An Analysis of the Femoral Head / Stem Taper Lock for Orthopaedic Prostheses

A THESIS
Presented to
The Academic Faculty

by

Brian Schumacher

In Partial Fulfillment
of the Requirements for the Degree
Master of Science in Mechanical Engineering

Georgia Institute of Technology
December 1992

An Analysis of the Femoral Head / Stem Taper Lock for Orthopaedic Prostheses

APPROVED:

Dave McDowell, Chairman

William Hutton

Ray Vito

Wade Fallin

Gretchen Rhodes

Date Approved by Chairman 12-15-92

ACKNOWLEDGEMENTS

I am very grateful to the people who have made my graduate work possible. First to my advisor Dr. McDowell for his guidance and understanding throughout my graduate career. To Georgia Tech for giving me the opportunity to go to graduate school. To Wade Fallin and Gretchen Rhodes for their financial support, helpful assistance, and the facilities to conduct the various aspects of this project. To Mark Harbaugh for his help and guidance with the FEA modeling. To both Wade Fallin and Will Sauer for their editing and comments. To Smith and Nephew Richards for their financial support, use of their facilities and for providing me with this project. And finally to my fiance Karen Metzler and her roommate Valerie Nail for their help in typing and editing till late at night and without whom I would not have finished on time.

TABLE OF CONTENTS

	Page
THESIS APPROVAL PAGE	ii
ACKNOWLEDGEMENT	iii
LIST OF TABLES	vi
LIST OF FIGURES	vii
SUMMARY	x
CHAPTER	
I. INTRODUCTION AND BACKGROUND	1
History And Modularity Of Hip Prostheses	
Taper Mechanics	
Test Specimens	
Hip Dislocation and Head Disassembly	
Hip Forces During Gait	
Taper Corrosion	
Problems with Particle Debris	
Test Variables	
II. INSTRUMENTATION AND EQUIPMENT	25
Measurements and Equipment Used	
Profilometer	
Air Gage and CMM	
III. PROCEDURES	29
Cleaning of Testing Parts	
Static Testing	
Fatigue Testing	
Impact Load and Pull-off	

Metal Ion Release
Fatigue Solution Filtering
SEM
Finite Element Analysis

IV. RESULTS AND DISCUSSION 47

Finite Element Analysis Results
Angle Mismatch
Static Testing Pull-off Loads
Taper Lock Friction
Roughness Results
Fatigue Testing Pull-off Loads
SEM
Metal Ion Release Results
Particle Count Results
Distal and Proximal Contact Theories
Impact Head Assembly and Pull-off Loads

V. CONCLUSIONS AND RECOMMENDATIONS 89

APPENDIX 92

REFERENCES 104

LIST OF TABLES

	Page
Table 1. Hip Load Values	13
Table 2. Taper Design Names and Parameters	19
Table 3. Measurements and Equipment	25
Table 4. Finite Element Analysis Results	48
Table 5. Strain Gage Results	57
Table 6. Diameter, Angle, and Angle Mismatch	61
Table 7. Static Testing Pull-off and Displacement Results	66
Table 8. Roughness Results	71
Table 9. Fatigue Testing Pull-off Results	73
Table 10. Metal Ion Results	79
Table 11. Impact Loading and Pull-off Results	87

LIST OF FIGURES

	Page
Figure 1. Drawing of the skeleton, the hip joint, and a hip prosthesis	2
Figure 2. Femoral Head and Short Taper Stem	4
Figure 3. Head preloading attachment	6
Figure 4. Drawing of the femoral head	8
Figure 5. Pictured from left to right are Fatigue, Proximal, Polished, and Sleeved tapers, a sectioned femoral head, and a hip prosthesis.	9
Figure 6. Drawing of a Proximal taper	11
Figure 7. Hip force calculation for a one legged stance	13
Figure 8. Drawing of a hip prosthesis	14
Figure 9. Drawing of different specimens	19
Figure 10. Profilometer profiles	20
Figure 11. Distal and proximal contant	22
Figure 12. Sleeve design	22
Figure 13. Head Assembly by direct impact strike and by striking a controlled impactor	24
Figure 14. Profilometer measurement setup	27
Figure 15. Air gage measurement setup	27
Figure 16. Static and preloading test set up	31
Figure 17. Axial pull-off test set up	31
Figure 18. Fatigue testing setup	34
Figure 19. Fatigue loading disk and Fatigue holding fixture	35

Figure 20. Finite Element Model head and taper 43

Figure 21. FEA head pressure distribution curve 44

Figure 22. FEA nodes with head pressure distribution and taper fixation 44

Figure 23. Rosette strain gage locations 46

Figure 24. FEA Proximal design with friction 49
(a. Hoop stress, b. Effective stress, c. Max principal stress,
d.. Min principal stress)

Figure 25. FEA Proximal design, frictionless (Hoop stress) 52

Figure 26. FEA Distal design, frictionless (Hoop stress) 52

Figure 27. FEA Proximal design with friction 53
Displacement in the x direction

Figure 28. FEA Distal design with friction 54
(a. Hoop stress, b. Effective stress, c. Max principal stress,
d. Min principal stress)

Figure 29. FEA Conforming design with friction 58
(a. Hoop stress b. Effective stress c. Max principal stress
d. Min principal stress)

Figure 30. Average angle mismatch between the head and the taper 63
(a. Total graph, b.Expanded graph)

Figure 31. Static testing pull-off 65

Figure 32. Friction values from preloads and pull-off loads 65

Figure 33. Roughness Results 70
(a. All roughness values, b. Proximal and Distal roughnesses,
c. Polished roughness, d. Rough roughness)

Figure 34. Fatigue loading pull-off 72
(a. Total graph, b. Expanded graph)

Figure 35. SEM pictures of the distal and proximal ends of the 76
different taper designs.
(a. Proximal, b. Distal, c. High preload, d. Polished)

Figure 36. Metal ion release results 78
(a. Metal ion results for Co, Cr, and Ti, b. Cobalt ion results,
c. Chromium ion results, d. Titanium ion results)

Figure 37. Cobalt chromium particle and energy dispersive analysis 82

Figure 38. Filtered titanium particles 84

Figure 39. Impact Load Testing 86

Figure 40. Pull-off testing after impacting heads onto the tapers 86

SUMMARY

A total hip prosthesis consists of a main structural stem, a spherical head, and extensions. The connection between the head and stem is accomplished by a male / female conical taper lock. This study considered the interface connection between the head and stem.

Cobalt chromium heads and titanium stems were analyzed because of their biocompatibility and wide use in industry. The surface roughness and taper angle were the primary variables studied. The assembly load, the assembly procedure, and the number of part connections were the secondary variables studied. In this investigation, only the taper was changed and the head was taken from existing stock from Smith and Nephew Richards of Memphis Tennessee. There were seven different head / taper lock designs tested to evaluate the the variables listed above.

In this study, a 2-D axisymmetric finite element (FE) analysis of the conical taper was used to determine the relative displacements and the stress distributions in the head and taper under loading conditions. They showed that for different taper angles the maximum hoop, effective, and principal stresses were always at the head / taper contact region. The Distal contact design had the highest stresses, but they were still well below the ultimate strength of the material. This Distal design makes initial contact between the taper and head at the rim of the head. Most of the designs investigated had initial contact at the proximal end inside the head. The FE displacement and stress results were similar to the static testing and strain gage experimental results.

Both static and fatigue testing were conducted on the head / taper lock. The head / taper combinations were loaded in compression and the metal ion release, particle debris,

relative displacement, and pull-off loads were measured. The static testing showed that the head pull-off loads had a linear relationship with the preload. For the different roughnesses and taper angles the pull-off load was usually 53% of the preload. From the profilometer and SEM analysis the contact region showed plastic deformation, but there was not a consistent trend in the roughness (Ra) values between the low and high static loads

In the fatigue testing the specimens were loaded at 1,100 lb cyclic load for 1 million cycles in Ringer's solution, and these results showed more significant differences between the different designs. In this study, the Distal contact design had a higher head pull-off load and much lower metal ion in solution. High pull-off loads would demonstrate a stronger mechanical lock and the lower metal ion content would show less contamination escaping into the body. One head / taper connection was preloaded very high to 3,000 lbs before fatiguing and it had a much larger pull-off load and reduced metal ion content. This would be expected because for higher preloads the locking strength is better. Another design that incorporated a sleeve connection between the head and taper showed a much higher metal particle amount after filtering with up to 52 million titanium particles after the fatigue test which was similar to a year of use. This could be attributed to the additional connection. It should be noted that the wear debris caused by the head / cup articulation can cause 50 billion particles per year, which is much greater than the wear from the head / taper lock. However, it is always beneficial to reduce metal ions and particles from contaminating the body.

With the mechanical integrity and contamination to the body as key design issues, the best overall design based on the methods used in this study was the design with Distal contact. It was superior in static and post fatigue pull-off tests and it had a lower metal ion release rate. It should be noted that in this study, the fatigue testing was conducted for only one million cycles and from the literature it was found that further tests of ten to twenty million cycles should be conducted in the future to develop stronger conclusions. From the

literature it was also found that a very important issue in this type testing is the quality of the taper and head manufacturing. Poor quality with proximal or distal contact would not be beneficial.

A study of the different surface roughnesses did not reveal any consistent advantage of one over the other. They were relatively similar in mechanical integrity and contamination to the body. Also there was no correlation found between the small variations in angle mismatch between the head and taper in pull-off loads or metal ion content. Angle mismatches of greater than the angles used in this study would be required to show significant differences.

Another item variable investigated was the assembly procedure of putting the head onto the taper. It was determined that a higher assembly load causes the head to lock on better and to have less metal ion release. In order to consistently accomplish this, it was proposed to use a device that applies a known controlled impact load. The current procedure involves a surgeon striking the head manually with a surgical mallet , which results in a large variation in the impact loads applied. The spring loaded controlled impactor device was investigated and proved to work well. It applied a more consistent impact load to the head / taper connection than a manual direct strike. This study also indicated that using a device like this would ensure a strong mechanical lock with less metal ion contamination to the body.

CHAPTER I

Introduction and Background

History And Modularity of Hip Prosthesis

Total joint implants are used to replace deteriorated joints. This study focuses on the hip as shown in Figure 1. A total hip prosthesis primarily consists of a main structural stem, a spherical head as shown in Figure 1. The connection between the head and stem of the implants was accomplished by a male / female conical taper lock. This study will consider the interface connection between the head and stem.

Hip joint implants are a significant and important part of the orthopaedic industry. Hip joint implants accounted for 816,000 orthopaedic implants in 1988 which was 12.5% of the implant distribution; this accounted for the largest percentage of the artificial joint implants (1). By comparison, knee implants accounted for 8% and all others were 4.4% of the total implant distribution.

In hip implants today, the femoral head is usually a separate modular piece. The method of fixing the head to the stem is by a male / female tapered cylindrical connection. The taper is generally referred to as a Morse Taper, but this is a misnomer. The "Morse Taper" is the standard name given to most tapered cylindrical parts. The "Morse taper" originated in the 1880's and was published in the "American Machinist" journal in November 1884 (2). The manufacturer of the morse taper was the Morse Twist Drill and Machine Company of Bedford, Massachusetts. The tapers were defined primarily by a name, diameter, and the taper per foot. Originally there were six different taper sizes and today there are seven different Morse taper sizes. The average Morse taper included angle

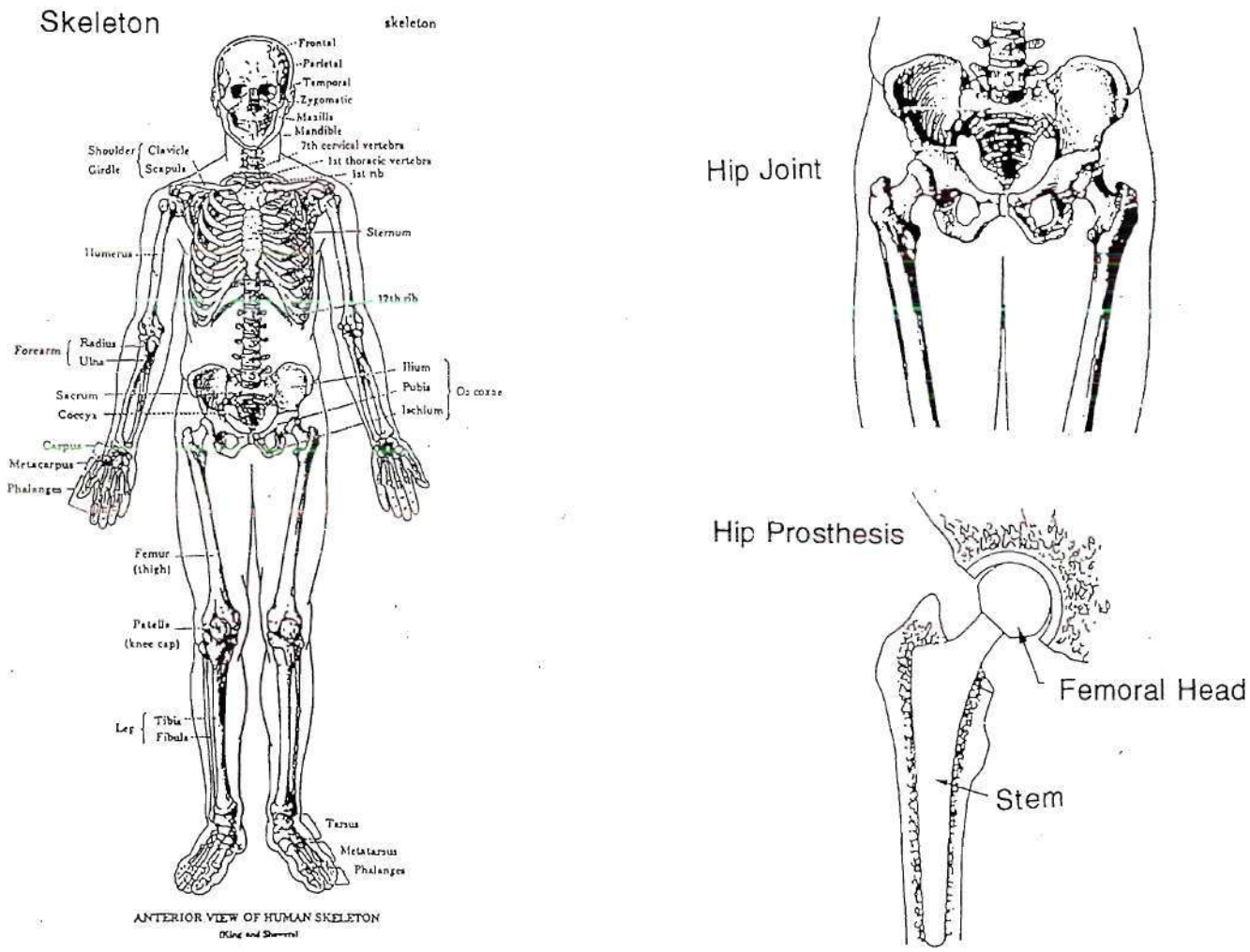

Figure 1. Drawing of the skeleton, the hip joint, and a hip prosthesis

is 5/8 inches per foot or 5.96° (3). This angle and diameter does not match the orthopaedic tapers used today even though the "Morse taper" label is still used.

Smith and Nephew Richards of Memphis, Tennessee was the innovator of modularity for the head-neck interface. In 1982 they introduced the first modular ceramic head design for the Autofor hip. The main idea behind having modular heads was the ability to have one material for the stem which fixates to the bone and carries the load and another material for the head which articulates with the acetabular cup as shown in Figure 1. Titanium is more flexible than cobalt chromium or stainless steel and this flexibility avoids stress shielding ,and bone resorption (4,5,6). For stable implants, titanium is very biocompatible and allows the bone to form a tight interface. Titanium (Ti-6Al-4V) is a material that is widely used in industry for the stem. In this study titanium was the material used for the stem taper. However, titanium is not a good material for articulation with the UHMWPE acetabular cup. It produces a high amount of both polyethylene and titanium wear (7,8,9). Ceramic heads have the lowest friction and best wear properties but are much more expensive and for this study they were not as available. Cobalt chromium heads have very good wear characteristics, are more affordable than ceramic heads, and therefore were used in this investigation. Cobalt chromium heads are the leading alternative available on the market today to ceramic heads. Figure 2 shows a head and short taper bar.

Another advantage of a modular head and neck is a reduced inventory because of the many sizes offered. Modularity also allows the surgeon to make changes in the neck length intraoperatively and allows removal of the head in a revision operation. Several choices of head sizes were generally offered including 22, 26, 28 and 32 mm outside diameter. Three neck lengths inside of the head, or taper depth length, are generally offered and they include +0, +4, and +8 mm sizes. The different lengths give the surgeon the ability to make fine adjustments in the head extension if needed.

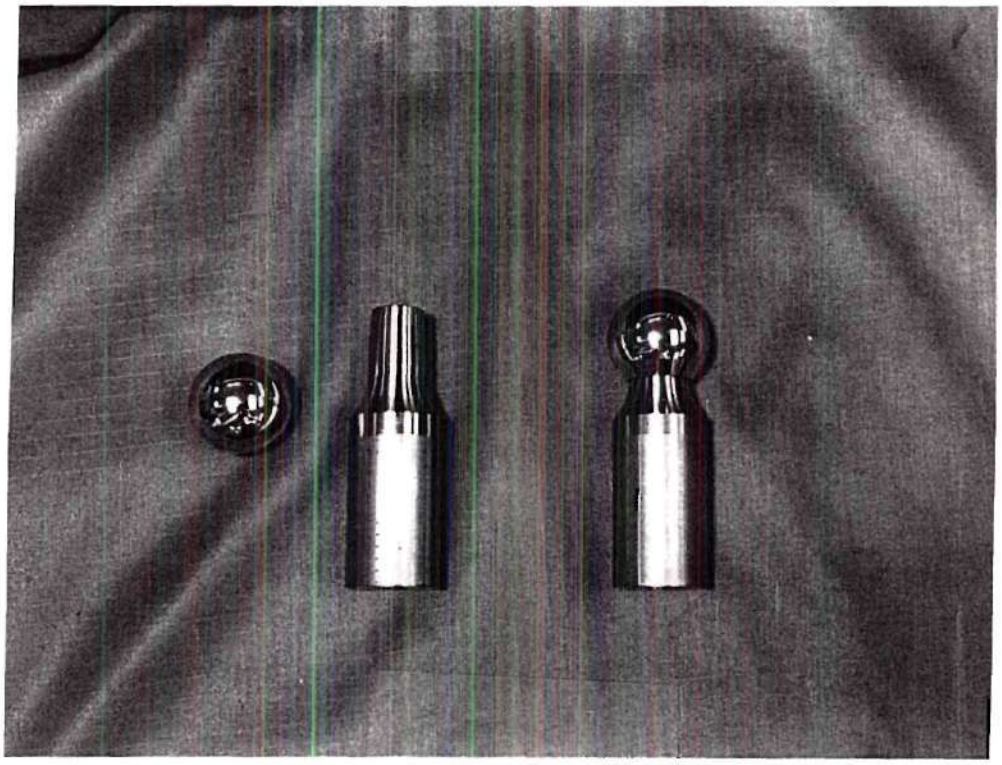

Figure 2. Femoral Head and Short Taper Stem

Taper Mechanics

The physical mechanism that holds the head and taper together is friction as seen in Figure 3. There are two types of taper lock designs. Tapers with inclusive angles between 0° and 8° are self locking and tapers with angles greater than 12° are self releasing (10,11). Self-locking designs transmit torque without additional fixation while self-releasing designs require an additional positive latching mechanism to transmit torque. Most orthopaedic companies have tapers between 2° and 6°. The tapers between 8° and 12° are in a transition regime between these two types. As the taper angles get smaller, the force to disassemble the two parts is higher, but the amount of load it can withstand is reduced. Larger angled tapers are able to withstand more axial loading because the stresses are reduced. The taper lock is a simple compact design that is self-centering and is very strong mechanically. It can resist both axial and torsional loads and is very well suited for the femoral head/taper connection.

Test Specimens

The selection of materials and sizes for this testing was based on their wide use in industry and the reasoning previously discussed. The test specimens or components used in this research include cobalt chromium (Co-Cr) femoral heads (ASTM F-799) and short titanium (Ti-6Al-4V ELI Alloy) taper stems as shown in Figure 2. The heads are essentially a sphere with a part through tapered hole. The heads are composed of 66% cobalt, 28% chromium, and 6% molybdenum and are machined from wrought bar stock. The bar stock is made by forging, followed by hot rolling and cold finishing. The outside sphere and female taper surfaces are both manufactured by CNC turning of the bar stock. After the head is machined the outer surface is polished. The femoral heads used in this research were stock Smith and Nephew Richards heads (cat #12-9935), and a 28 mm

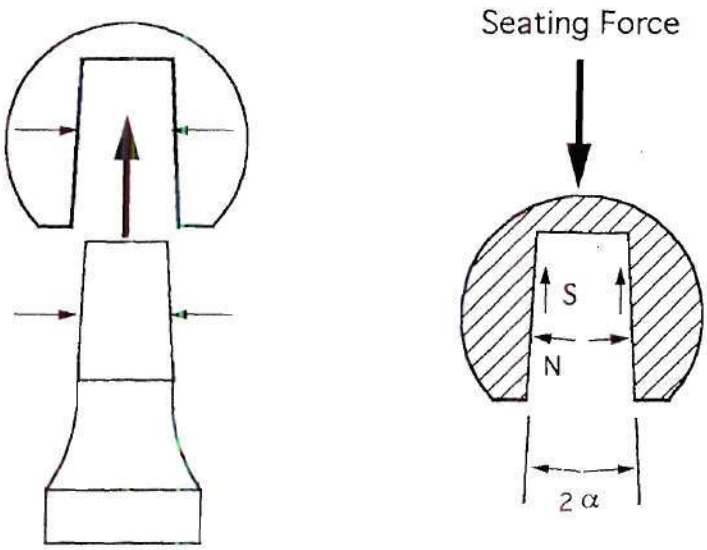

Figure 3. Head preloading attachment

outside diameter head size was used. Figure 4 shows the schematic of the heads used. The four sizes available include 22, 26, 28, and 32 mm in diameter but, the 28 mm size was chosen because it has the highest percentage use in industry. The neck length, which corresponds to the taper hole depth, was +0 mm standard. This results in the deepest hole depth into the head. The other sizes available include +4 mm and +8 mm which correspond to more shallow holes and longer head extension. The +0 was chosen because it has the largest contact area which should increase the total friction to improve the taper lock. With the taper angle and surface roughness as key issues in this study, having the largest area of contact was beneficial to make comparisons between different designs. The material properties of both titanium and cobalt chromium are shown below (12,13).

	Modulus of Elasticity (ksi)	Ultimate (ksi)	Yield (ksi)	Poisson's ratio
Ti-6Al-4V	16.5×10^3	125	115	.35
Co-Cr	31×10^3	170	120	.30

The titanium short taper stems used in the testing are not stock catalog products. Due to high costs, it is not practical to do this type testing with full hip stems. Therefore, a short cylindrical bar with a tapered end is used as can be seen in Figures 5 and 6. This is a standard testing practice and is much more effective and quicker to manufacture. The bar or tapers, as they will be called, are 3" long and 1" in diameter. The tapered end is identical to the tapered end of a full hip stem and Figure 6 shows the drawing of the Proximal taper The hip stem and taper are both made of 90Ti-6Al-4V (90% titanium, 6% aluminum and 4% vanadium). Titanium was chosen because of its wide use in industry. The tapers were machined from the hot-rolled and cold-finished bar stock. The taper was tapped and threaded on the end for testing fixture fixation and then the other end was CNC-turned to form the tapered surface. The CNC turning process was the controlling factor in changing

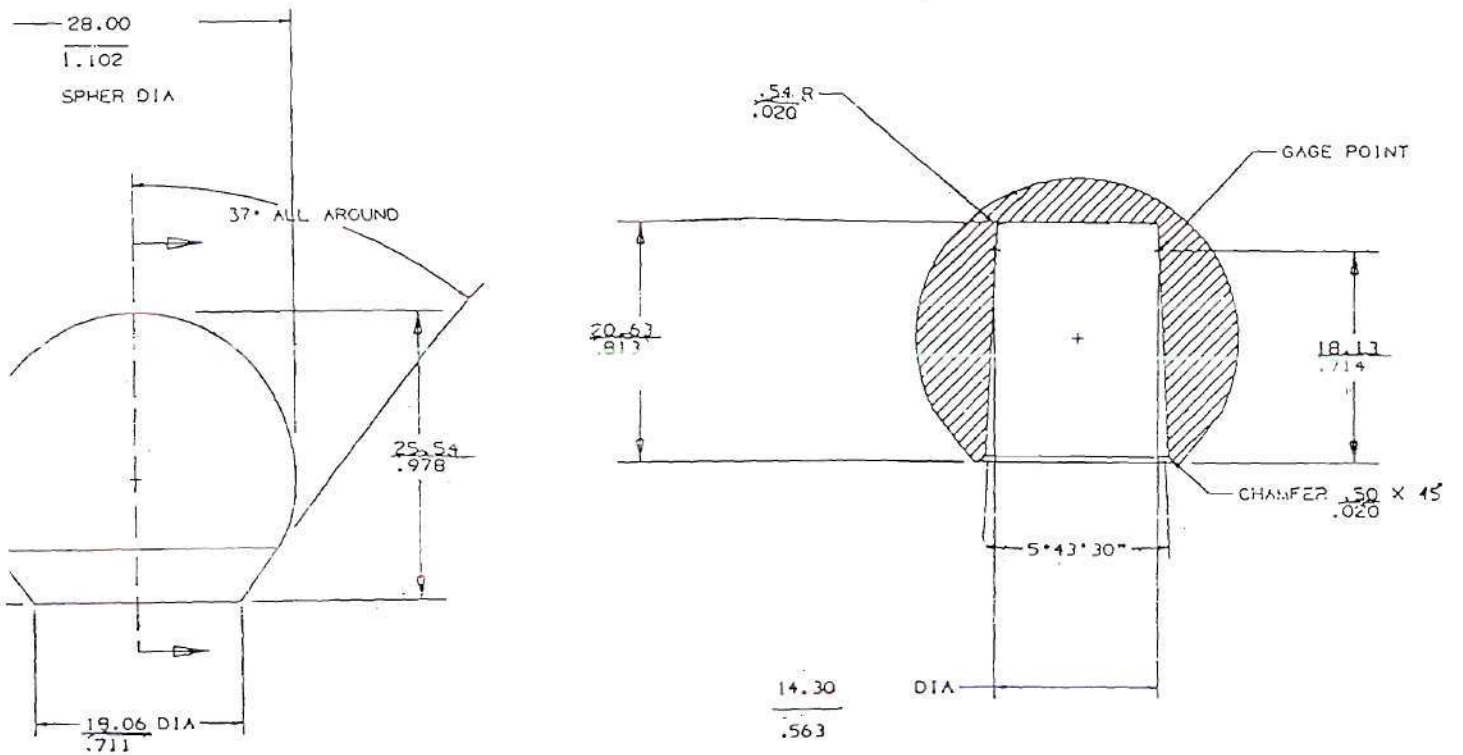

Figure 4. Drawing of the femoral head

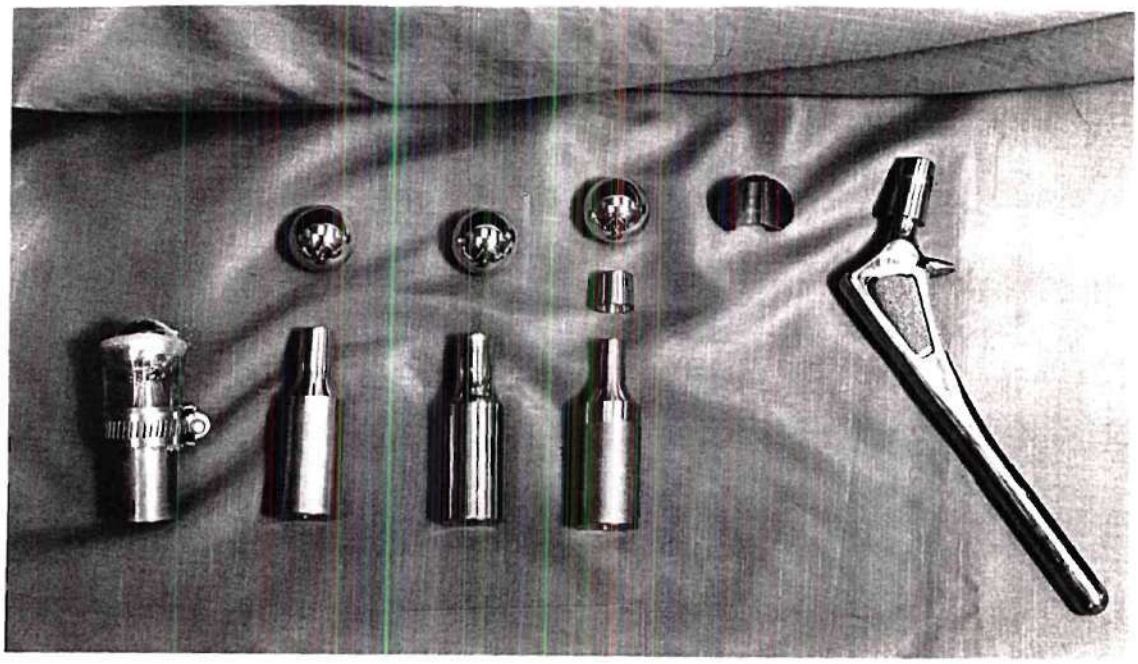

Figure 5. Pictured from left to right are fatigue, standard, polished, and sleeved tapers, a sectioned femoral head, and a hip prosthesis.

the angle and roughness of the taper surface. The normal taper surface is actually a "threaded" surface. The threads are extremely short and spaced far apart. The threaded taper surface deforms due to the forces applied to the surface and the taper conforms to the head. The rougher surface should ideally conform more, providing better fixation with the head. This conformance may allow for lower tolerance standards. If, however, the threads are too "sharp" it can cause particles to shear off which is not desirable. The diameter of the small end of the taper is 0.564" which is the Proximal design end diameter at the defined gage point. The taper angle is 5° 43' 30" - β' [+0 -λ'] and the roughness is 50-60 Ra (roughness average). The β and λ are proprietary information to Smith and Nephew Richards. These values are the base line design in this experiment. These tapers were made in the Smith and Nephew Richards specialty products and manufacturing facilities.

Hip Dislocation and Head Disassembly

There are several reasons why it is important to have a strong mechanical lock between the head and taper. The more common and most important issue with the taper lock is the wear debris and metal ion release. However, the mechanical locking strength is another important issue. This can be measured by the pull-off forces after preloading the heads with a press fit. The mechanical locking strength is important from a wear debris standpoint because if the head becomes loose, a large amount of debris will be generated and this is not desirable

Under normal in vivo conditions the head is compressed onto the taper by the acetabular cup and there is no tensile loading to pull the head off. However, under rare circumstances, there is a tensile force which acts to remove the head. This disassembly has only occurred a few times in vivo (14,15,16). The times that it has occurred have been after the hip has dislocated from the acetabular cup and a closed reduction (realignment of

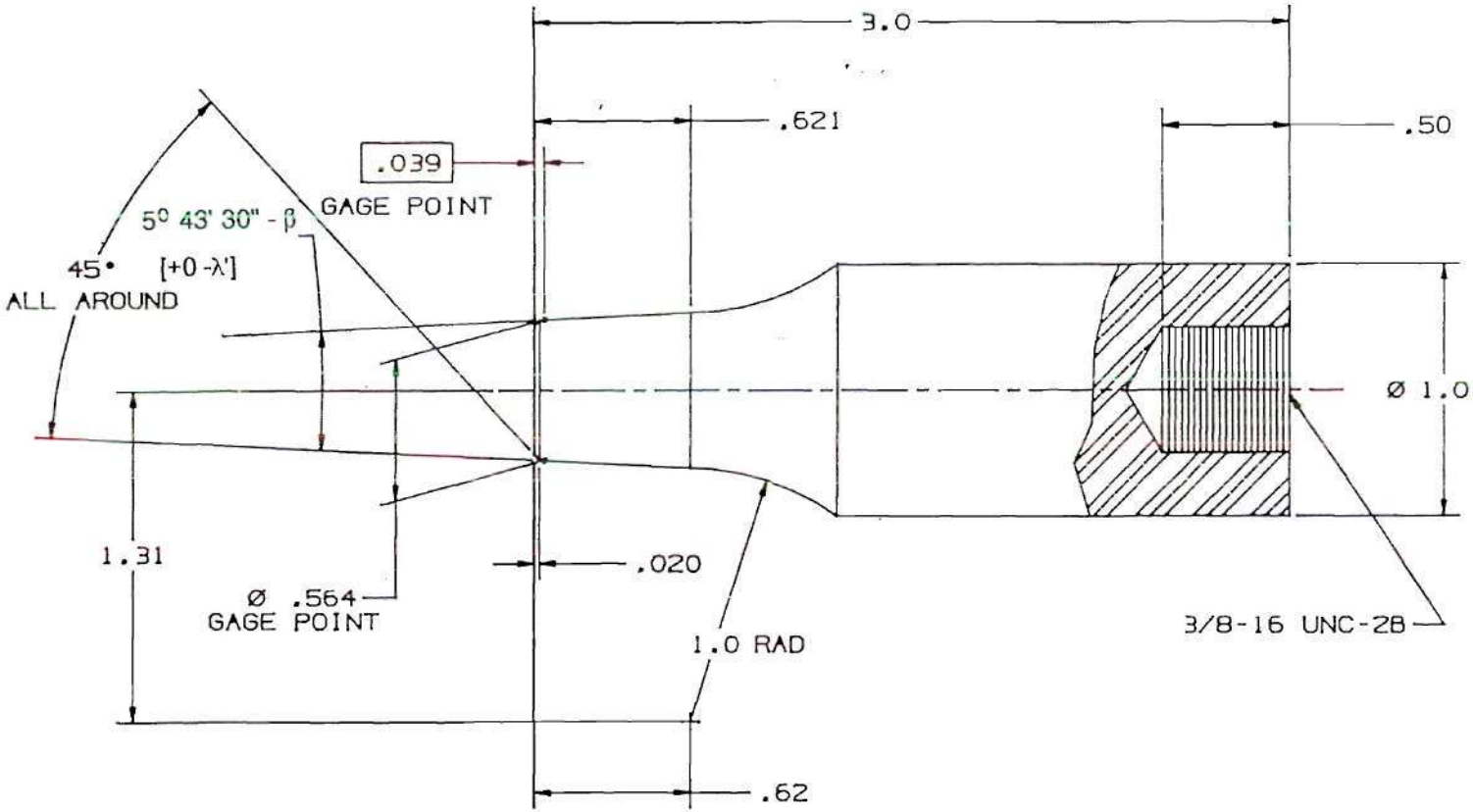

Figure 6. Drawing of a Proximal taper

the hip) was attempted. The edge of the head was caught on the edge of the acetabular cup and after much force on the leg to reset the joint, the head disassembled from the taper. The patient had to immediately undergo surgery to remove the loose femoral head and to assemble a new head. This has happened only a few times but is a very undesirable result because surgery must be performed. Proper sizing of the hip prosthesis can reduce the chances of dislocations. However, the head must remain intact under these circumstances. The disassembly could have been caused by an inadequate impact preload of the head on the stem; this topic will be discussed later. Another cause could have been a poor design or poor manufacturing of the taper and head.

Hip Forces During Gait

Previously discussed have been the benefits of modularity, the basics of the taper lock and the materials used in this study. Now to be addressed are the loads that the hip is normally subject to during several different activities. The forces in the hip are typically determined in comparison to the body weight (BW). The forces on a hip are approximately 3 times BW for a a one-legged stance and 4.3 times BW for the beginning of the single-support period of gait (17). This additional load is caused by the counterbalance of the abductor muscles keeping the body balanced and is illustrated in Figure 7. Williams reported the hip loads for other activities and is shown in Table 1 (18). The hip load values are shown for a person with a body weight of 160 which is the average weight of a man and much higher than an average weight of a woman.

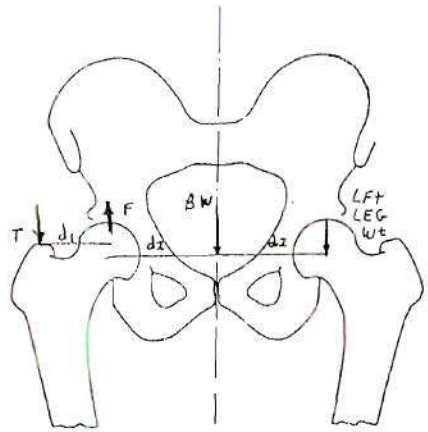

d1 = 2.75 in d2 = 5.95 in
Total BW = 175 lb BW = 119 lb Lft Leg = 28 lb
$\Sigma Fy = 0 = T + F + BW + \text{Lft Leg}$
$\Sigma M = 0 = BW\,(d2) + T\,(d1) - \text{Lft leg}\,(2 * d2)$
$F = 3\ BW$

Figure 7. Hip force calculation for a one-legged stance

Table 1. Hip Load Values

Action	Body Weight	Hip Load
2 legged stance	0.3 BW	48
1 legged stance	3.0 BW	480
Walking	4.3 BW	688
Jogging	7.0 BW	1,120
Running	8.0 BW	1,280
Walking Stairs	5.0 BW	800

Seven times body weight for a 110 lb person is 770 lbs and for a 250 lb person is 1,750 lbs. Obviously, the first solution to reducing hip loading is to lose weight.

In the fatigue testing a cyclic load ranging from 110 lbs to 1,100 lbs was conducted for 1 million cycles. This is a simulation of a man jogging continuously for a year. The load chosen was comparable and higher than that typical of other studies of similar nature.

The angle of the loading was the next issue. The problem occurs that the muscles attached to the femur acts in several directions. It would be desirable to apply a single load in laboratory testing that would reproduce similar loading and strains as the actual in vivo loading. From a study conducted at Richards, it was determined that with stem and taper at physiological angle that a vertical load was the best approximation of the magnitude and distribution of strains obtained in a hip system (19). This was done for the hip at an in vivo angle of 10° adduction which is the ISO Standard (20). It is also confirmed by C. Dingman and Rohlman et al that the 0° load case best approximated the mid stance phase (19,21). Therefore, this 0° load with the hip at its in vivo angle was used in the fatigue testing. With the 49° neck angle and 10° adduction, the resulting angle is 39° with the taper axis, as shown in Figure 8.

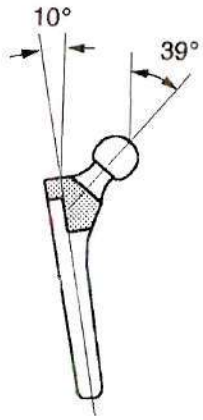

Figure 8. Drawing of a hip prosthesis

Taper Corrosion

The next issue to be discussed deals with some of the results of the continuous loading and of having modular components in the body. As mentioned earlier, the issue of wear debris and metal ion release are very important issues, and this section discusses corrosion of the taper lock. Corrosion is influenced by several things including the surface finish, design geometry, oxygen concentration, pH, mechanical stresses and the presence of proteins (22, 23). The largest problems with corrosion is that it can lead to a loss in the

mechanical taper lock integrity due to a loss of material and it has the potential for adverse effects in the body.

Definitions (23,24,25):

Corrosion - Any surface discoloration caused by chemical reaction of metal.

Pitting - Any form of surface material removal caused by chemical processes.

Fretting - Material removal caused by mechanical removal of surface oxides and substrate due to apparent micromotion

Galvanic corrosion - An accelerated reaction caused by the electrochemical coupling of two metals of significantly different corrosion resistance.

Crevice corrosion - It is corrosion that occurs in a crevice where tight contact between mixed or similar metals leads to damage of the protective passivation layer, which cannot then reform due to oxygen depletion.

In crevice corrosion the chemical reaction is dissolution of a metal into its respective ions and oxygen to hydroxide (oxidation M=M+e, reduction $0_2 + 2H_20 + 4e = 4OH-$). Oxygen is depleted resulting in excessive positive charge, which causes negative chloride ions to contaminate the crevice (23,26). The pH can be two to three times lower than normal, which corresponds to the acidity being two to three times higher than normal. Fontana stated that to function as a corrosion site, a crevice must be wide enough to permit liquid entry, but sufficiently narrow to maintain a stagnant zone. For this reason crevice corrosion usually occurs at openings a few thousandths of an inch or less in width. (25, 27).

There are several opinions as to what type corrosion occurs at the head/taper connection. Collier reported that he attributed the extensive metal loss to galvanic corrosion (22). He stated that the in vivo electrochemical connection of the cobalt chromium and titanium materials causes galvanic corrosion. He based this on the fact that he only saw corrosion on mixed metal head/taper connections (CoCr / Ti) and not on similar metal connections (CoCr / CoCr). However, all of his implants with mixed metal head/taper connections were from the same manufacturer and the design was not taken into consideration. Other research has shown that the significant factor is the quality of manufacturing and the mismatch between the head and taper (23). Dr. Galante reported

from retrievals of the Harris-Galante hip that there was evidence of crevice corrosion (24). Other research has also stated that galvanic corrosion is not occurring (23,24,26). Mathiesen found corrosion in like-metal taper locks which showed that crevice corrosion occurred (23, 28). This was due to poor mechanical fitting of the head and taper which left a large crevice. Some researchers, including Bauer et al, think that fretting initiates corrosion and that corrosion then consumes the initial fretted region (23, 24, 27). Slight fretting may occur with very large head/taper mismatch but this is only for poorly designed taper connections and poor manufacturing. Also, it has been found that larger tolerances result in more corrosion, which may be attributed to crevice corrosion.

From the literature and experimental research the primary corrosion appears to be crevice corrosion that is initiated or accelerated by fretting, but is not galvanic corrosion (23, 26). It has been shown that a well designed mixed metal head/taper combination with good manufacturing results in no corrosion. From Sauer et al , 18 titanium stems with cobalt chromium heads were retrieved periodically three to five years in vivo (23). Also, similar fatigue mechanical testing testing was conducted in Ringers solution. The results of their study of retrievals and testing were similar to the fatigue testing of this study. From visual analysis there was no evidence of corrosion and there were very few surface changes; the original machine marks were still visible and intact in both studies. The SEM results from Sauer et al testing showed that there was little or no evidence for material removal or pitting on the tapered surfaces.

Collier et al did not consider the mechanical design into the effects of corrosion and this could be a very large factor. Two studies, Sauer et al and Collier et al, evaluated the CoCr / Ti material combinations at a 3 to 5 year follow-up (22,23). Collier et al showed crevice corrosion and Sauer et al showed no corrosion for the mixed-metal combinations. Collier et al also tested like-metal combinations (CoCr / CoCr) and found no corrosion. Collier attributed the start of corrosion to the mixed-metal combination because the like-

metal combination did not have significant corrosion. However the design of the like-metal and mixed-metal combinations were different and this was not taken into account. This showed that the design and manufacturing of the taper had a greater effect than the type of metal combination . This showed that galvanic corrosion is not the issue of concern, but design and manufacturing related issues are the explanation.

Titanium has the best crevice corrosion characteristics while cobalt chromium can suffer from crevice corrosion. For galvanic corrosion the passive film must be disturbed (26). However, both titanium and cobalt chromium repassivate very quickly so any damage to passive films during impaction are easily corrected (23, 26, 29). Crevice corrosion is created by a crevice conditions between the head and taper. With good design and manufacturing, this problem can be reduced.

Fretting and corrosion may lead to a degradation of the mechanical lock and to increased metal ions. The metal ions were measured in this study to determine the contamination to the body. The articulation between the Co-Cr heads and the acetabular cup has ten times greater metal ion release than the head/taper connection. The wear from the articulation between the Co-Cr heads and the acetabular cup was about 18 ppm/yr of cobalt compared to 0.75 ppm/yr (ppm = parts per million) for the head / taper connection (26). The differences in wear debris is due to the difference in motion between the articulation between the head and cup and the a mechanical lock between the head and taper. Titanium oxide and chromium oxide protect the bulk material. Titanium alloy films do not dissolve and will maintain protection even under the local acidic conditions. However, the cobalt chromium passive film will dissolve (26). Metal ions (m+) react with water in solution to produce H^+ ions. As the H^+ ions increase, the environment becomes more and more acidic if it is not diluted (26). As the metal ions increase the acidity increases and this causes the cobalt alloy's passive oxide film to become less stable. Metal attack then becomes easier and can lead to crevice corrosion (26).

Problems with Particle Debris

Ever since modular prosthesis design has been used in orthopaedic implants, wear debris and metal ion release have become important issues. The wear particles produced can cause several problems including macrophagic osteolysis. Amstutz stated that the release of particles will result in significant bone loss around the implant site (30). Particulate debris is an activator of macrophages and these macrophages can cause bone resorption. Mathiesen et al stated that the tissue surrounding an implant with many wear particles were black in color and has been shown to cause inflammation and extensive necrosis of the tissue (28). Also foreign body giant cells are present and cause destruction of the media. Other problems of metal particles discussed include biological effects with metabolic, bacteriological, and immunogenic consequences, and possible carcinogenic effects (28). It is obviously not beneficial to have metal ions and wear debris in the body.

Test Variables

With the background of the wear issues, loading conditions, and hip material, next to be discussed are the variables being investigated in this study. In this case study, five different parameters were investigated. The primary variables investigated were the taper roughness and the taper angle. The secondary variables include the number of connections, the preload amount, and the head assembly procedure. The different parameters are shown in Table 2 and in Figure 9 below. The parameters are described in more detail in the following sections.

Table 2. Taper Design Names and Parameters

Name	Roughness (Ra)	Taper Angle (°)	Comments about Taper
Proximal	50 - 60	5° 43' 30" - β' [+0 -λ']	Proximal with angle mismatch from β' to 2λ+β '
Rough	118 - 122	Proximal	Rough surface
Polished	6 - 14	Proximal	Extremely smooth surface
Distal	Proximal	5° 43' 30" + β + λ' [+λ' -0]	Head rim contact with same angle mismatch as Proximal
Sm Prox	Proximal	5° 43' 30" - β - 4λ' [+0 -λ']	Large angle mismatch with proximal contact
Hpreload	Proximal	Proximal	3000 lb preload before fatiguing (All others 450 lb preload)
Sleeve	Proximal	Proximal	Sleeve between head and taper (Extra Connection)

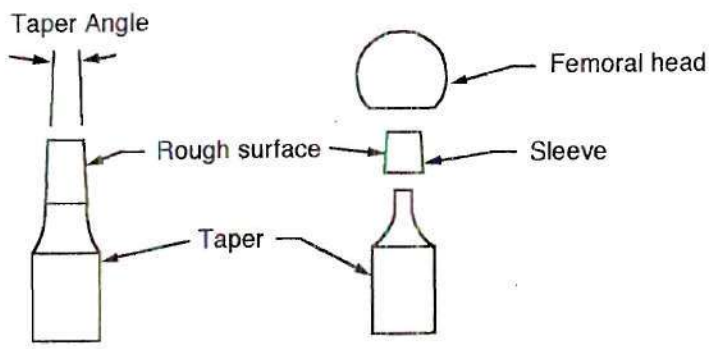

Figure 9. Drawing of different specimens

The roughnesses investigated were chosen as two extremes from the base line roughness of 50 m" Ra. The "Polished" surface was very smooth and the "Rough" surface had over double the Ra value as shown in Figure 10. The profiles shown are examples of

1. Base line - 58 μ" Ra

2. Rough Surface - 120 μ" Ra

3. Polished Surface - 3.6 μ" Ra

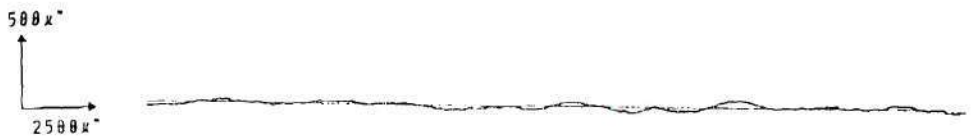

Figure 10. Profilometer profiles

the best surfaces manufactured. Along with the roughness, the other primary parameter involves the angle of the taper. The taper angles were also chosen for both proximal and distal contact. The exact angle tested are proprietary information to Smith and Nephew Richards, but the different angle are shown below with a λ tolerance and β and λ used to define the angle.

Taper Angles

1. Proximal Contact	5° 43' 30" - β' [+0 -λ']
2. Distal Contact	5° 43' 30" + β + λ' [+λ' -0]
3. Less Proximal Contact	5° 43' 30" - β - 4λ' [+0 -λ']

The "Proximal" impinges with the head proximally, which is at the inner most part of the head and at the end of the taper as shown in Figure 11. The angle mismatch between the head and taper varied from β' to $2\lambda+\beta'$ for the "Proximal " design , always with proximal contact. These values were determined from the maximum and minimum angles that the head and taper could have and still be in tolerance for the study. The "Distal" design was chosen with the same angle mismatch as the Proximal design but with distal contact. This contact was at the rim of the head opening as shown in Figure 11. Therefore the Distal design had a β' to $2\lambda+\beta'$ angle mismatch between the head and taper. The distal contact was chosen to determine the effect of this entirely different contact region. The "SmProx" for small angle and proximal impingement was chosen to determine the effect of a large angle mismatch. This would measure the effect of having a larger tolerance band and having a small region of contact. The angle mismatch for this design was $\beta + 4\lambda'$ to $\beta + 6\lambda'$.

The secondary variables included three items; the number of connections, the preload amount, and the head assembly procedure. The number of taper connections refers to the number of parts connected together between the stem and the head. The standard condition tested included a direct connection between the head and stem. The alternative incorporated a sleeve between the head and taper shown in Figures 5 and 12. The taper diameter was reduced to 0.404" end gage point diameter. This sleeve provides more sizes

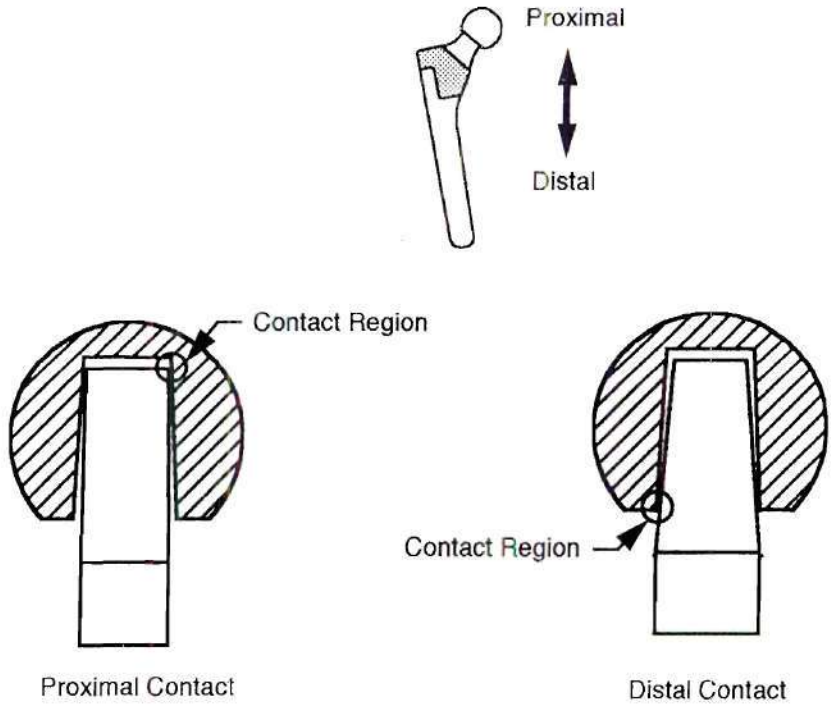

Figure 11. Distal and proximal contact

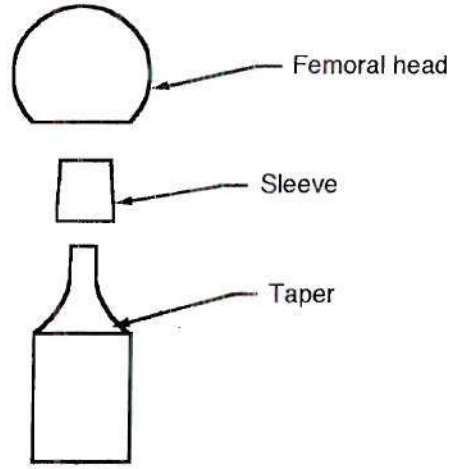

Figure 12. Sleeve design

and fine adjustment because it is offered in two sizes. The effect of having two coupled connections was tested, and it was referred to as "Sleeve" in the tables and figures.

The next secondary variable involved the preload level. The preload was the amount of load applied to the head in order to lock it onto the taper. In all of the testing, 450 lbs of static load was applied. In this case, 3000 lbs load was applied to the head before the fatigue testing. Therefore, it was called "H preload" to designate a high preload. This load was chosen because it was the maximum static load tested and it was desired to investigate the effects of a very high preload before fatigue. In all cases, the same fatigue load was used, which was a cyclic load from 110 to 1,100 lbs.

The last variable was the head assembly procedure. The current surgical procedure employs impact of the head on the taper by striking an impacting bar (which has a cupped delrin tip) with a surgical mallet three times, which is essentially striking the head directly as shown in Figure 13. This leaves a wide range for variability in the load that is applied. The static loading during the testing involved a precise load applied at approximately 0.1 inches per minute. The rate was increased manually, but a uniform slow rate was attempted. The proposed design to be investigated involved applying the load to the head with a controlled load impactor instead of the load being applied by striking with a surgical mallet directly and this controlled impactor is also shown in Figure 13.

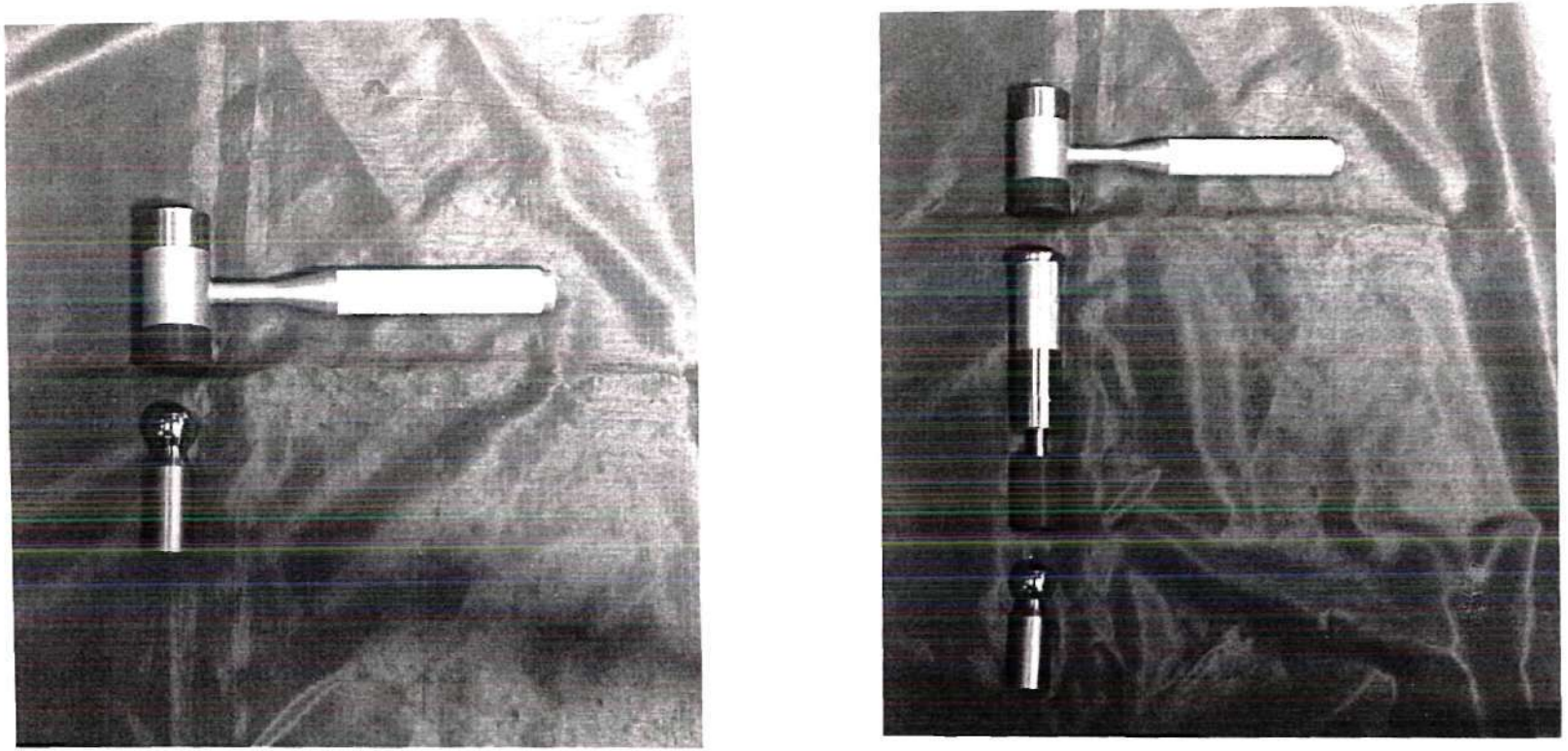

Figure 13. Head Assembly by direct impact strike and by striking a controlled impactor

CHAPTER II

Instrumentation and Equipment

Measurements and Equipment Used

Listed below, in Table 3, are the different variables measured and the equipment that was to conduct the measurement and the brand of the equipment used.

Table 3 Measurements and Equipment

Measurement	Equipment
Diameter	(Air Gage and CMM)
Taper angle	(Air Gage and CMM)
Roughness	(Profilometer)
Surface Pictures	(Scanning Electron Microscopy, SEM)
Preload & Pull-off Loads	(MTS 810)
Relative Displacement	(Dial Gage)
Particle Count	(SEM)
Metal Ion Release	(ICPMS Method)
Cleaning	(Ultra sonic with Micro)

Air Gage -	Air Gage Company, Pneumatic gage with a minitron electronics column. Accuracy of 0.00005" and .0042°.
CMM -	Brown and Sharp
Profilometer -	Tokyo Seimitsu Company, Surfcon profilometer with accuracy of 0.0000005".
SEM -	Smith and Nephew Richards material research division and Hitachi S-800
MTS 810 -	MTS Corp, Servohydraulic testing machine.

Dial Gage -	Mitotoyo, Accuracy of 0.0001" and range of 0.01.
ICPMS Method -	Teledyne Wah Chang Albany.
Ultrasonic Cleaning -	Branson 5200, Branson Ultrasonic Corporation.
Micro solution -	International Product Corporation.

Profilometer

The surface roughness of the contacting region of the surfaces of the head and taper were measured. The measurement length varied depending on the uniformity of the part but the normal measurement length was 0.35". The Vmag was 2000 and the Hmag was 200, and the travel speed was 0.012 "/s. All of these values were chosen as standard values to conduct the measurements for the roughness and type parts being investigated. The tapers and heads were placed in a precision vise to hold the parts for a measurement of the stylus moving along the surface as shown in Figure 14. The vise was pivoted in such a way to level the top of the taper's angled surface and the inside of the head's angled surface. The profilometer was located on a granite top which was on a dynamic pneumatic table. This essentially put the parts and profilometer on a cushion of air which prevented any vibrations of the surroundings from effecting the measurement. The Ra is the roughness average measurement and was used in this study as the comparison for the difference in roughness between the designs. It is the arithmetic average of all departures of the roughness profile from the center line within the evaluation length (lm) and is the standard roughness measurement.

$$Ra = \frac{1}{lm}\int_0^{lm} |y|\, dx$$

In using the profilometer, at least two heads and two tapers were measured after each static load for each part variable. Also, the fatigue specimens were measured before and after testing.

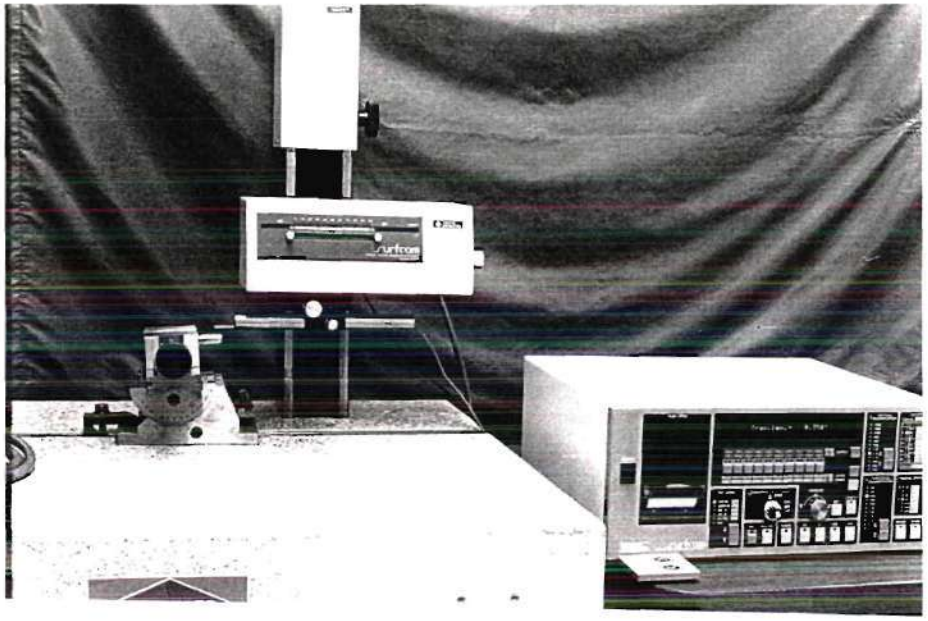

Figure 14. Profilometer measurement setup

Figure 15. Air gage measurement setup

Air Gage and CMM

Along with the roughness, the diameter and taper angle of each part were also measured. The small diameter or gage point diameter and angle of the taper surface and the inside of the femoral head were measured with an air gage shown in Figure 15. An air gage shoots two streams of air and when a part is set inside the cylinder there is a pressure change. From this pressure change the diameter and angle can be determined. The part was set inside the air gage and the value read from the LED column. Initially the heads and tapers were measured with a coordinate measuring machine (CMM) in order to compare to the air gage measurements. For each measurement 50 points were taken around the circumference of each part. These points were taken at three locations along the taper. The diameter and angles measured were similar for the 27 heads and tapers measured. In fact the air gage had a better accuracy than the CMM. The roundness error was the only value that the CMM could measure that the air gage could not. The roundness error of the tapers was usually less than 0.0005" and the heads were usually less than 0.0003". This was determined to be small enough that the parts were made very well and that the CMM did not need to be used. The CMM measurements took a much longer time to perform. Therefore, the air gage was used for the remainder of the diameter and angle measurements conducted.

CHAPTER III

Procedures

Cleaning of Testing Parts

Before any testing, all of the heads and tapers were thoroughly cleaned and, while conducting testing, great effort was taken to keep the parts clean. While handling parts, gloves without powder were worn. This prevented the parts from being contaminated by physical contact or by glove powder. The procedure for cleaning the parts is listed below. This kind of cleaning has been conducted previously at Richards and has proven to be effective (31).

1. All heads, tapers, and tubing were wiped off with a clean cloth.
2. All glass and plastic containers used in cleaning was ultrasonically cleaned in Micro* and then dDI water (double deionized water) for 10 minutes each.
3. The tapers were ultrasonically cleaned with acetone for 10 minutes , micro for 12 minutes, and then dDI water for 12 minutes. The heads and tubing were ultrasonically cleaned in micro for 12 minutes and then dDI water for 12 minutes.
4. The parts were set to dry under a vented hood.
5. During transport and storage the parts were placed in a large plastic container with padding and a lid. The heads were also set into individual plastic containers. This was all used to prevent contamination or damage of the parts.

* Micro - International Products Corp. Cat # 6732

Static Testing

After both measuring and cleaning, the static testing was conducted. There were 6 tests conducted for each of the separate parameters, which resulted in 36 heads and stems being tested for the 6 different parameters. Six parts were tested for each to facilitate some measure of statistical significance of the testing. To fix the stem, it was screwed onto the threaded fixture and the head was placed on the taper as shown in Figure 16. Two marks were made on the head and taper in order to assemble the head on the taper in repeated fashion. The head was always loaded to 30 lb and then the dial gage was set to read the relative displacement between the head and the taper. This 30 lb initial load was applied in order to produce the same starting point for every test. This loading prevented the head from being slightly angled at the start of the static loading. The tests were conducted in an MTS 810 servohydraulic testing machine. The heads were assembled by manually increasing the compressive load with a uniform slow rate at approximately 0.1"/minute. This method of assembling the head and taper were conducted up to a load that will be referred to as the preload because it was the load applied prior to removing the head or further loading. An acetabular cup, which was cemented into a delrin cylinder, was used to apply the compressive load. In vivo the head articulates with and is loaded through the acetabular cup therefore this set up provided similar loading conditions.

The first test involved loading the head onto the taper up to 450 lbs. Next the head was removed using the specially designed fixture that uniformly pulled the head off the taper. The heads were pulled off with a steel box frame fixture that was self-aligning due to a universal joint connected to the fixture as shown in Figure 17. The bottom plate of the four-sided box had a hole that the taper slid through and then two semicircular rings were inserted to fit under the head. The MTS 810 was then set to remove the head at 0.1"/min and the peak pull-off load was recorded. The heads were then placed in a plastic case and

Figure 16. Static and preloading test set up

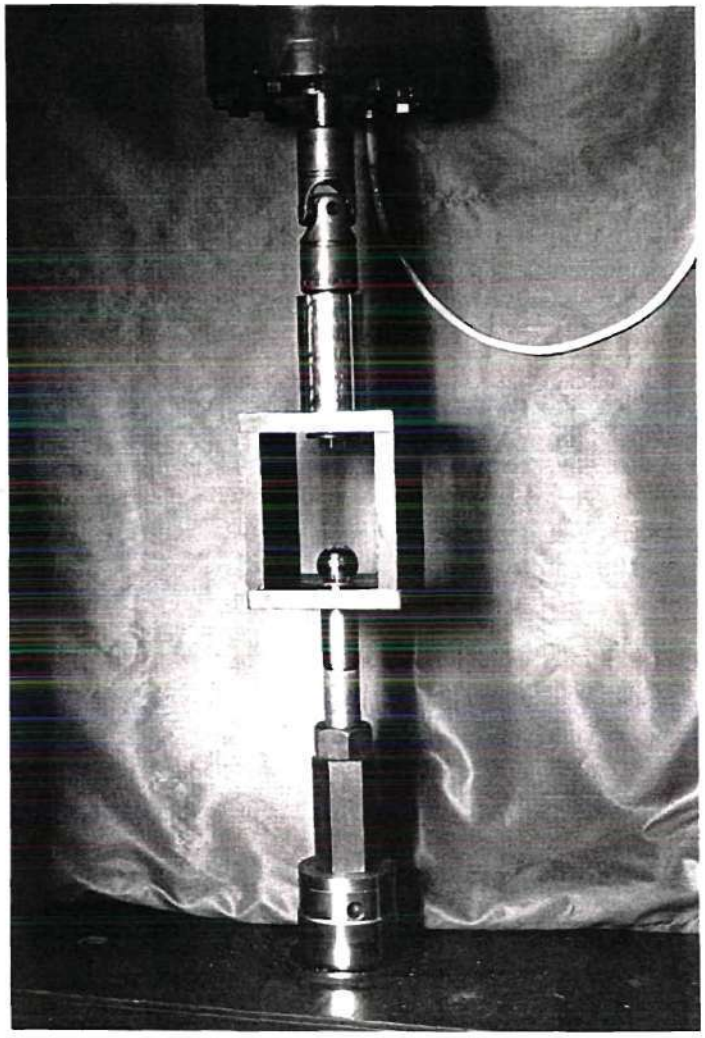

Figure 17. Axial pull-off test set up

put in the plastic box along with the tapers. Care was taken to not damage the parts during handling. The roughness of the head and taper were then measured with the profilometer. The head was then placed back on the same taper in the same position by lining up the marks that had been put on both parts. The head was then loaded to 750 lb, and the same process was repeated. All of the loads include 450, 750, 1100, 1500, 2000, 2500, and 3000 lbs. There were six heads and tapers of each separate design that were tested this way. The load was always increased in order as apposed to a random or decreasing order of loading so that the deformation of the head and taper would always be increasing. If a part had been loaded to 3,000 lbs and then 450 lbs the part would have come off much easier because there would not have been as much plastic deformation on the contact surfaces of the parts. The reason the same parts were reused for the increasing load was due to cost and the validity of conducting the test in this manner (32,33).

In between each load, a profilometer measurement was taken of two out of the six parts for each separate design except the SmProx and Sleeved. These two were only measured before 450 lbs and after 3000 lbs. Before each load the head was placed on the same location on the taper by lining up the marks on each part in order to reduce any variability in how the head and taper were put together. The head was then loaded onto the taper as described above.

Fatigue Testing

Similar to the static testing, all of the parts were cleaned and measured before fatigue testing. During all of the fatigue testing, care was taken to keep all parts clean to prevent contamination. The parts were assembled with an MTS 810 to 450 lbs at approximately 0.10 "/min. with the same procedure as the static loading. The parts were then placed in a plastic storage box and covered to reduce contamination. Before testing, micro was poured over the assembled parts and then dDI water was poured over them in

order to ensure that the parts were clean. The parts were set under a vented hood to dry. After drying, the clean vinyl tubing was slid over the taper bottom as shown in Figures 5 and 18. This tubing was chosen because of its past use and because it does not contaminate the solution. A quick clamp was used to press the tubing up 2/3 of the way on the head. This was done under a vented hood or in a clean room to prevent contamination. Epoxy glue was used to seal the top of the tubing on the head. It was set aside for at least two hours to let the glue dry and then a hose clamp was put on the tubing bottom below the taper region as shown in Figure 18. The top edge of the tubing was filed to prevent the loading disk from hitting the tubing while fatiguing. Anywhere from immediately to several days, the part would wait before Ringers solution was injected. Ringers solution is a salt saline solution . It was chosen because it is similar to body fluids and is used as a standard in industry for fatigue testing. Ringers is also used as an IV solution. This solution promotes corrosion which was a factor investigated in this study. Using a solution also had the benefit of capturing the metal ions and metal particle for analysis.

The Ringers solution was inserted with a new sterile syringe each time. The 3 ml syringe was inserted into the side of the tubing toward the top. Enough solution was inserted to fill the chamber around the taper region, which was approximately three milliliters. The solution was injected just before that part was fatigue-tested. The syringe holes were not sealed to ensure a pressure release when the loading disk pressed on the top edge of the tubing. The part was then set into the fixture with the syringe holes facing upward in order to prevent leakage and then the set screw on the fixture was tightened. The fixture and fatigue set up are shown in Figure 18. The dimple in the loading disk was aligned with the top of the femoral head and then the fixture base was tightened down. The part was loaded for one million cycles from 110 to 1,100 lbs at approximately $\pm$ 10 lbs, and this was conducted at 11 Hz. Note that the assembly preload for the fatigue testing was 450 lbs. After loading, the contaminated Ringers solution was removed with a new sterile syringe and

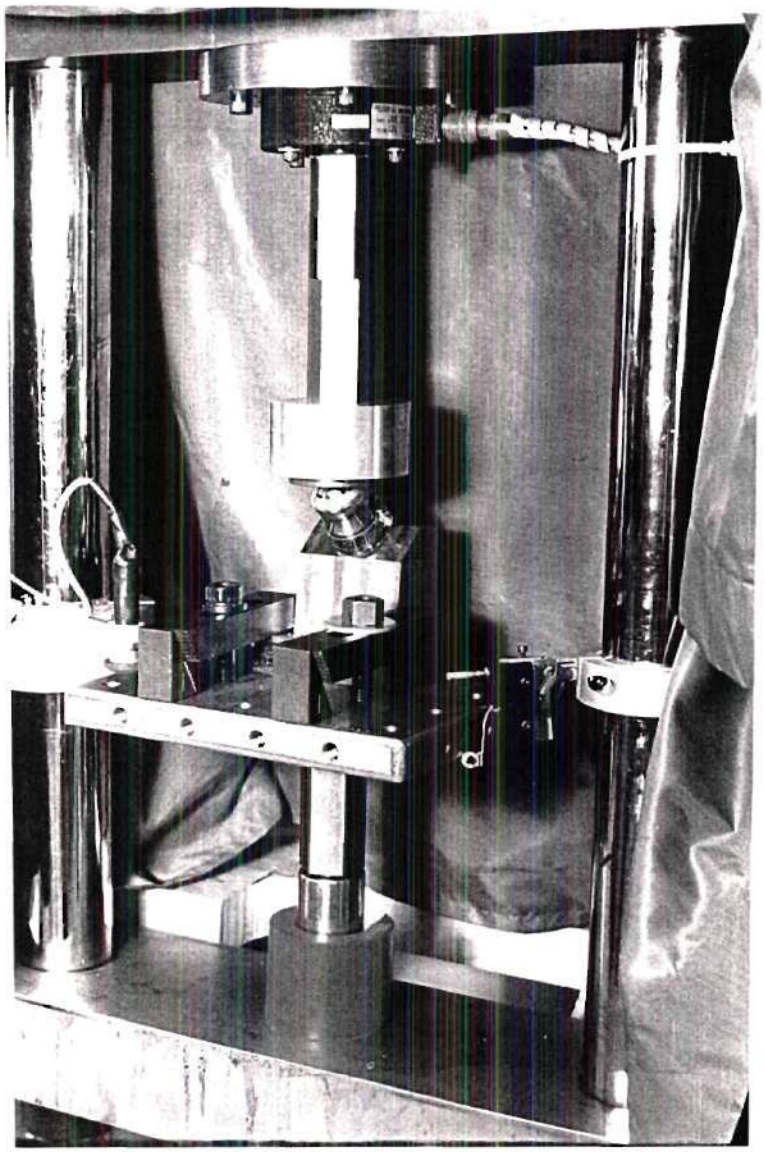

Figure 18. Fatigue testing setup

then inserted into a polyethylene plastic container. The Ringers solution was removed under a vented hood or in a clean room in order to prevent contamination. The container was stored in a refrigerator until it was sent off for metal ion release analysis. The tubing was then cut off with a scalpel and the head was pulled off at 0.1 "/minimum and the load was recorded with the same procedure as discussed earlier for the static testing.

In the fatigue and static testing, six of each different design was tested. This resulted in 42 heads and stems for fatigue testing with seven different parameters. The 1,100 lb fatigue load was chosen as a conservative value of almost seven times an average 160 lb man's weight, which was discussed earlier and which was comparable with testing conducted by others (34, 35, 36 ,37). The loading rate was relatively low compared to other similar testing. A person walks at up to 3 Hz but due to time constraints this was not feasible. The 11 Hz rate was closer than the typical 20 or 30 Hz rate used by many other researchers (34, 35, 36 ,37). Also, the metal ion content should be higher for lower rates so that comparisons could be made easier between designs. One million cycles was chosen because it was felt that it would be long enough to produce metal ions and particles so that comparisons could be made between different designs. Fricker stated that even after 1,000 cycles fretting would be apparent (38). Also Dr. P. Kovacs, Manager of Surface Research for Richards, stated that there would be sufficient metal ion release after 1 million cycles in order to determine a difference between the design parameters (personal communication 6-92). The number of cycles and loading rates resulted in 25.3 hours of testing time per part, which was conducive to changing tests each day. This testing was conducted for a relatively short time period in order to do a large number of tests so that comparisons could be made between many different designs. For longer tests the proportionality of results between designs may differ from the test time chosen, but the trend should be similar. It should be noted that the conditions chosen in the fatigue testing are an approximation of in vivo conditions, but it is very difficult to exactly simulate what occurs in the body. Therefore,

only from clinical trials can true results be obtained.

The angle of the loading was determined from the stem design and the physiological alignment. The neck stem angle on the hip was 49° and with the in vivo angle of 10° adduction, the resultant was 39° loading as shown in Figures 8 and 18. This angle was chosen from the ISO Standard. Dingman and Rohlmann et al showed that the load angle that best represented in vivo stresses and strains was at this 39° (19, 21). To apply the load to the head a delrin disk with a small spherical dimple was used. The loading disk and holding fixture are shown in Figure 19. The delrin was used because it was similar to the acetabular cup material which is UHMWPE. For applying the load it would be ideal to use an acetabular cup but because of the tubing around the head this was not feasible. Instead, a delrin disk with a divot was used to apply a smaller distributed load. The base fixture was made of stainless steel and a set screw was used to hold the taper tight.

Impact Load and Pull-off

The static and fatigue testing that was conducted in this study always involved a compressive static loading of the head onto the taper. This procedure was used in order to have a consistent preload which eliminated a variable. However, the surgical procedure involves striking the femoral head with a surgical mallet three times. This procedure had the potential for a wide range of preloads applied to the head. It would be desired to have a known and high preload instead of leaving it up to the surgeons discretion. This issue of the head assembly procedure was investigated as a secondary variable in this study.

The impact load was measured by striking an impulse hammer and the peak load was recorded on a digital peak meter. Both devices were made by PCB Piezotronics, Inc., with the hammer model 86B20 and meter model 451B. The range of the hammer was 5,000 lbs with a sensitivity of 1 lb. A surgical mallet was used to strike the force hammer and this was an approved method for determining the peak load (39). The surgical mallet

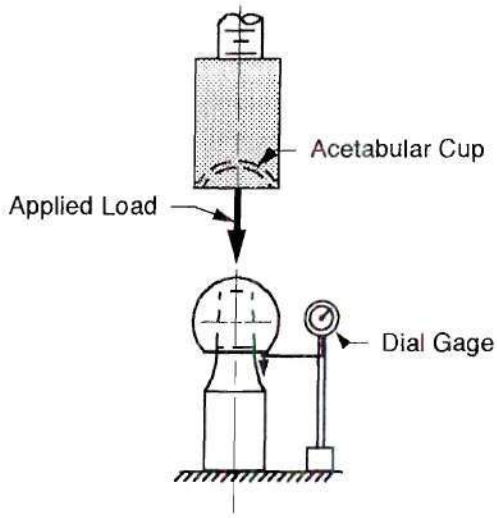

Figure 16. Static and preloading test set up

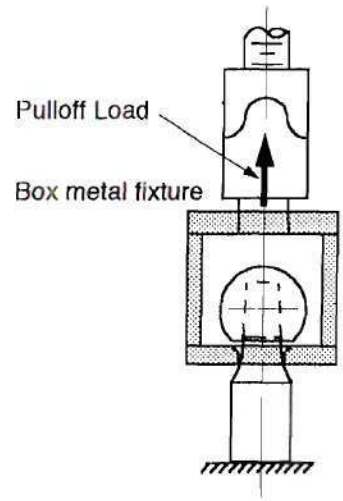

Figure 17. Axial pull-off test set up

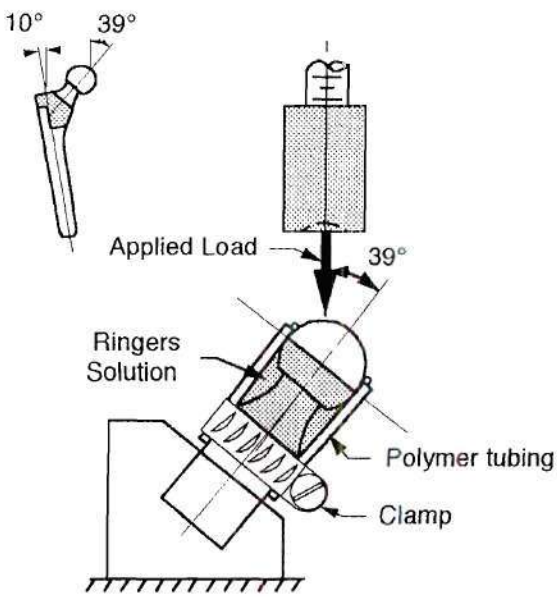

Figure 18. Fatigue testing set up

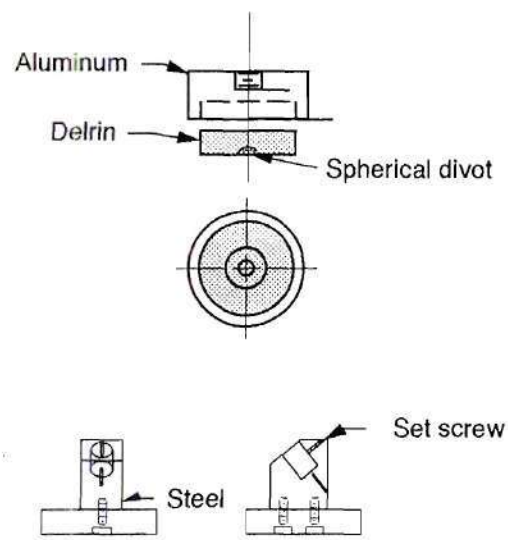

Figure 19. Fatigue loading disk
and Fatigue holding fixture

was securely placed on the counter top and the rubber end was removed so that there was direct contact between the delrin end of the surgical mallet and the steel end of the impulse hammer. The end of the impulse hammer was removed so the strike would not be damped.

Both medium (average) and heavy strikes were tested with approximately 20 strikes of each kind. Since it is desired to have a known load, a controlled impactor was also tested. This was the same impact tool used for the Richards modular hip distal extension. The controlled impactor is spring-loaded; it compresses to a certain point and then releases with a high impact and load click and is shown in Figure 13. This click was the indicator that the impact load had been applied. The impact load of the controlled impactor was tested by holding it against the impulse hammer and compressing it with different techniques. One technique involved striking the controlled impactor with a surgical mallet and the second involved pushing the impactor manually until the impact load was applied. The need for striking the controlled impactor is due to the surgeon's need to assemble the head onto the taper from a distance. There was probably not enough space for the surgeon to push the controlled impactor. However, since the controlled impactor was designed to be pushed, the two techniques of pushing and striking were investigated. In all cases the impulse hammer was securely placed on the counter top and was loaded.

Next, six heads were assembled by striking the controlled impactor and six were assembled by striking with a surgical mallet . The heads were then removed with the same static removal fixture and procedure discussed earlier. The self-aligning box frame was used and the heads were pulled off at 0.1"/minute . The impact loads and pull-off loads were then compared to the previous static testing.

Metal Ion Release

After the fatigue testing, the solution was removed with a syringe and later analyzed for metal ion content. The amount of metal ion release was probably the most important part of this research. Metal particles escaping into the body may contribute to osteolysis and are a particular concern with modular prostheses. Measuring the metal ion release is one of the best ways to predict the amount of metal particulate which could potentially contaminate the peri-prosthetic tissues. It is desirable to have as little particulate debris as possible.

Kovacs et al have shown a direct correlation between metal ion concentration and fretting wear (particulate) volume (40). They stated that the use of metal ion concentration measurements for basic research were valuable and strongly recommended. Analyzing the metal ion release results showed the potential contaminants of metal ions and wear debris that could get into the body.

The contaminated Ringers solutions were sent to Teledyne Wah Chang for analysis of the solutions for metal ions. The analysis was done by inductively couple plasma source mass spectrometry or ICP/MS. The following is a description about the technique of ICP/MS provided by Teledyne.

The specimen was taken into solution, diluted, and aspirated into a horizontally mounted inductively coupled plasma. The resulting atomic ions were introduced into a quadruple mass spectrometer. The ions were detected by a multiplier with real time data acquisition performed by a high speed multi-channel analyzer. An integrated, PC-based data system, provided both instrument control and data reduction/calibration.

Fatigue Solution Filtering

Along with the metal ion analysis, some solutions were analyzed for particle counts. For each fatigue parameter two solutions were filtered. A 25 mm 0.2 micron polycarbonate double membrane filter was used in filtering the contaminated Ringers. A polycarbonate filter was used because its smooth texture and proper pore size made it easy to view particles when using the SEM. The filtering procedure is described below. The glass cylinders, beakers and the filter apparatus were ultrasonically cleaned in Micro and then dDI water for 10 minutes each. The filter apparatus and glassware were then allowed to dry. The filter was placed on the filter apparatus and the top class cylinder was placed on the filter and a glass dish was placed on top to prevent dust from accumulating on the filter. Fifty ml of dDI water was poured over the filter. The contaminated Ringers was shaken and then poured into the water. This helped to distribute the particles over the filter. The glass dish was placed on top again and a vacuum was applied. The vacuum was necessary to pull the solution through the filter because of the filter's extremely small pore size. The solution was pulled through the filter into a glass beaker. Another 50 ml of dDI water was poured into the plastic container and shaken to clean out the plastic container and this dDI water was poured onto the filter. The vacuum was continued for 10 minutes after all of the solution visually appeared to be filtered. This ensured that all of the solution had been filtered and aided in drying the filter. The solution was then poured into a new plastic container and stored in the a refrigerator and the filter was placed on a filter pad and put in a plastic dish with the lid off. This plastic dish was placed in a glass petri dish and the top of the petri dish was placed on them to prevent contamination. They were then set aside to let the filter dry. After drying, the plastic lid was then placed on the filter and it was set aside to be viewed by the SEM.

SEM

The filters were analyzed on the SEM by J. Varnavas, a Research Technician for Richards. The filter was gold-sputtered and secured to a block for SEM viewing. Each filter was then viewed to determine the size, kind, and number of particles. The SEM can be used to analysis the number of particles on the filters. The filters were analyzed by using the feature scan image analysis software on the Link microanalysis computer, which found the particles by their chemical content and counted them.

The SEM was also used to view the specimen surfaces and pictures were taken after fatiguing. A Hitachi S-800 SEM at Georgia Institute of Technology was used. The pictures were taken at 350 X and used to compare the distal and proximal ends of the tapers.

Finite Element Analysis

Along with this mechanical testing and analysis, the mechanical performance of the head/taper connection was studied by using Finite Element Analysis (FEA). The IDES software package was used to construct the model and ANSYS was used to solve it. The material properties for Ti and Co-Cr were listed earlier and the same values were used again in the FEA model. Ti had an elastic modulus of 16.5×10^3 ksi and a poisson's ratio of 0.35 and Co-Cr had an elastic modulus of 31×10^3 ksi and a poisson's ratio of 0.30 (12,13). The material was assumed to be linear elastic and homogeneous. The ANSYS element used was Stif 42 for the taper and head elements and Stif 12 for the gap elements. Stif 42 is a 2-D four node isoparametric solid element. It is designed as a biaxial plane element or as an axisymmetric element (41). The element is defined by four nodal points having two degrees of freedom at each node with translations in the nodal x and y directions. Stif 12 is a 2-D interface element, and it can support compressive loads in the normal direction to the surface

and shear in the tangential direction (41).

The same head design was used in each model. The angle mismatch was investigated by changing the angle of the taper. The taper angles included conforming with 0° mismatch, proximal contact with 11° mismatch, and distal contact with -11° mismatch. The relative head/taper displacement was compared to the experimental relative displacement. The stress in the head and in the taper was investigated in order to better understand the taper lock mechanism.

Both frictionless and friction models were analyzed. The friction model was primarily investigated because it was more representative of the true conditions. Also, in the model the material properties for the head and stem were the same as the parts experimentally tested. A 2-D model with axisymmetric finite elements was used to create the model of the head and taper and gap elements were used to create the interface between the head and taper as shown in Figure 20. Visually the model consisted of half of a taper and half of a head. With the axisymmetric element this surface was revolved 360°, essentially creating a solid head and taper.

A distributed load was applied to the top of the head. The loading of a femoral head by an acetabular cup was determined by M. Harbaugh, Senior Research Engineer for Richards and this was made into a load curve. This loading was equivalent to a pressure distribution of 1,125 lbs. This curve was used to determine the amount of load required for each element across the top of the femoral head. The width of each element was determined and the distance to the center of each element was measured. These two values were used to determine the load for each head element. A uniform load was applied normal to each element that required a load. Results are shown in Figure 21. The base of the taper was fixed and all other elements were free to displace as shown in Figure 22.

The gap elements were defined with an angle and a stiffness. The angle used was the half of the average between the head and taper angles , which was 2.85^o. The stiffness was

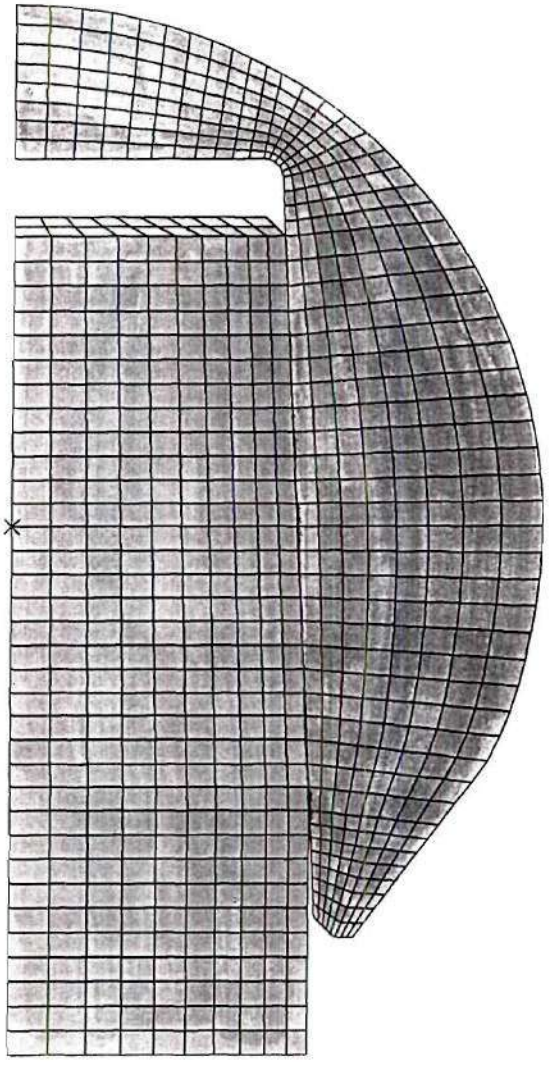

Figure 20. Finite Element Model head and taper

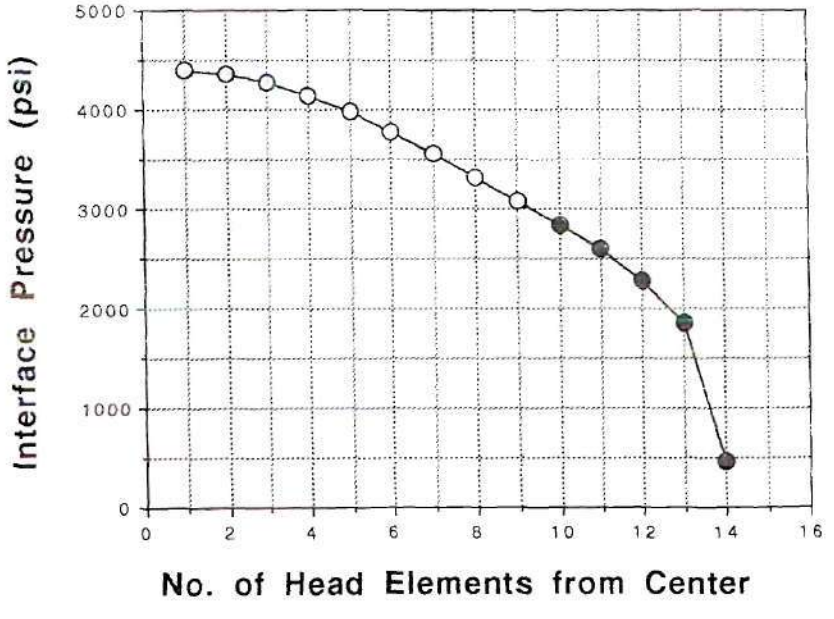

Figure 21. FEA head pressure distribution curve

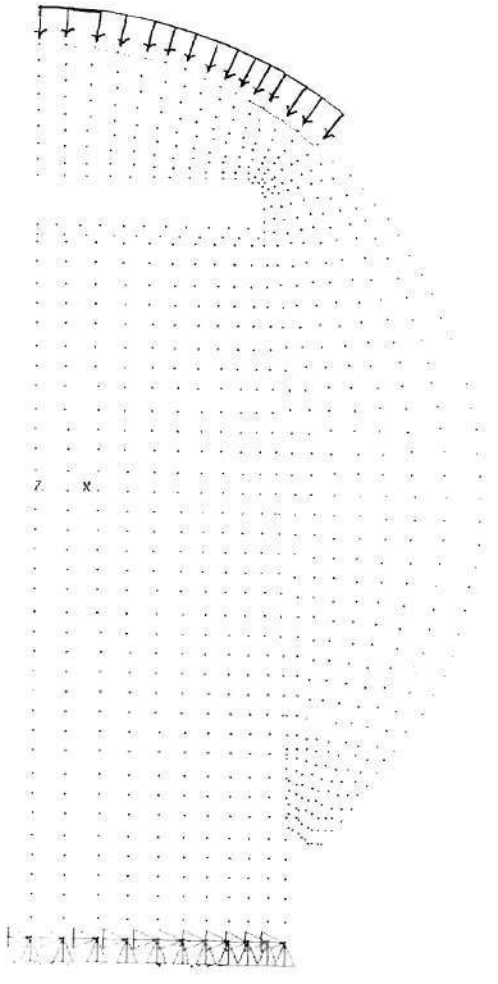

Figure 22. FEA nodes with head pressure distribution and taper fixation

determined by investigation of the element stiffness (AE / L) of the model without friction and altering that to determine the required stiffness. A test was conducted comparing different stiffness values with the percent change of hoop stress and the displacement. With a higher stiffness the result becomes more accurate but has more difficulty converging. The best stiffness was calculated by multiplying the maximum element stiffness by 1, 10, 100, and 1000 and comparing these results to each other. The stiffness 10 times the maximum element stiffness resulted in a 0.4% change in the hoop stress and displacement. Therefore, the value of 0.17×10^9 lb/in/radian was used for the stiffness.

A coefficient of friction of 0.15 was used. This was determined from Fessler et al from experimentation by determining the friction from the angle, preload, and pull-off load of the heads and tapers (42,43). The number of load steps was also evaluated. With no friction, one load step can be used, but with friction the load must be broken up into many steps. This is because friction is path-dependent. The higher the number of steps the longer it will take to converge, but the more accurate it would be. Five, ten, and fifteen load steps were investigated. Ten load steps were determined to be sufficient and were used in the testing. The different load steps were accomplished by multiplying the calculated distribution load on each element by $\frac{1}{10}$ and $\frac{2}{10}$ and this was increased until $\frac{10}{10}$ was reached. This provided the 10 step increase of the load so that an accurate solution could be reached. The parts of the FEA program that would be of interest are shown in the appendix.

The stresses that were investigated for the different models include the hoop stress, effective stress, maximum and minimum principal stresses. The hoop stress is simply the circumferential stress, which is in the direction coming out of the page. The maximum and minimum principal stresses were calculated, and the equation for effective stress is shown on the next page.

$$\text{Effective} = \sqrt{\frac{3}{2}} \left(\sigma_{ij}' \ \sigma_{ij}' \right)^{\frac{1}{2}}$$

For a check of the FEA model the displacement of the head was measured during static testing and the stresses and strains were measured by adhering strain gages to the side of a head. Rosette strain gages were used and the Proximal and Distal designs were tested. The gage was located on the side of the femoral head as shown in Figure 23. Only one gage was required since the loading was axial and the head and taper were both symmetrical. The heads were loaded on the MTS with the same procedure and loads as the static testing. The stresses were calculated and compared to the FEA results.

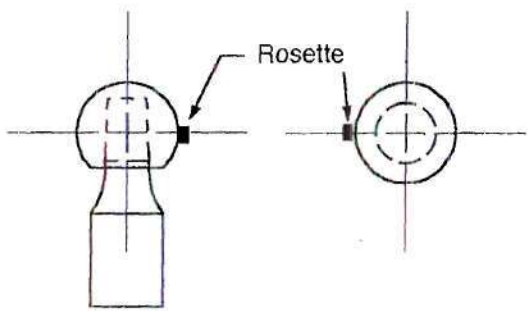

Figure 23. Rosette strain gage location

CHAPTER IV

Results and Discussion

All of the bar graphs show one standard deviation of error. The calculations of statistical significance is shown in the appendix. A t distribution was used to approximate the statistical distribution of the case comparing two average values with different variances. The analysis was conducted for 95% significance, therefore $\alpha = 0.05$

Finite Element Analysis Results

Figure 20 shows the FEA model of the head and taper. Table 4 shows all of the FEA results of the different models and loadings tested. For each analysis the maximum and minimum stresses were recorded. All of the FEA figures shown are for the 1,125 lb loading case. For all of the designs the stresses were below the ultimate of Ti and Co-Cr which are 125 Ksi and 170 Ksi respectively. Even up to loads of 3,000 lbs, the stresses did not come close to the ultimate strength for the materials used.

The results of the proximal contact model with a friction of 0.15 are shown in Figure 24 with the hoop stress, effective stress, maximum principal and minimum principal stresses shown respectively. The hoop stress in the head was mostly tensile with a maximum of 22,747 psi at the inside of the head vertically about the taper. This was because of the expansion of the head on the taper due to the proximal contact. The displacement was 0.00892" which was similar to the displacement measured experimentally. The largest compressing hoop stress was -36,836 psi and was located at the outside top of the head and

Table 4. Finite Element Analysis Results

	Load	Relative Displacement (in)	Hoop stress Min (psi)	Hoop stress Max (psi)	Effective Stress Min (psi)	Effective Stress Max (psi)	Max Principle Min (psi)	Max Principle Max (psi)	Min Principle Min (psi)	Min Principle Max (psi)
Proximal frictionless	1,125.0	0.019855	-73,105	37,771	-	-	-13,899	38,133	-107,731	979
with friction	112.5	0.003174	-19,959	5,665	140	23,444	-4,517	6,123	-31,480	174
	675.0	0.007464	-33,264	16,366	228	39,352	-10,050	16,366	-49,215	459
	1,125.0	0.008919	-36,836	22,747	264	47,135	-10,906	22,747	-54,947	581
1 cycle	675.0	0.008743	-37,467	18,155	175	45,016	-10,900	18,196	-55,319	473
1cycle	112.5	0.008510	-38,120	16,116	150	42,310	-10,562	19,884	-55,371	1148
Distal Frictionless	1,125.0	0.020056	-55,565	54,455	-	-	-28,535	54,455	-109,527	710
With friction	300.0	0.006449	-22,757	15,788	30	40,618	-12,837	15,788	-45,964	781
	675.0	-	-25,336	16,991	49	41,784	16,706	16,991	-46,609	495
	1,125.0	0.009764	-33,384	25,570	104	57,198	-21,714	25,570	-60,603	652
	3,000.0	0.018106	-54,966	48,878	272	100,850	-36,084	48,878	-100,562	575
Conforming with friction	112.5	0.000054	-3,409	2,449	16.1	5016	-1,327	2,449	-4,924	37

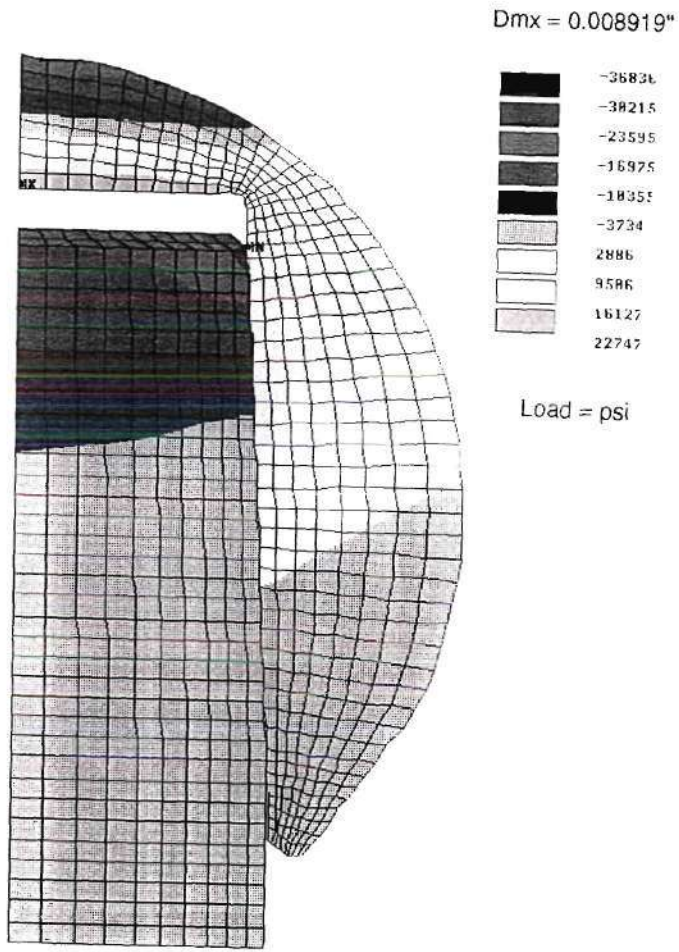

24.a Hoop stress

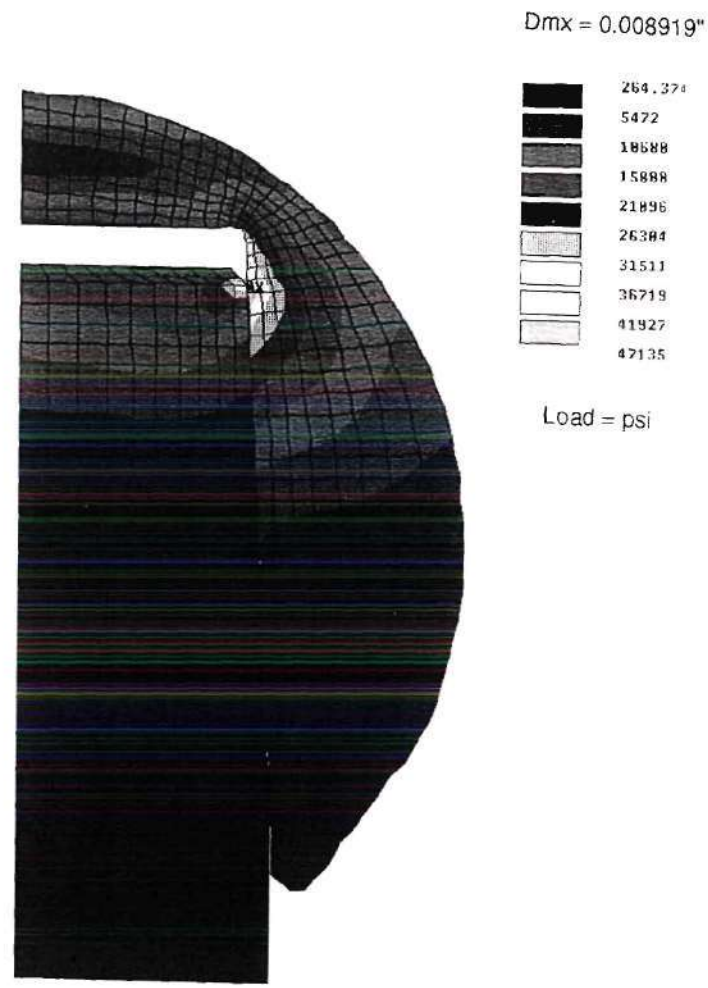

24.b Effective stress

Figure 24. FEA Proximal design with friction
(a. Hoop stress, b. Effective stress, c. Max principal stress, d. Min principal stress)

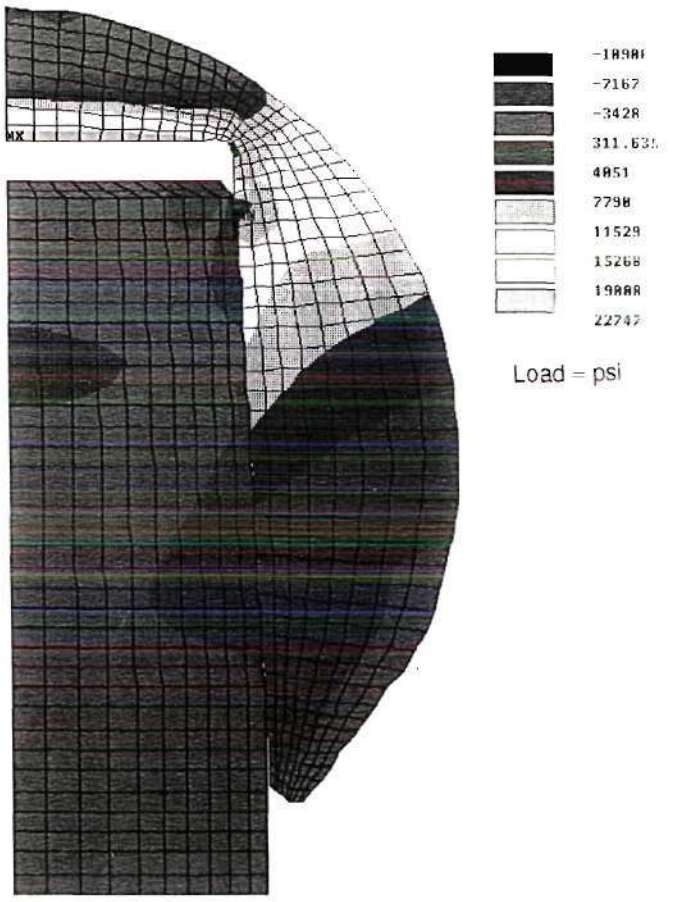

24.c Maximum principal

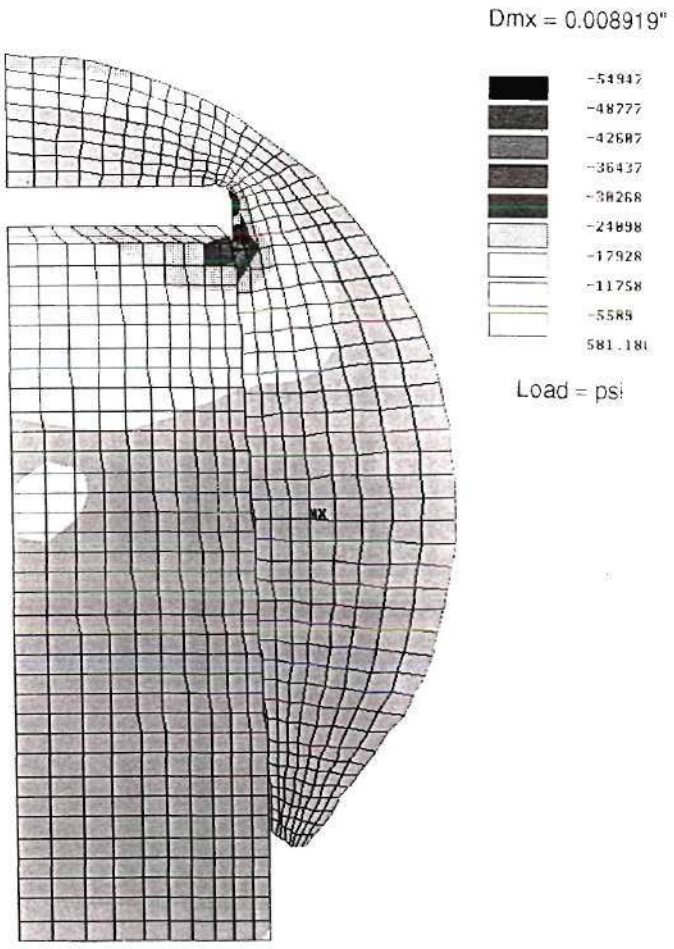

24.d Minimum principal

Figure 24. FEA Proximal design with friction
(a. Hoop stress, b. Effective stress, c. Max principal stress, d. Min principal stress)

at the top contacting region of the taper. Figure 24.b shows the effective stress and the maximum occurred at the initial contact point with a value of 47,135 psi. The maximum and minimum principal stresses are shown in Figures 24.c and 24.d. The largest tensile maximum principal was the same as the maximum tensile hoop stress with a value of 22,747 psi. The largest compressive maximum principal was -10,908 psi and was located at the contact region on the taper and at the outside top of the head.

These values along with the hoop stress would be expected because of the expansion and bending of the head due to the proximal contact region. The most compressive minimum principal stress for both the head and taper was at the proximal contact point with a value of 54,947 psi.

The frictionless model for the proximal contact design had higher tensile and compressive stresses and are shown in Figures 25 and 26 and Table 4. This would be expected because the displacement was much greater with a value of 0.0198". This caused the head to expand more and the taper to compress more. The maximum tensile hoop stress and maximum principal stress was located along the inside area of the head as shown in figure 25 with a value of approximately 38,000 psi. This agrees with the thick wall vessel theory. Figure 27 shows the displacement in the x direction. As expected the taper was compressed with a maximum at the contact point of 0.522×10^{-3}". The head had a maximum expansion movement at the contact region with a value of 0.523×10^{-3}".

The distal contact design without friction is shown in Figure 26 . The relative head displacement was similar to the Proximal design with a value of 0.200". The maximum hoop stress in tension was 54,455 psi and located at the distal contact region of the head. The maximum compressive hoop was located at the distal contact region of the taper.

Again for the Distal contact design, a friction of 0.15 was used and all of the figures shown were for 1,125 lbs loading conditions. The displacement of 0.00976" was slightly greater than the Proximal design as shown in Figure 28. As expected the maximum and

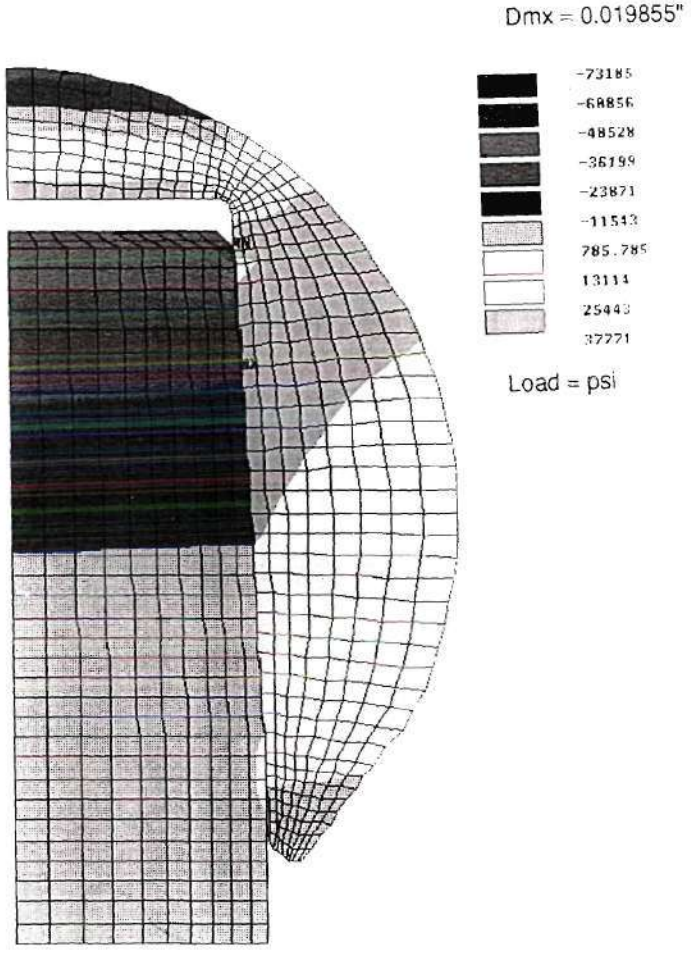

Figure 25. FEA Proximal design, frictionless (Hoop stress)

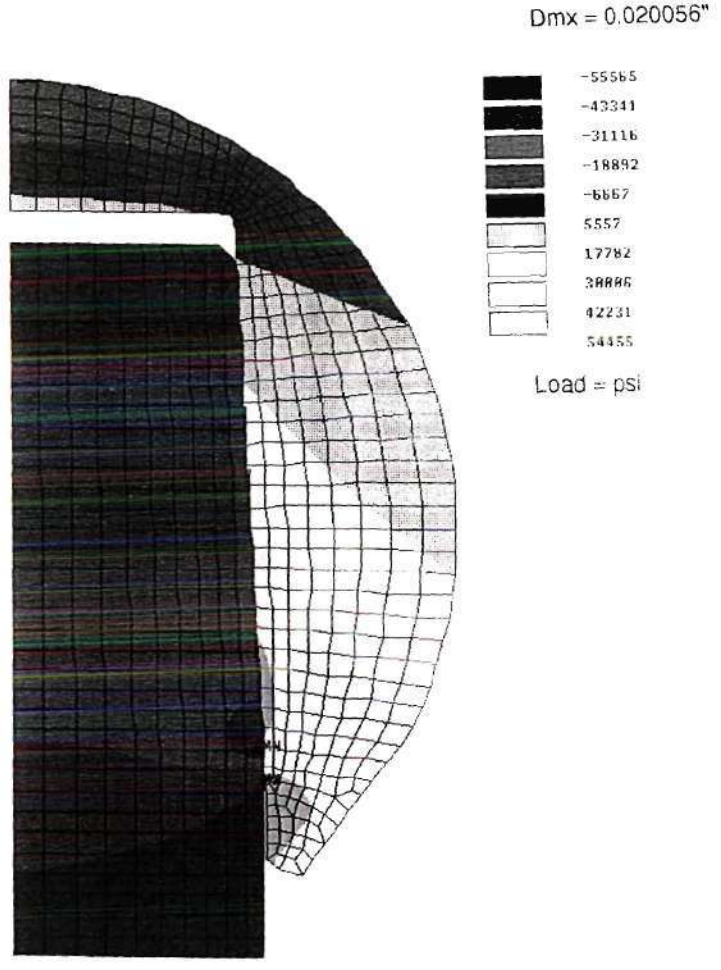

Figure 26. FEA Distal design, frictionless (Hoop stress)

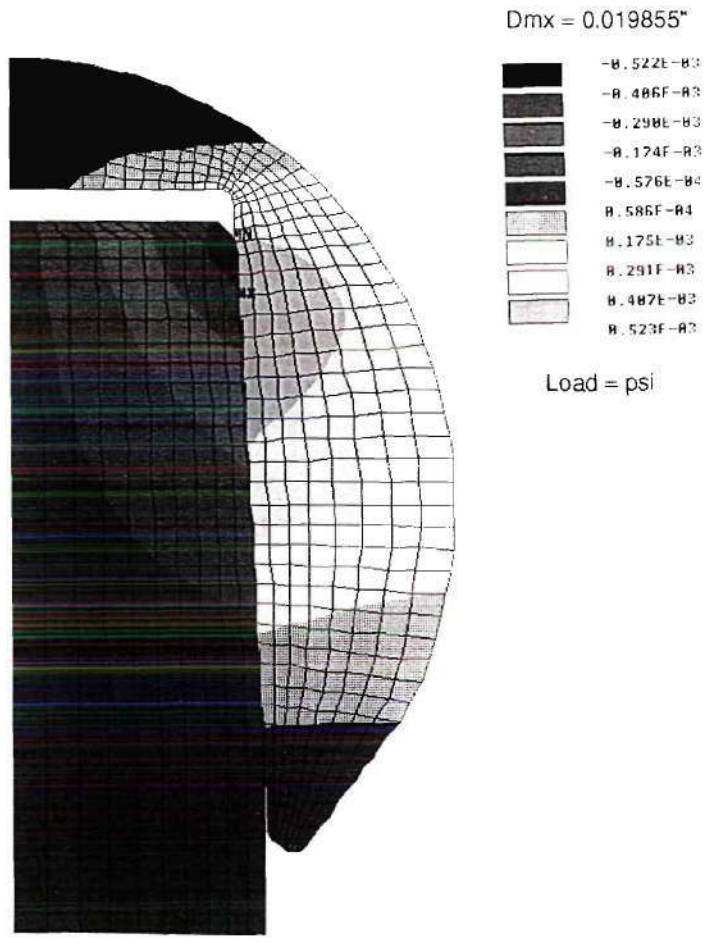

Figure 27. FEA Proximal design with friction
Displacement in the x direction

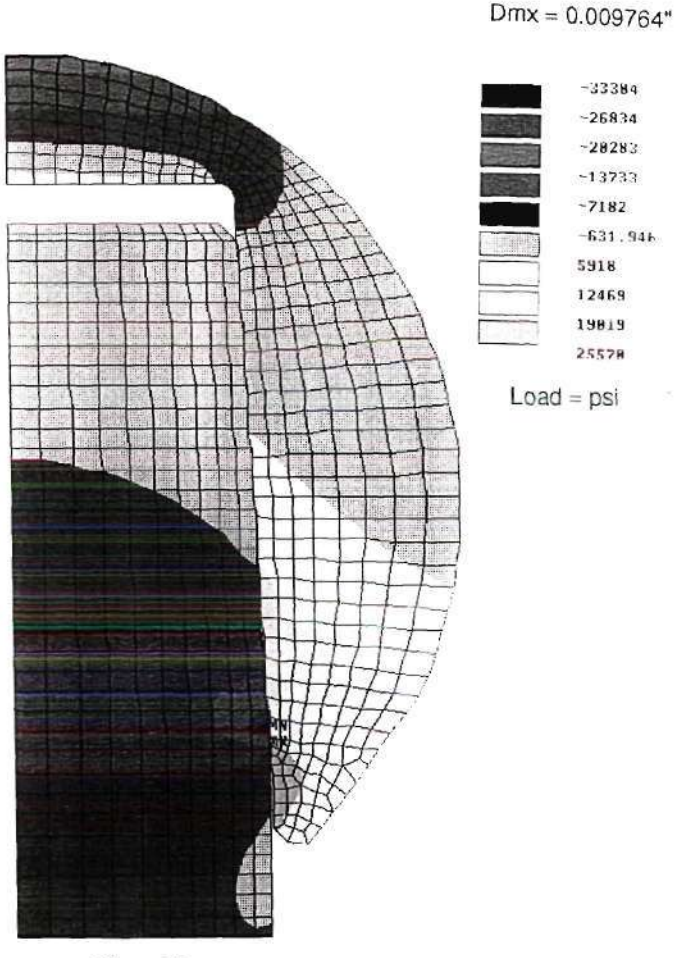

28.a Hoop stress

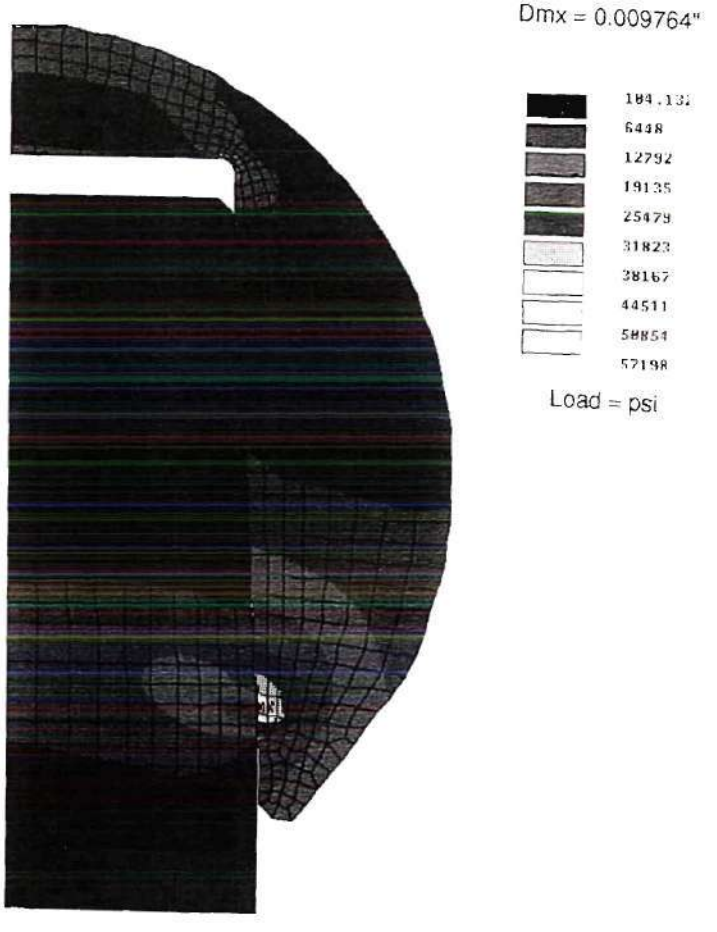

28.b Effective stress

Figure 28. FEA Distal design with friction
(a. Hoop stress, b. Effective stress, c. Max principal stress, d. Min principal stress)

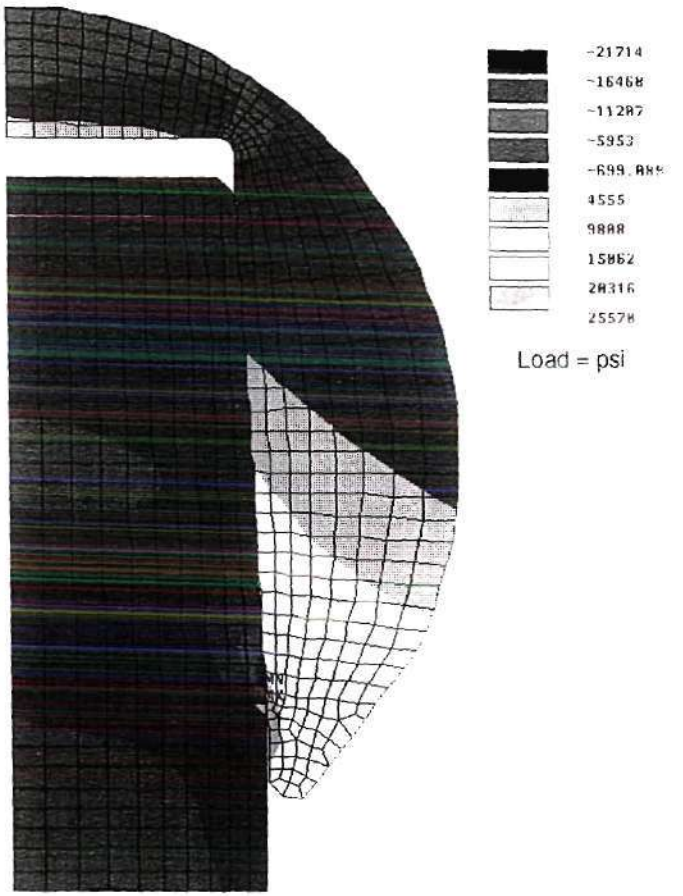

28.c Maximum principal

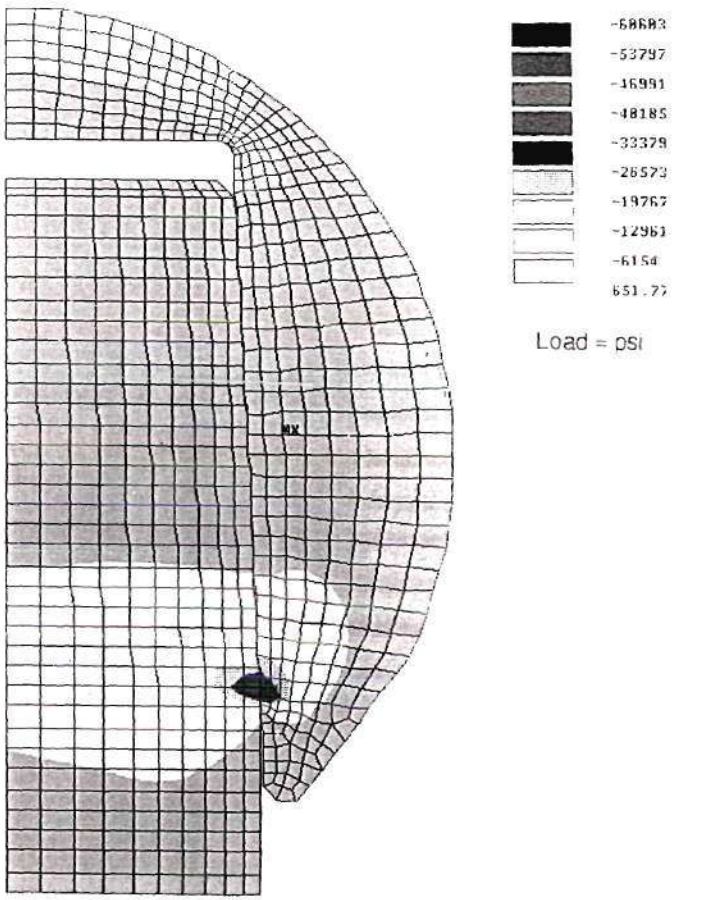

28.d Minimum principal

Figure 28. FEA Distal design with friction
(a. Hoop stress, b. Effective stress, c. Max principal stress, d. Min principal stress)

minimum hoop stresses and principal stresses were located at the contact region with the head being in tension and the taper being in compression. The maximum tension in the head had a value of 25,578 psi and the maximum compression in the taper was -21,714 psi for principal stress and -33,308 psi for hoop stress. The effective stress shown in Figure 28.b. The maximum stress value was in the head at the contact point with a value of 57,198 psi. The minimum principal showed a compressive value of -60,603 psi in the head and taper at the contact point.

Strain gaging was done with the proximal contact and distal contact designs. The results are shown in Table 5. The strain gages were adhered to the sides of the femoral head and the results of the strain gage and FEA model were similar.

The conforming design was only loaded to 112.5 lbs. The load was distributed over a larger region and therefore the stresses were reduced as shown in Figure 29 and the displacement was less than the Proximal and Distal designs. The displacement was 0.54×10^{-4}" and for the Proximal design it was 31.7×10^{-4}". The maximum tensile hoop stress and maximum principal stress was 2,449 psi and it was distributed over a large part of the inside surface of the head. The maximum compressive hoop and maximum principal were at the proximal contact part on the taper with a value of -3,409 hoop and -1,327 psi principal.

The effective stress in Figure 29.b shows the maximum of 5,016 psi in the head at the contact proximal point. The minimum principal stress shows a compression of -4,924 psi in the head and taper at the proximal contact point. Because of the conformity, all of the stresses were much lower than compared to the other designs. However, this would not be a design that could be manufactured practically. From all of the FEA analyses, the displacements were similar to the experimental displacements and the stresses were much lower than the yield and ultimate values of the materials.

M. Harbaugh analyzed a similar 2-D FEA model of a head and taper connection. He had similar displacements and stress results for all of the different angles and loads analyzed (43).

Table 5. Strain Gage Results

Proximal	0 load	450 lb	750 lb	1100 lb	1500 lb	2000 lb	2500 lb	3000 lb
Max principal stress (psi)	-120		-400	340	1590	3300	5180	6900
Min principal stress	-220		-1460	-1010	-320	390	970	1250
Shear stress	50		530	670	950	1450	2110	2820
Max principal strain (ue)	-2		1	21	54	103	158	210
Min principal strain	-6		-43	-36	-26	-19	-19	-26
Shear strain	4		-57	-70	-81	122	177	237
Distal	**0 load**	**450 lb**	**750 lb**	**1100 lb**	**1500 lb**	**2000 lb**	**2500 lb**	**3000 lb**
Max principal stress (psi)	460	1360	2180	3330	4910	6590	7920	9880
Min principal stress	-120	-90	-50	100	770	540	270	1540
Shear stress	290	720	1110	1620	2070	3020	3820	4170
Max principal strain (ue)	16	45	71	107	151	207	253	304
Min principal strain	-8	-16	-23	-29	-23	-46	-68	-46
Shear strain	24	61	94	136	174	254	321	350

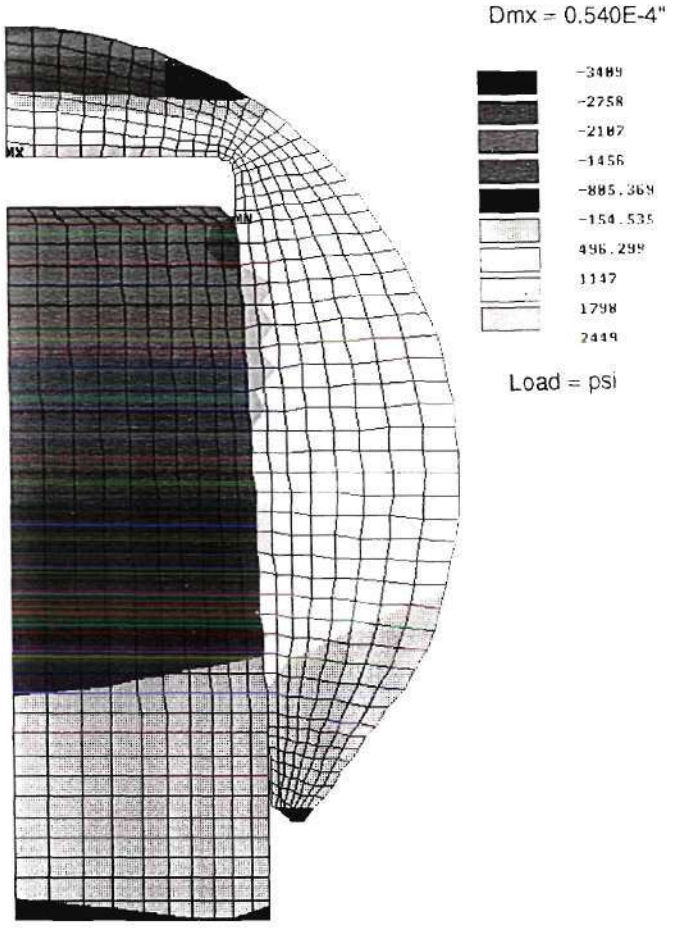

29.a Hoop stress

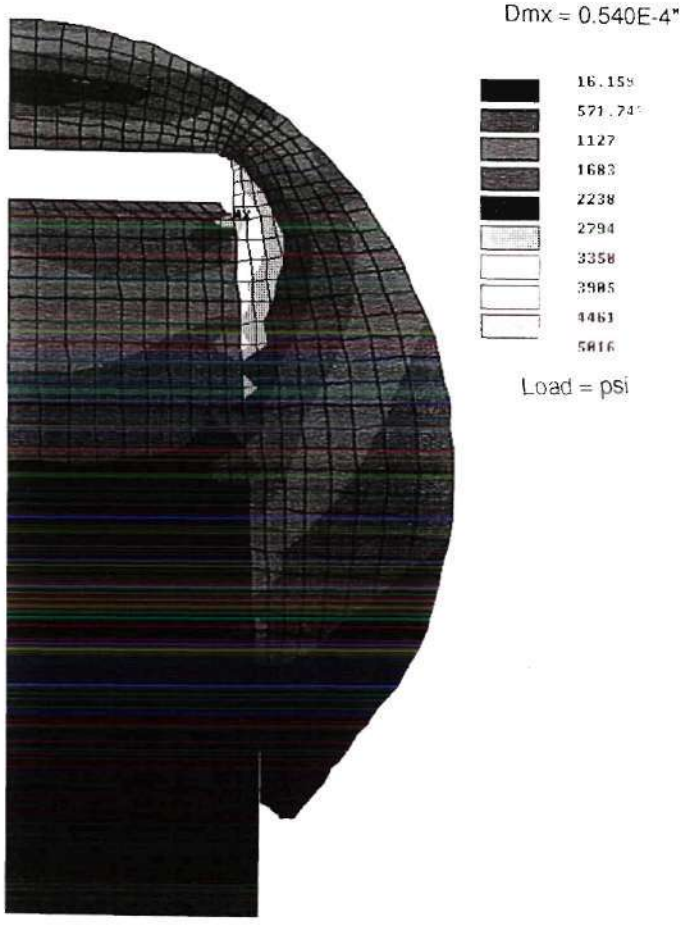

29.b Effective stress

Figure 29. FEA Conforming design with friction
(a. Hoop stress b. Effective stress c. Max principal stress d. Min principal stress)

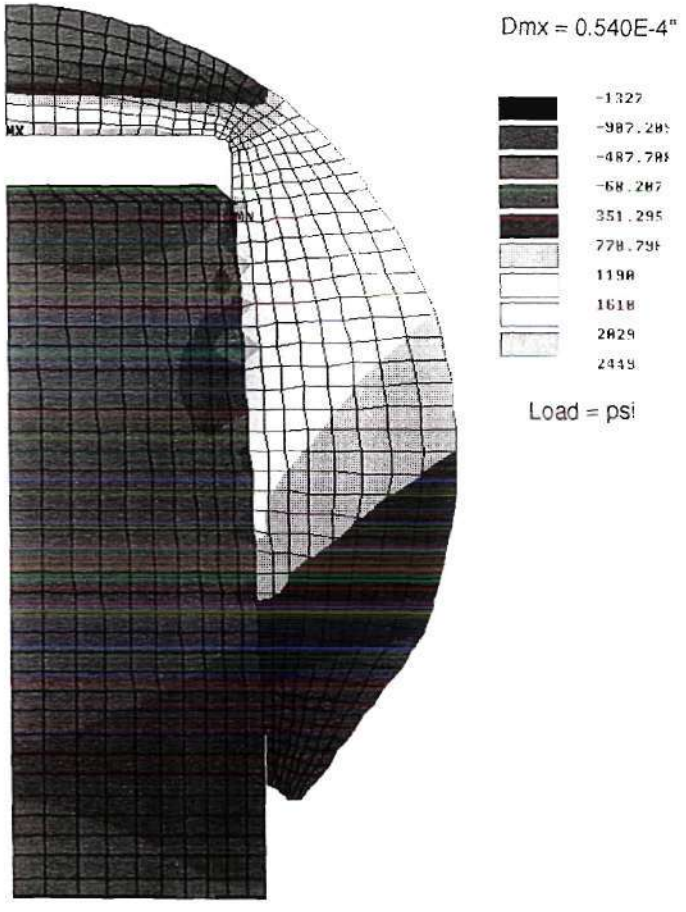

29.c Maximum principal

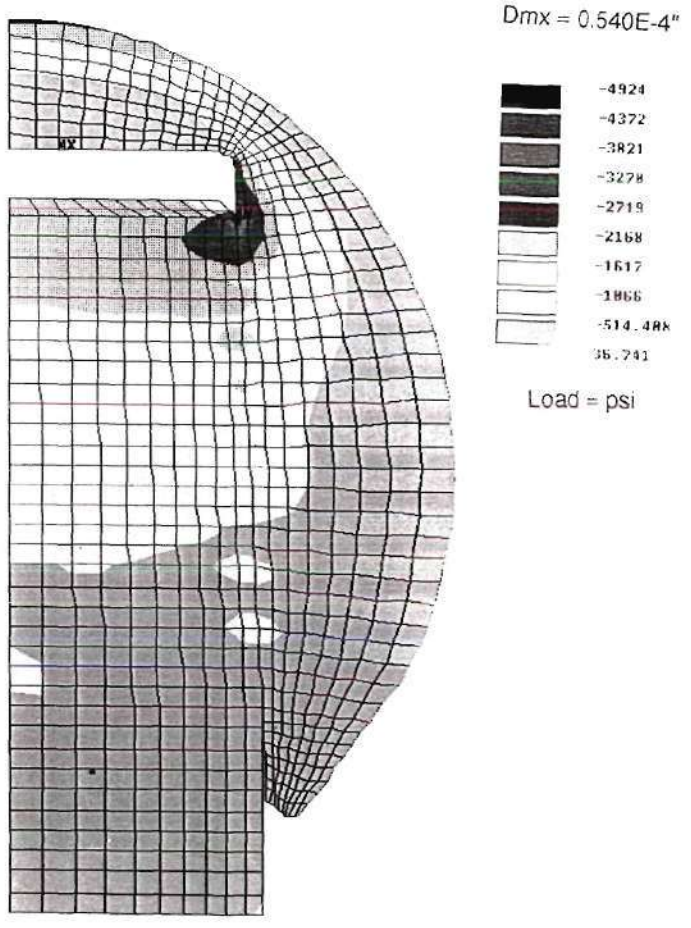

29.d Minimum principal

Figure 29. FEA Conforming design with friction
(a. Hoop stress b. Effective stress c. Max principal stress d. Min principal stress)

Angle Mismatch

Along with the FEA model, experimental tests were conducted. Before testing, all of the parts were measured for diameter angle and roughness. The diameter and angle of the heads and tapers were measured with an air gage as described earlier. For each different test parameter the diameter and angle were well within the study's design tolerances. The diameter and angle for both the heads and tapers is shown in Table 6. The angle mismatch was determined for each separate head/taper combination from the air gage results. The angle mismatch between the head and taper for each test parameter was averaged and is shown in Figure 30.a. The average was determined from the twelve head/taper combinations that were used for the static and fatigue testing. As expected, the SmProx was the only angle mismatch that was significantly different from the other parameters with a value of 25 min ($p<.05$). Figure 30.b shows an expanded view of the other five parameters. For this study the expected angle mismatch was $\beta + \lambda$ minutes. As shown the average mismatch values fell on both sides of the expected value from 4.6 min for the Distal to 7.2 min for the Sleeve. Also, the Proximal deviations were small with a maximum of 0.83 min for the "Rough" which showed that the parts were manufactured consistently. Only the angle was evaluated and not the diameter because the two parts would have to come in contact where the diameters were equal. However, the diameter and angle were both measured to make sure that they were the correct size.

Also within one design parameter there was no correlation found between the mismatch amount and the pull-off loads after static testing, pull-off loads after fatigue testing, or metal ion release. The small changes in angle mismatch for one design was so small that no consistent trends could be found relating the larger mismatches and lower pull-off loads. The mismatch was not large enough to see a difference in performance. However differences were found between the Sm Prox design and the Proximal design showing that large mismatch differences do affect the taper lock performance.

Table 6. Diameter, Angle, and Angle Mismatch

No.	Stem Diam	Stem angle	Head Diam	Head Angle	Ang mismatch
POLISHED					
1	0.5641	40.75	0.5643	46	5.25
2	0.5642	42.50	0.5640	46	3.5
3	0.5632	42.50	0.5638	46.5	4
4	0.5633	41.00	0.5639	46.5	5.5
5	0.5638	39.00	0.5639	46.5	7.5
6	0.5641	42.00	0.5640	46.5	4.5
7	0.5632	42.60	0.5637	47	4.4
8	0.5640	42.60	0.5636	48	5.4
9	0.5642	42.50	0.5638	46	3.5
10	0.5637	41.00	0.5642	46	5
11	0.5638	42.60	0.5639	46.5	3.9
12	0.5637	40.50	0.5640	45.25	4.75
Ave	0.5638	41.6292	0.5639	46.3958	4.7667
StDev	0.0004	1.17	0.0002	0.6696	1.1058
ROUGH					
13	0.5645	40.00	0.5637	46.5	6.5
14	0.5639	40.00	0.5641	46	6
15	0.5648	39.50	0.5639	46.5	7
16	0.5648	40.00	0.5635	46.5	6.5
17	0.5640	40.50	0.5641	46	5.5
18	0.5648	40.00	0.5641	46.5	6.5
19	0.5643	40.75	0.5643	45.5	4.75
20	0.5642	41.00	0.5639	46.5	5.5
21	0.5639	41.00	0.5640	48.25	7.25
22	0.5641	41.50	0.5635	47	5.5
23	0.5644	41.00	0.5638	48	7
24	0.5643	41.00	0.5642	46	5
25	0.5645	40.00			
26	0.5642	40.00			
27	0.5646	41.00			
Ave	0.5643	40.48	0.5639	46.604167	6.083333333
StDev	0.0003	0.59	0.0003	0.8080	0.8280
Proximal					
30	0.5641	40.50	0.5642	46.25	5.75
31	0.5643	40.00	0.5641	46.75	6.75
32	0.5639	40.75	0.5641	47.5	6.75
33	0.5643	40.00	0.5642	46.25	6.25
34	0.5647	40.50	0.5641	46.75	6.25
35	0.5641	40.50	0.5643	46.5	6
36	0.5642	40.50	0.5639	46	5.5
37	0.5641	40.25	0.5640	46	5.75
38	0.5642	40.50	0.5639	46.5	6
39	0.5642	40.50	0.5639	46.5	6
40	0.5642	40.00	0.5639	46.5	6.5
41	0.5642	40.00	0.5641	46	6
42	0.5645	40.00	0.5639	46.75	6.75
43	0.5643	40.50	0.5637	46.5	6
44	0.5643	40.50	0.5641	46.5	6
48	0.5645	40.25	0.5640	46.5	6.25
Ave	0.5642	40.3281	0.5640	46.484375	6.15625
StDev	0.0002	0.25	0.0001	0.3705	0.3750

Table 6. Diameter, Angle, and Angle Mismatch (continued)

No.	Stem Diam	Stem angle	Head Diam	Head Angle	Sleeve Diam	Sleeve Angle	Ang mismatch
SLEEVE							
70	0.564	39.75	0.5642	46	0.56	38.5	7.5
71	0.5642	40	0.5641	46	0.56	39	7
72	0.56425	40.5	0.5640	46.5	0.56	39.5	7
73	0.5641	40	0.5642	46.5	0.56	39	7.5
74	0.5642	40	0.5642	46.5	0.56	40	6.5
76	0.5643	40.75	0.5641	47.5	0.56	39.5	8
77	0.56425	40.5	0.5643	46.5	0.56	38.75	7.75
78	0.56455	40	0.5642	47	0.56	39	8
79	0.5645	39.5	0.5640	46.25	0.56	40	6.25
80	0.5645	39.5	0.5642	47.5	0.56	40	7.5
81	0.5645	39	0.5642	46.75	0.56	40.5	6.25
88	0.56445	40					
89	0.56415	40					
Ave	0.5643	39.9615	0.5641	46.6364	0.56	39.4318	7.2045
StDev	0.0002	0.4660	0.0001	0.5168	0.0002	0.6334	0.6502
H PRELOAD					Ang mismatch		
90	0.5646	40.5	0.5642	46.25	5.75		
91	0.5646	40.25	0.5640	46.75	6.50		
92	0.5645	40	0.5639	46.5	6.50		
93	0.5643	40.5	0.5640	47	6.50		
94	0.5643	40.5	0.5640	46.25	5.75		
95	0.56425	40.5	0.5639	47.25	6.75		
99	0.5643	40	0.5639	46	6.00		
Ave	0.564407143	40.3214286	0.5640	46.5714286	6.25		
StDev	0.0002	0.2378	0.0001	0.4499	0.41		
SM PROX							
121	0.5645	22.25	0.5640	47	24.75		
122	0.5645	23	0.5640	47.5	24.50		
123	0.56475	21.5	0.5638	47.5	26.00		
124	0.56465	21.5	0.5638	47	25.50		
125	0.5643	22.25	0.5639	47	24.75		
126	0.5643	22	0.5638	47.25	25.25		
127	0.5643	22.25	0.5640	46.75	24.50		
128	0.5642	23	0.5640	47	24.00		
129	0.5642	22.5	0.5638	47.5	25.00		
130	0.5648	21	0.5640	46.75	25.75		
131	0.5645	21.75	0.5638	46.75	25.00		
Ave	0.564454545	22.0909091	0.5639	47.0909091	25.00		
StDev	0.0002	0.6252	0.0001	0.3015	0.59		
DISTAL							
50	0.5634	51.5	0.5640	46.5	-5.00		
51	0.5635	51.5	0.5638	46.5	-5.00		
52	0.5636	51.5	0.5637	47.25	-4.25		
53	0.5635	51.25	0.5640	46.5	-4.75		
54	0.5635	51.5	0.5639	46	-5.50		
55	0.5635	52	0.5637	47	-5.00		
56	0.5637	51.5	0.5639	46	-5.50		
57	0.5637	51	0.5640	46.5	-4.50		
58	0.5637	51	0.5640	46.5	-4.50		
59	0.5635	51	0.5640	46.5	-4.50		
60	0.5632	50.5	0.5637	47.5	-0.30		
61	0.5635	51.5	0.5639	46.75	-4.75		
63	0.563	50.5	0.5640	46.5	-4.00		
Ave	0.5635	51.2500	0.5639	46.6154	-4.43		
StDev	0.0002	0.4330	0.0001	0.4284	1.32		

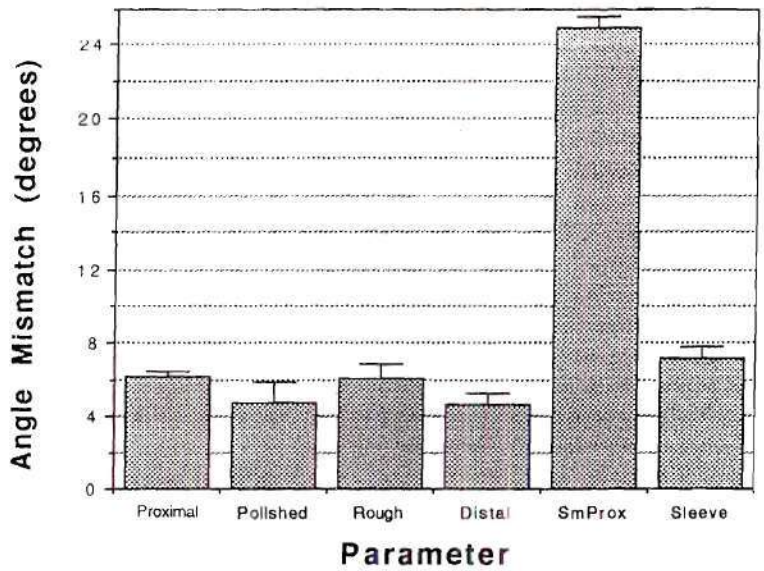

Figure 30.a Total graph

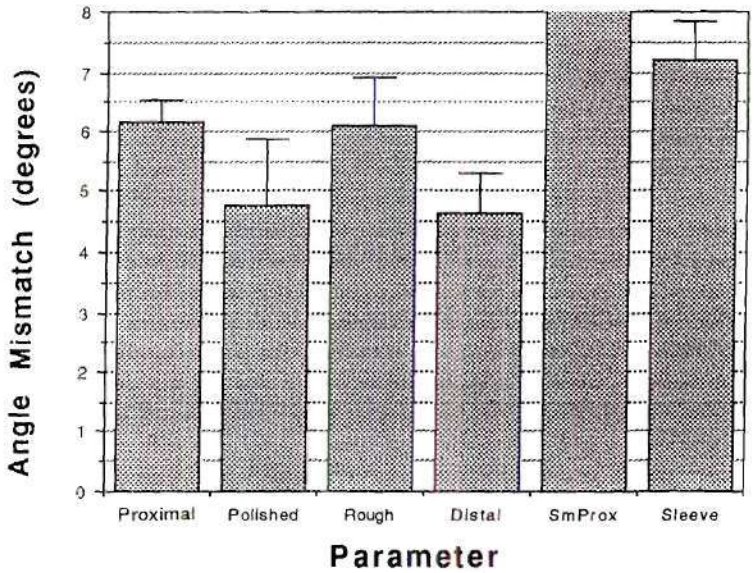

Figure 30.b Expanded graph

Figure 30. Average angle mismatch between the head and the taper
(a. Total graph, b.Expanded graph)

Static Testing Pull-off Loads

After measuring the parts, they were experimentally tested. The results from the static testing are shown in Figure 31 and Table 7. The graph shows the discrete points of the measured pull-off load for each respective preload of 450, 750, 1100, 1500, 2000, 2500, and 3000 lbs. It is not a continuous graph but the points were connected to show the trend. It was desired to have high pull-off values. A higher pull-off load would represent a stronger mechanical lock and this should have less wear debris and fewer problems. The lines in the figure are difficult to distinguish and this shows that the pull-off loads are very similar for all of the different designs. The pull-off loads were expected to vary more between designs but the pull-off was typically about 53% of the preload. This could be attributed to the fact that the same material combinations were used for each different design. The graph also shows the linearity of the relationship between the preload and pull-off load.

All of the designs had very similar results up to 1,500 lbs preload and then there was some separation between the designs. It was surprising that the SmProx had the highest pull-off values at the high preload values because it had the larger head/taper angle mismatch. The Distal and Sleeved design had the next highest pull-off values with average percentages of preload values of 54.4 % and 53.7 %. All of the designs had similar values except the Rough design which consistently had a pull-off load average of 47.5 % of its preload.
At 1500 lb none of the pull-off loads were significantly different from the Proximal design ($p<.05$). At 3000 lb the Proximal design was significantly different than the Rough and SmProx designs. The Rough design was also significantly different than the Distal and Polished designs.

The loads that a hip would experience in a typical 160 lb person would be below the 1,500 lbs separation point on the curve, which is 9.4 times that persons body weight. Heavier people under more strenuous loading could experience the higher loads but this

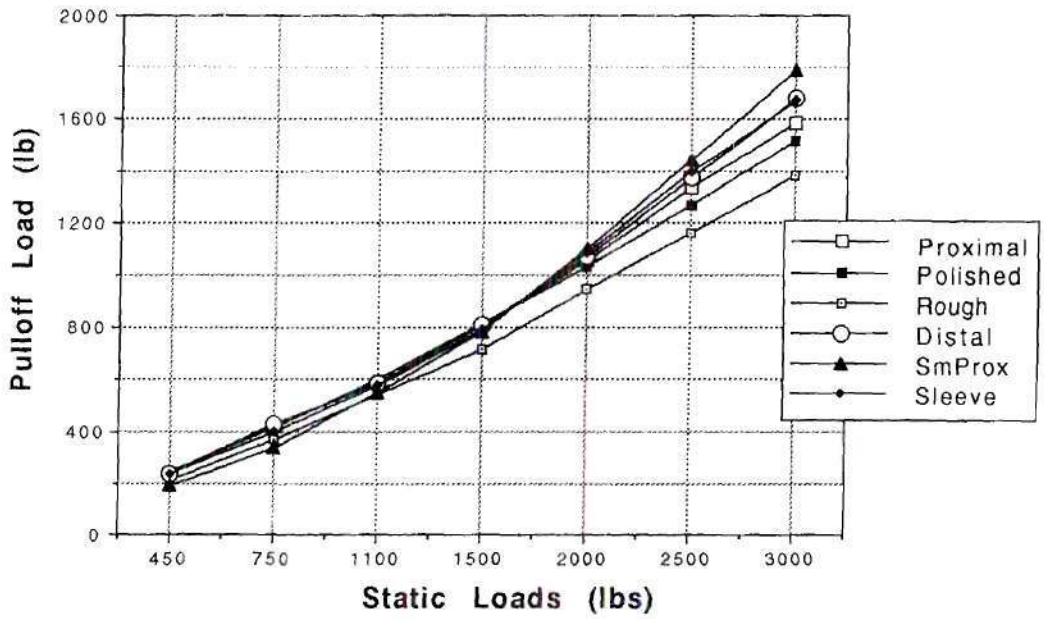

Figure 31. Static Loading Pulloff

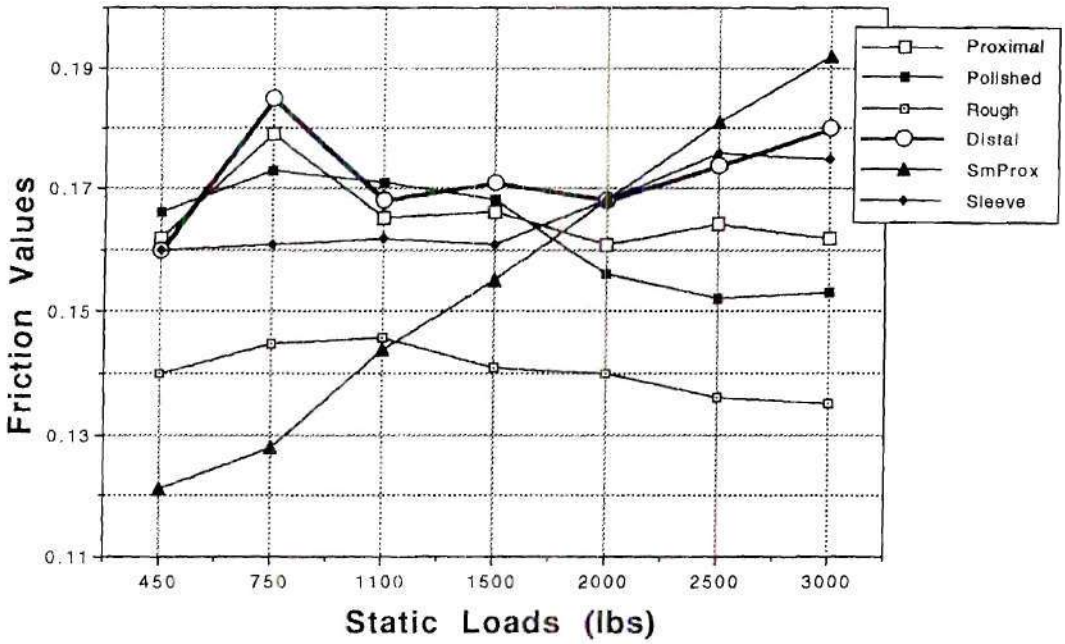

Figure 32. Friction values from preloads and pulloff loads.

Table 7. Static Testing Pull-off and Displacement Results

	preload 450		preload 750		preload 1100		preload 1500			preload 2000		preload 2500		preload 3000	
	displace (inches)	pulloff (Lbs)	displace (inches)	pulloff (Lbs)	displace (inches)	pulloff (Lbs)	displace (inches)	pulloff (Lbs)		displace (inches)	pulloff (Lbs)	displace (inches)	pulloff (Lbs)	displace (inches)	pulloff (Lbs)
	450		750		1,100		1,500			2,000		2,500		3,000	
Polished									Polished						
1	3.5	255.8		437.6	7.7	658.8	10.4	914.8	1	9.5	1,134.8	13.4	1,344.0	14.9	1,594.0
3		219.7	6.6	362.4	7.3	550.0	10.3	744.0	3	10.7	940.0	13.4	1,186.4	15.5	1,469.6
4		273.6	6.7	444.8	6.5	610.4	11.2	777.6	4	11.2	934.4	14.2	1,176.4	16.1	1,406.8
6	5.0	219.5	7.1	385.6	9.5	575.6	10.4	788.8	6	10.5	971.2	14.1	1,189.6	15.4	1,469.6
7	4.5	254.5	5.7	440.0	7.9	615.2	10.1	839.2	7	9.0	1,142.0	12.6	1,345.6	14.4	1,674.4
12	4.1	226.2	6.6	388.8	10.8	610.4	9.3	820.4	12	9.7	1,088.4	13.0	1,357.6	14.2	1,512.8
Average	4.26	241.55	6.53	414.40	8.28	603.40	10.28	814.13	Average	10.10	1,031.80	13.45	1,266.60	15.08	1,521.20
Std Dev	0.62	22.79	0.51	35.17	1.58	37.23	0.61	59.49	Std Dev	0.83	95.58	0.62	90.56	0.72	97.21
Friction		0.166		0.173		0.171		0.168	Friction		0.156		0.152		0.153
	displace 450	pulloff	displace 750	pulloff	displace 1,100	pulloff	displace 1,500	pulloff		displace 2,000	pulloff	displace 2,500	pulloff	displace 3,000	pulloff
Rough									Rough						
13	4.6	204.8	4.3	357.6	7.8	514.4	11.0	687.2	13	9.5	884.8	13.5	1,088.4	14.7	1,298.4
14	4.7	200.0	4.1	357.2	7.5	543.2	8.5	740.4	14	8.3	1,037.2	13.0	1,232.8	12.3	1,438.0
15	4.8	210.6	4.8	356.0	8.7	523.6	9.9	689.6	15	10.4	878.8	14.5	1,093.6	14.5	1,302.8
16	4.3	217.0	4.1	370.4	7.5	555.2	10.0	709.2	16	8.8	974.4	12.2	1,176.4	13.4	1,428.8
17	5.3	235.8	5.9	372.4	6.8	538.0	10.0	708.4	17	9.4	922.0	13.5	1,141.2	14.4	1,373.6
18	4.3	214.7	6.1	376.0	9.5	563.0	13.0	754.0	18	9.3	999.2	13.2	1,218.8	13.5	1,444.4
Average	4.67	213.82	4.88	364.93	7.96	539.57	10.39	714.80	Average	9.28	949.40	13.32	1,158.53	13.80	1,381.00
Std Dev	0.37	12.46	0.90	8.96	0.98	18.43	1.50	27.06	Std Dev	0.71	64.38	0.75	61.49	0.91	67.15
Friction		0.140		0.145		0.146		0.141	Friction		0.140		0.136		0.135
	displace 450	pulloff pulloff	displace 750	pulloff	displace 1,100	pulloff	displace 1,500	pulloff		displace 2,000	pulloff	displace 2,500	pulloff	displace 3,000	pulloff
Proximal									Proximal						
31	4.2	205.2	5.5	375.0	8.4	505.8	8.1	719.0	31	11.0	960.0	12.5	1,217.2	11.8	1,421.6
33		246.6	4.8	438.8	7.4	572.2	8.9	770.2	33	10.4	1,009.6	11.7	1,309.2	12.5	1,583.6
40	4.9	205.2	5.7	361.0	7.2	528.2	9.8	731.2	40	9.5	955.2	12.0	1,230.4	1.2	1,537.2
41	5.0	216.2	6.8	380.8	8.4	536.8	7.4	733.2	41	10.0	975.6	11.4	1,234.4	12.4	1,489.2
42	3.3	234.4	5.3	412.4	7.0	610.0	7.5	841.0	42	9.2	1,092.4	9.9	1,390.4	12.7	1,675.6
43	3.8	230.2	5.6	429.0	7.5	606.2	8.5	844.6	43	9.0	1,107.2	10.3	1,390.4	12.6	1,655.2
44	4.2	328.4	6.2	558.8	8.1	762.6	9.0	1,013.4	44	9.9	1,286.8	11.8	1,559.6	12.2	1,760.0
Average	4.23	238.03	5.70	422.26	7.71	588.83	8.17	807.51	Average	9.86	1,055.26	11.37	1,333.09	10.77	1,588.91
Std Dev	0.65	42.71	0.64	66.79	0.58	86.12	1.01	104.45	Std Dev	0.70	119.17	0.94	123.94	4.23	116.77
Friction		0.162		0.179		0.165		0.166	Friction		0.161		0.164		0.162

Table 7. Static Testing Pull-off and Displacement Results (continued)

	preload 450		preload 750		preload 1100		preload 1500			preload 2000		preload 2500		preload 3000	
	displace (inches)	pulloff (Lbs)	displace (inches)	pulloff (Lbs)	displace (inches)	pulloff (Lbs)	displace (inches)	pulloff (Lbs)		displace (inches)	pulloff (Lbs)	displace (inches)	pulloff (Lbs)	displace (inches)	pulloff (Lbs)
	450		750		1,100		1,500			2,000		2,500		3,000	
Distal									Distal						
50	4.5	238.2	5.5	426.2	6.5	586.2	7.0	804.2	50	9.8	1,099.2	11.8	1,424.4	11.2	1,803.6
51	4.2	246.0	5.6	434.4	7.5	593.0	7.1	798.8	51	10.0	1,040.4	12.5	1,290.4	14.9	1,538.8
52	4.4	232.8	6.8	427.0	6.9	581.8	7.2	779.4	52	9.8	1,011.6	10.0	1,287.2	13.7	1,552.4
53	4.3	235.0	6.2	434.6	6.2	588.8	8.5	805.6	53	9.8	1,034.4	12.1	1,328.4	14.0	1,606.8
54	4.1	219.2	5.6	412.8	7.7	597.6	8.9	876.0	54	9.6	1,185.2	11.2	1,538.4	13.0	1,928.8
55	3.7	228.2	6.0	426.6	7.1	586.2	8.5	805.2	55	9.9	1,054.8	12.0	1,360.8	13.7	1,650.8
Average	4.20	233.23	5.95	426.97	6.98	588.93	7.53	811.53	Average	9.82	1,070.93	11.60	1,371.60	13.42	1,680.20
Std Dev	0.28	9.09	0.50	7.94	0.57	5.61	0.76	33.11	Std Dev	0.13	63.09	0.89	96.24	1.25	154.67
Friction		0.160		0.185		0.168		0.171	Friction		0.168		0.174		0.180
	displace 450	pulloff	displace 750	pulloff	displace 1,100	pulloff	displace 1,500	pulloff		displace 2,000	pulloff	displace 2,500	pulloff	displace 3,000	pulloff
Sleeve									Sleeve						
75	5.5	209.2	9.5	377.8	10.0	569.8	14.1	783.0	75	13.2	1,088.4	18.7	1,419.2	19.4	1,754.8
79	5.6	199.8	8.2	327.8	10.7	523.0	11.7	722.8	79	15.1	944.8	17.5	1,268.8	18.9	1,539.2
80	5.3	193.6	6.9	324.2	8.8	506.0	10.9	741.2	80	12.8	934.8	16.3	1,242.4	20.7	1,535.2
81	5.5	232.8	7.5	396.6	9.7	562.4	11.0	785.2	81	13.9	1,055.2	16.3	1,382.8	18.4	1,628.8
88	4.8	321.2	8.7	520.0	10.8	692.0	10.8	899.0	88	12.4	1,262.0	17.0	1,492.8	18.2	1,806.8
89	5.4	261.4	6.6	418.6	8.6	631.2	9.7	812.6	89	14.2	1,214.0	16.2	1,562.0	18.0	1,761.2
Average	5.35	236.33	7.57	394.17	9.77	580.73	11.37	790.63	Average	13.60	1,083.20	17.00	1,394.67	18.93	1,671.00
Std Dev	0.29	48.46	1.12	72.12	0.93	69.72	1.49	62.22	Std Dev	0.99	134.96	0.98	124.42	1.00	119.33
Friction		0.160		0.161		0.162		0.161	Friction		0.168		0.176		0.175
	displace 450	pulloff	displace 750	pulloff	displace 1,100	pulloff	displace 1,500	pulloff		displace 2,000	pulloff	displace 2,500	pulloff	displace 3,000	pulloff
SmProx									SmProx						
121	6.2	194.4	9.1	341.6	11.5	564.4	14.0	796.6	121	16.7	1,083.2	19.2	1,441.2	22.0	1,823.2
122	6.0	213.6	8.8	317.8	9.3	517.6	12.0	707.8	122	16.6	1,053.2	19.1	1,353.2	21.2	1,722.0
123	6.1	201.0	8.9	368.4	11.8	611.2	13.0	879.0	123	18.8	1,178.0	18.6	1,487.6	20.7	1,842.8
124	6.5	175.2	9.9	338.8	12.7	513.4	13.7	784.4	124	18.1	1,054.0	20.1	1,453.8	22.7	1,771.2
125	6.6	182.2	9.6	326.4	12.5	525.2	13.4	764.8	125	16.2	1,143.6	19.3	1,486.8	21.8	1,784.4
Average	6.30	193.28	9.26	338.60	11.56	546.36	13.22	786.52	Average	17.28	1,102.40	19.26	1,444.52	21.68	1,788.72
Std Dev	0.28	15.19	0.47	19.23	1.36	41.51	0.78	61.90	Std Dev	1.11	56.00	0.54	54.95	0.77	47.15
Friction		0.121		0.128		0.144		0.155	Friction		0.168		0.181		0.192

should be rare. Therefore, based on the static pull-off results, no major conclusions can be made that one design is better than another.

Taper Lock Coefficient of Friction

From the static testing the coefficient of friction was calculated using the preload and pull-off. The coefficient of friction of the head/taper connection can be determined from the following equation.

$$\mu = \tan \alpha \frac{(P_1 + P_2)}{(P_1 - P_2)}$$

P_1 = preload, P_2 = Pull-off load, α = half angle

This equation is more of a global perspective because it utilizes the preload and pull-off load to evaluate the coefficient of friction. In this study this evaluation was used to determine how the coefficient of friction for each different design parameter would be affected by increased loading. It was desired to have a high coefficient of friction value and for the value to not decrease at higher loads. These conditions would both be desirable for a strong mechanical lock. Figure 32 and Table 7 show the changes in the friction values for the different parameters as the static load was increased. This graph is difficult to follow but the general trend is for the friction to stay relatively constant. The Proximal and Polished designs slightly decreased and the Distal and Sleeve designs slightly increased as the preload was increased. The SmProx friction value increased with each preload increase with a value of 0.121 at 450 lbs and a value of 0.198 at 3,000 lbs preload. This could probably be attributed to a "digging in" effect. This increase was desired, but it had lower friction values at the lower loads which was not desired. The Distal design consistently had one of the highest friction values and was increasing with higher loads with a value of 0.171 at 1,500 lbs preload. Both of these conditions were favorable.

Roughness Results

Between each static load the surface roughness was measured. The results of the roughness tests did not show any significant linear trends. Figure 33 and Table 8 show the average results of the roughness measurements after the static testing. The Ra, average roughness, was plotted. There was not a consistent slope of the graphs, but the measurements showed the large differences between the different roughness designs. Therefore, it was beneficial to check the roughness to insure that the parts were manufactured properly.

Fatigue Testing Pull-off Loads

Along with the static testing the next testing involved fatiguing the parts. The average pull-off loads after fatigue testing are shown in Figure 34 and Table 9. As for both the static and fatigue testing, it was desired to have higher pull-off values because this would represent a better mechanical lock between the head and taper. The fatigue results carry more significance than the static testing because this testing was conducted under conditions more similar to in vivo loading. The cyclic loading of 1,100 lb for 1 million cycle loading was an approximation of a person running nonstop for a year. After fatiguing and disassembling the connection the parts were wet with Ringers solution on both the tapers and the heads as well as on top of the taper inside the head. This showed that the fluid was making its way into the contact region. However, with the naked eye there was no sign of corrosion on any of the parts and there was no visual sign of metal particles in any of the solutions. Corrosion is a very time-dependent phenomenon and in this study it would not be expected to see visible signs of corrosion because the testing only lasted 25 hours. Figure 33 shows that the pull-off load for the H preload, which was a 3,000 lb vs. 450 lb preload, had a significantly higher pull-off load and this would be

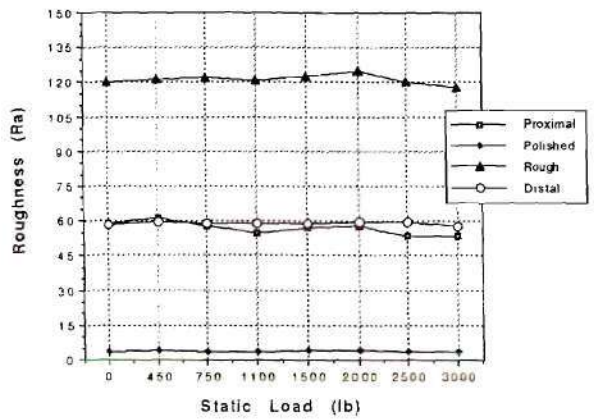

Figure 33.a All roughness values

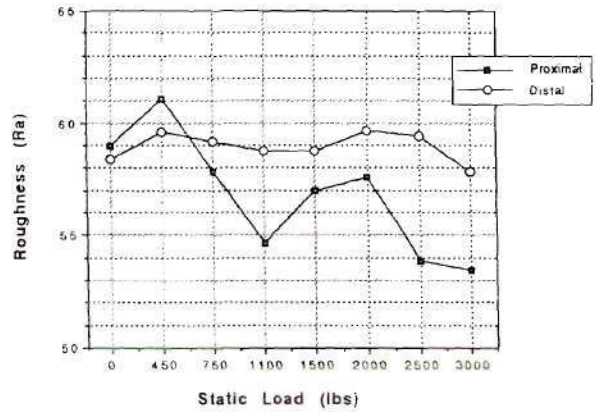

Figure 33.b Proximal and Distal roughnesses

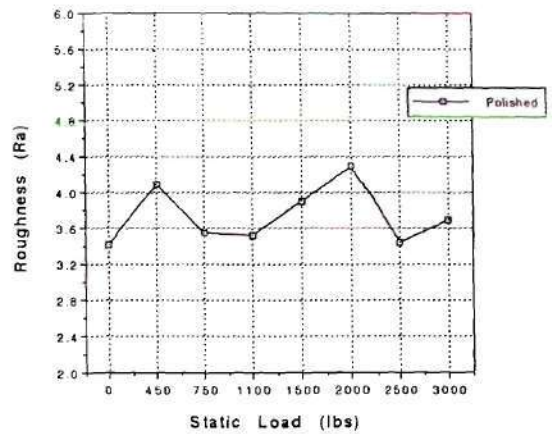

Figure 33.c Polished roughness

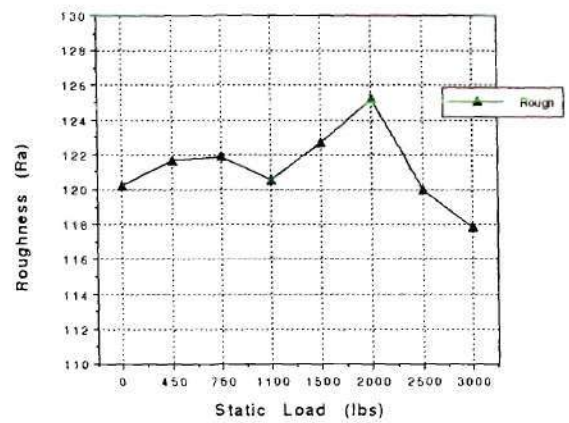

Figure 33.d Rough roughness

Figure 33. Roughness Results
(a. All roughness values, b. Proximal and Distal roughnesses,
c. Polished roughness, d. Rough roughness)

Table 8. Roughness Results

STATIC Ra	0 load	450 lb	750 lb	1100 lb	1500 lb	2000 lb	2500 lb	3000 lb		Fatigue Ra
Polished Ra	3.42	4.1	3.55	3.52	-	4.3	3.45	3.7		4.1
Rough Ra	120.26	121.63	121.92	120.58	122.7	125.2	120	117.85		120.15
Proximal Ra	58.98	61.1	-	54.65	56.97	57.6	53.85	53.43		55.75
Distal Ra	58.38	59.6		58.75	58.75	59.6	59.45	57.83		59.75
Sleeve Ra	79.3	-	-	-	-	-	-	79.1		88.5
H preload Ra	76	-	-	-	-	-	-	-		59.2
SmProx Ra	65.1	-	-	-	-	-	-	60.65		70.77

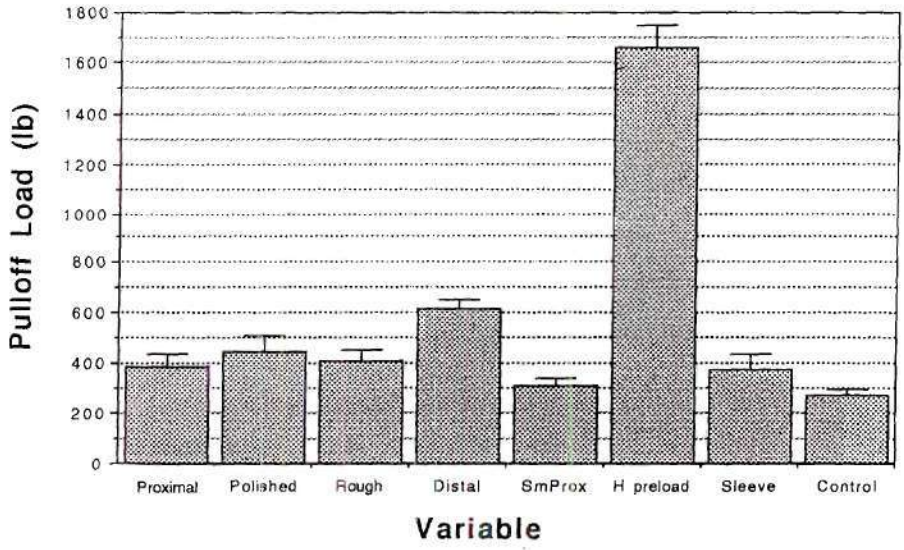

Figure 34.a Total graph

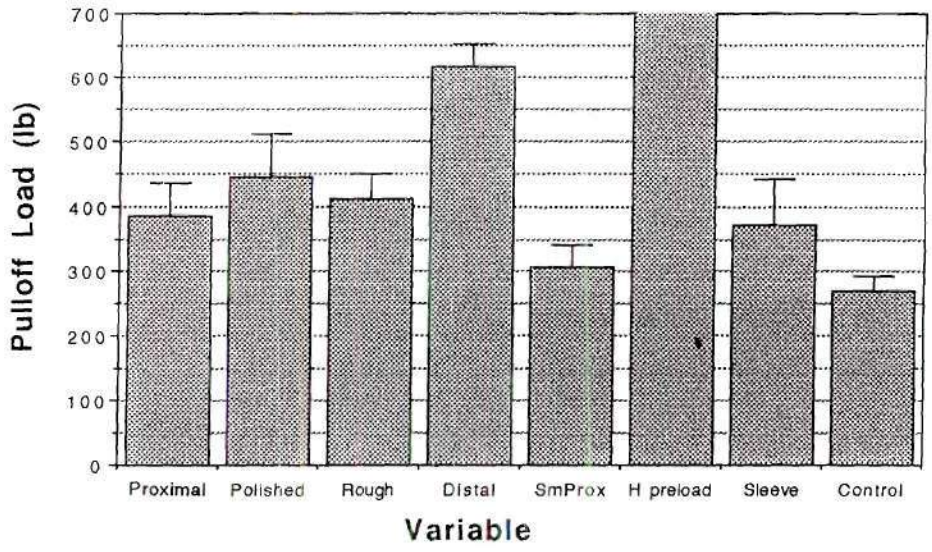

Figure 34.b Expanded graph

Figure 34. Fatigue loading pulloff
(a. Total graph, b. Expanded graph)

Table 9. Fatigue Testing Pull-off Results

Proximal	fatigue pulloff	Polished	fatigue pulloff	Rough	fatigue pulloff	distal	fatigue pulloff
30	337.8	2	589.0	12	401.0	56	657.8
32	349.2	5	383.0	19	456.0	57	586.4
34	357.4	8	479.0	22	450.0	58	553.6
35	469.8	9	450.0	24	347.0	59	643.2
38	363.8	10	409.0	26	393.0	60	624.6
39	434.6	11	407.0			61	634.0
		23/27	385.0				
Ave	**385.43**		**443.14**		**409.40**		**616.60**
STD	**48.94**		**67.69**		**40.13**		**35.71**

H preload	fatigue pulloff	sleeve	fatigue pulloff	SmProx	fatigue pulloff	Control	fatigue pulloff
90	1,486.2	70	382.0	126	369.6	140	250.0
91	1,661.0	71	375.0	127	274.8	141	264.4
92	1,806.2	72	508.4	129	290.0	142	245.0
93	1,676.2	74	297.0	130	302.4	143	313.6
94	1,671.2	76	335.6	131	294.0	144	273.2
95	1,631.4	77	334.8			145	277.0
99	1,735.2						
Ave	**1,666.77**		**372.13**		**306.16**		**270.53**
STD	**91.12**		**67.14**		**32.96**		**22.42**

expected ($p<.05$). The average H preload pull-off was 1,667 lbs after fatiguing. Comparing this result with the static testing showed that the pull-off load was not effected by the fatiguing. The pull-off load in the static testing was 1,589 lbs for the Proximal design with a 3,000 lbs preload. This result demonstrated that having a very high preload as compared to the actual in vivo hip loads should be very beneficial. This topic will also be addressed later. The other seven parameters are shown close up in Figure 33.b. The control on this graph represents a head/taper connection that was not fatigue loaded but did have Ringers solution inside its tubing for the same duration as a fatigue test. This measured the effect of the Ringers solution alone on the preloaded parts. As expected the Control pull-off was the same as the static tests so the Ringers had no effect on the mechanical lock for the 25 hour time duration. The Proximal, Polished, Rough and Sleeved designs were not significantly different from each other ($p<.05$). However, the SmProx had a significantly lower pull-off load and the Distal was significantly higher than the Proximal design with values of 306.2 and 616.6 lbs. respectively ($p<.05$).

Also with the 1,100 lb fatigue loading the expected value might be similar to the static pull-off of 53% of the loading. This would result in the pull-off load being about 600 lbs. The Distal design was the only design that had this result. All of the other designs were significantly lower than this 600 lb value. This shows that the fatigue loading did not adversely effect the Distal design but the other designs were affected. Also this result demonstrates that the method of increasing the load used in the static testing was valid because in this fatigue test the head was loaded directly to 3000 lb with similar results as the static testing. These fatigue pull-off results showed no significant difference between the different surface finishes of Proximal, Rough, and Polished ($p<.05$). However, these results were very favorable to using a high preload and designing with distal contact.

It should be noted, however, that this testing was for only 1 million cycles and a longer 10 or 20 million cycle follow-up study should be conducted to develop even

stronger conclusions. Also as in most laboratory testing, not every clinical factor was reproduced. Factors such as rotational forces, loading frequency, actual time, and actual conditions which lead to corrosion were not the same as in vivo conditions.

SEM

After fatiguing, the parts were viewed with the SEM and pictures were taken at 350 X magnification. Figure 35 shows the SEM pictures of the proximal and distal ends of representative tapers after the fatigue testing. This shows the region of plastic deformation. Figures 35.a and 35.b show the Proximal and Distal designs respectively. As expected each design had the wider band in the region where there is initial impingement. Figure 35.c shows the H preload and as can be seen the plastic deformation was very large at the region of initial contact . This was also expected because these parts were loaded higher than all others. The Polished parts are shown in Figure 35.d and they showed no signs of deformation. However, visually there were scratches that could be seen where the head contacted.

Metal Ion Release Results

Also after the fatigue test , the solutions were analyzed for metal ion content of Co, Cr, and Ti. Figure 36 and Table 10 show the metal ion release results. "Fresh" represents Ringers solution that was fresh from the manufactured container. Throughout all of the results it was expected that the Control and "Fresh" would both be lower than all other designs and this was the case. The average values were typically determined from four of the six tests because the other two were filtered for particle counting.

There were two issues involved in the metal ion results. The first issue was that as wear increases the mechanical lock is deteriorated due to third body wear and loss of material The second issue was that metal ion release predicts the metal contamination in the

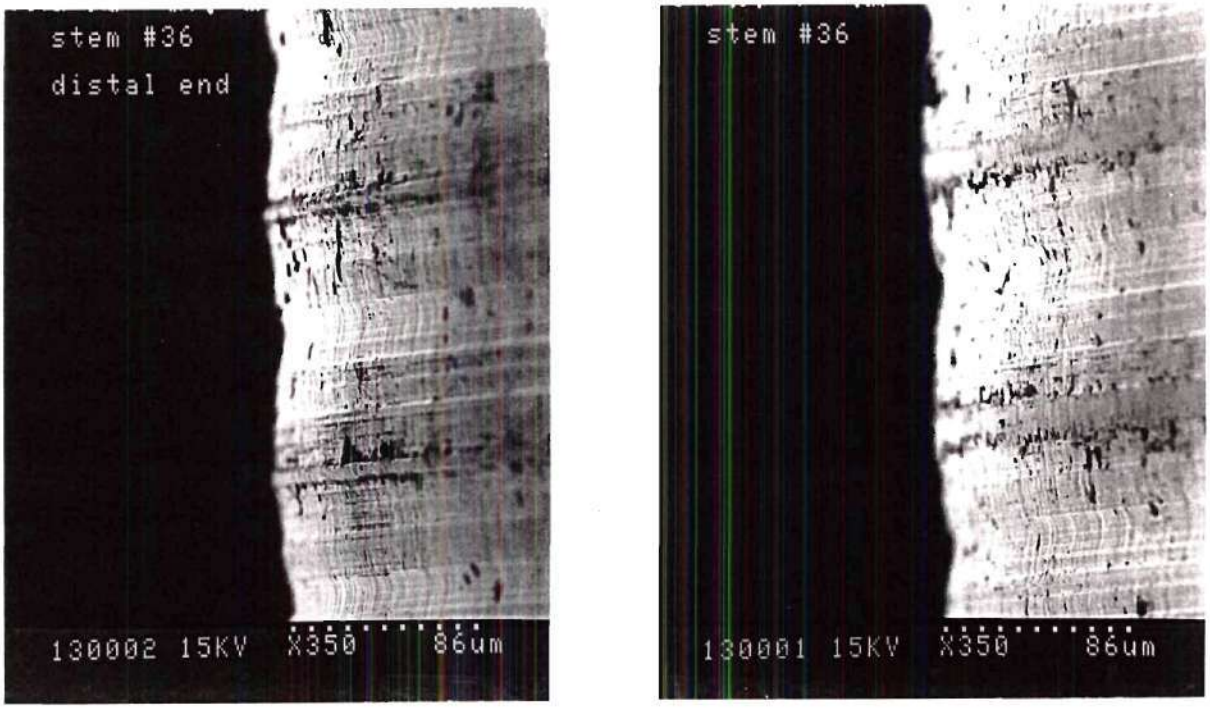

Figure 35.a Proximal

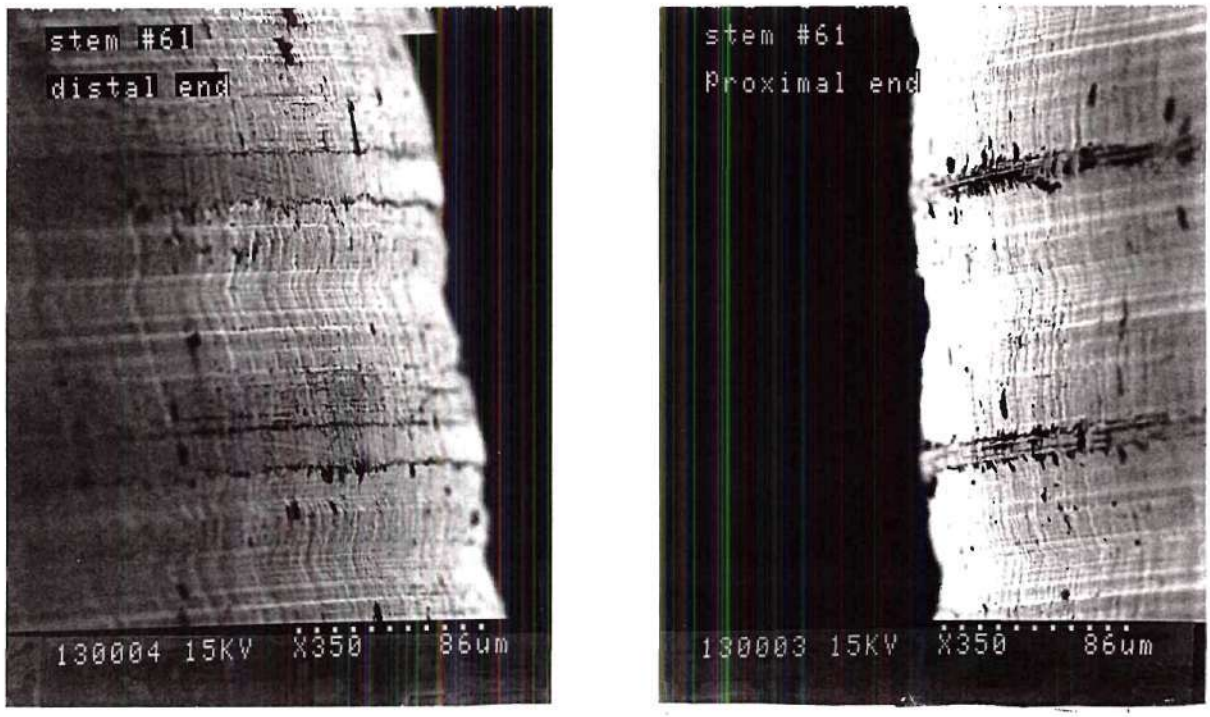

Figure 35.b Distal

Figure 35. SEM pictures of the distal and proximal ends of the different taper designs. (a. Proximal, b. Distal, c. High preload, d. Polished)

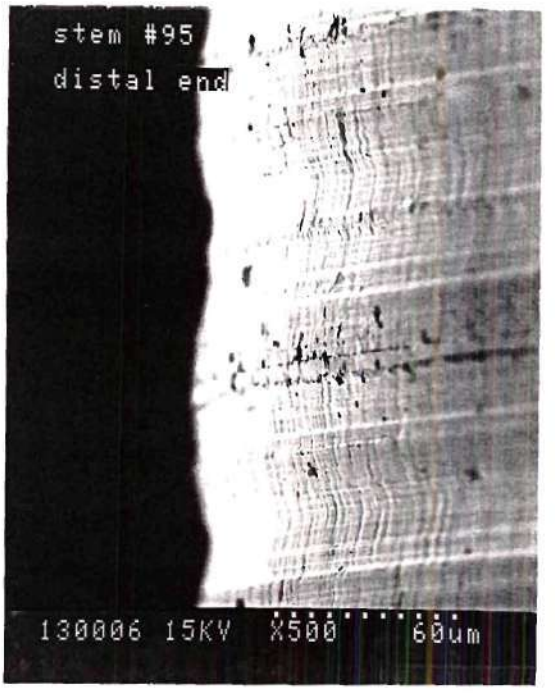

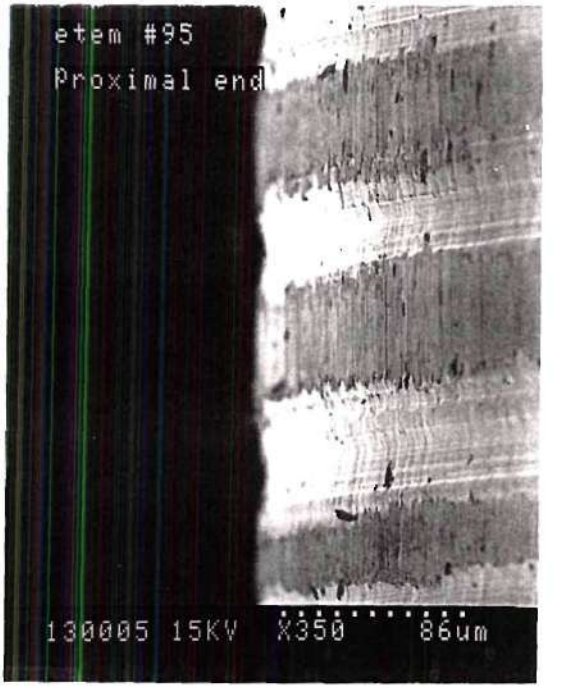

Figure 35.c High preload

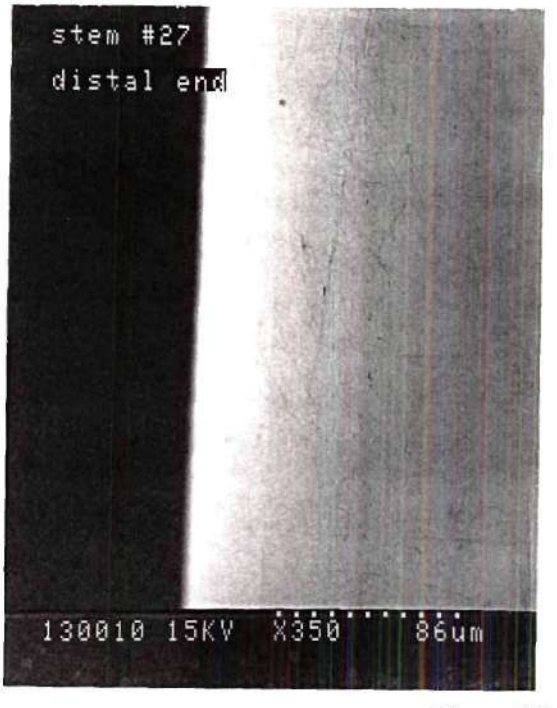

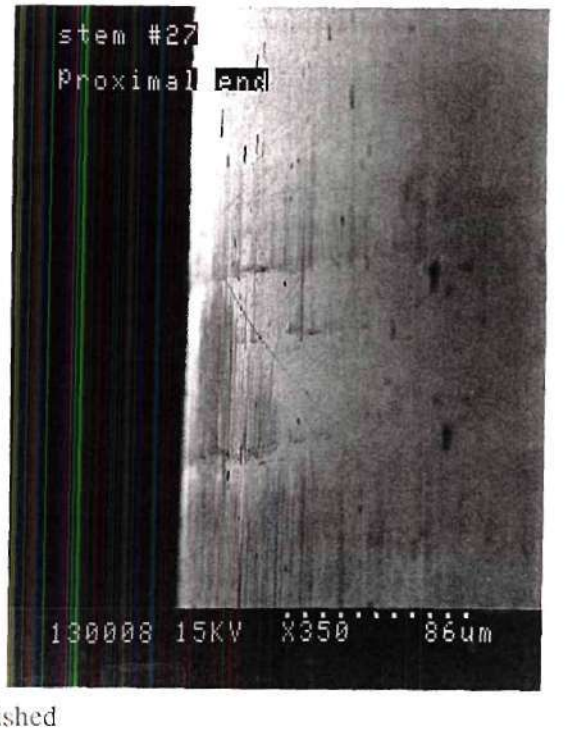

Figure 35.d Polished

Figure 35. SEM pictures of the distal and proximal ends of the different taper designs. (a. Proximal, b. Distal, c. High preload, d. Polished)

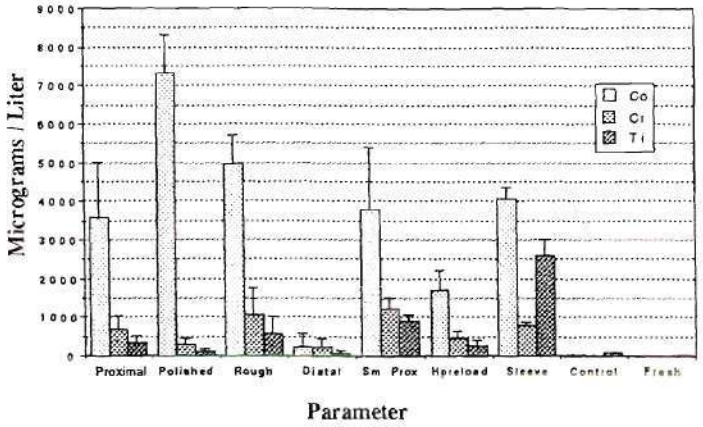

Figure 36.a Metal ion results for Co, Cr, and Ti

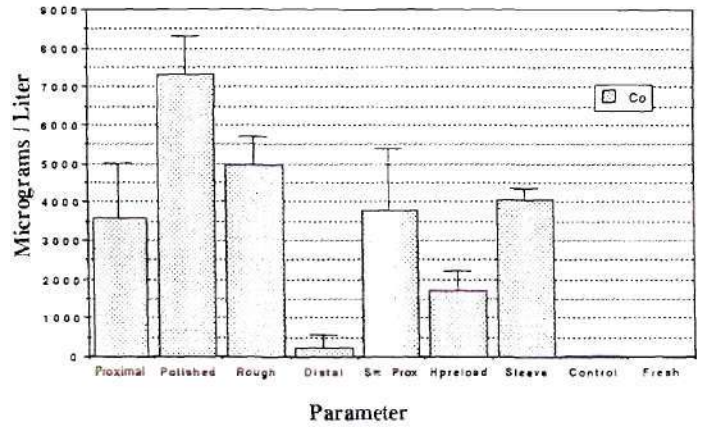

Figure 36.b Cobalt ion results

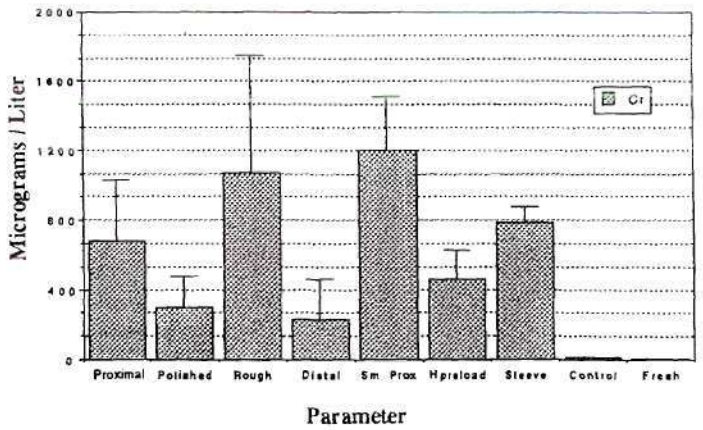

Figure 36.c Chromium ion results

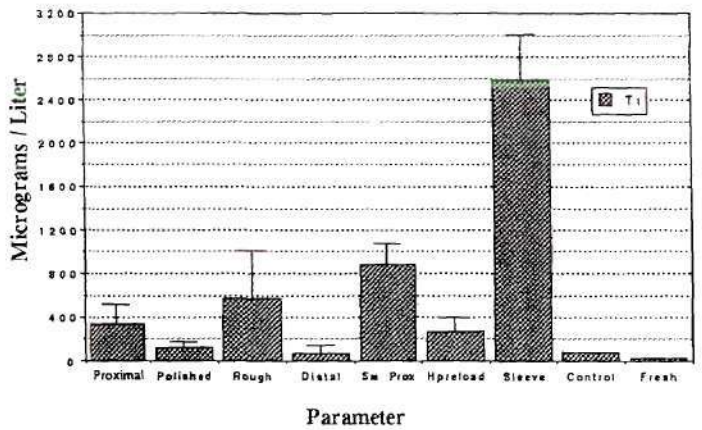

Figure 36.d Titanium ion results

Figure 36. Metal ion release results
(a. Metal ion results for Co, Cr, and Ti, b. Cobalt ion results,
c. Chromium ion results, d. Titanium ion results)

Table 10. Metal Ion Results

Rough	#	Co	Cr	Ti
	19	4,700	1,090	515
	20	5,240	1,860	1,150
	23	5,820	205	93
	26	4,060	1,130	555
Ave		4,955	1,071	578
stdev		752	677	435

Proximal	#	Co	Cr	Ti
	31	3,590	960	400
	32	2,070	525	440
	33	4,100	1,030	520
	38	2,470	165	61
	39	5,690	730	295
Ave		3,584	682	343
stdev		1,435	351	177

Distal	#	Co	Cr	Ti
	56	750	260	200
	58	93	40	160
	60	70	490	32
	61	55	160	23
Ave		242	238	104
stdev		339	191	90

Control	#	Co	Cr	Ti
	141	34	13	80
	142	37	12	82
	143	25	12	89
	144	23	12	80
Ave		30	12	83
stdev		7	1	4

Sleeve	#	Co	Cr	Ti
	70	4,240	745	2,110
	77	4,220	730	2,860
	79	3,760	890	2,790
Ave		4,073	788	2,587
stdev		272	88	414

polished	#	Co	Cr	Ti
	8	6,470	140	78
	10	7,170	480	180
	11	8,380	285	110
Ave		7,340	302	123
stdev		966	171	52

Hpreload	#	Co	Cr	Ti
	90	2,130	465	270
	93	2,040	660	69
	94	1,020	245	350
	95	1,630	465	375
Ave		1,705	459	266
stdev		506	170	139

SmProx	#	Co	Cr	Ti
	126	2,990	720	600
	127	4,720	1,230	910
	129	4,690	1,180	950
	130	5,170	1,330	840
	131	6,070	1,560	1,130
Ave		4,728	1,204	886
stdev		1,120	307	192

Fresh	Co	Cr	Ti
	1	6	32

body. Of the different materials in the two alloys, titanium is the best material for biocompatibility and cobalt is the worst. From Figure 36.a it can be seen that the amount of cobalt ions was much higher than the other elements and this was not desired. Figures 36.b, 36.c, and 36.d separate cobalt, chromium, and titanium onto separate graphs respectively. On Figure 36.b the Distal design was extremely low at 242 μg/l and the H preload also had a low value at 1,705 μg/l. This could be expected because of the high pull-off loads after fatiguing for these two designs. These values were low compared to 7,340 and 4,955 μg/l for the Polished and Rough designs respectively. The Distal design was significantly different from all of the different designs that were tested ($p<.05$). The design of the tapers and heads were the same for both the Proximal and H preload but the preload was different. The significant difference between them showed the benefit of using a high preload value ($p<.05$). This was the most significant graph because these values are much higher that the other elements. For both issues of mechanical integrity and body contamination this graph was significant because of its high values, and the Distal design had the best results.

The chromium results are shown in Figure 36.c. Again the Distal had the lowest metal ion release with a value of 238 μg/l. In this case the Polished and H preload designs both had low values of 302 and 459 μg/l respectively. The Rough and SmProx designs had high values of 1,071 and 1,204 μg/l. This could be expected because these two had lower pull-off values after fatigue testing.

The titanium graph showed that the Distal design had the lowest metal ion release again with a value of 104 μg/las shown in Figure 36.d. The Polished and H preload again had low values of 123 and 266 μg/respectively. The Rough and SmProx were both higher but this graph had the Sleeve parameter several times greater than the other parameters. The Sleeve had a value of 2,587 μg/l. This was not expected but could be explained by the extra titanium connection between the sleeve and the taper.

All of these graphs show that the Distal design had excellent metal ion release results and that a higher preload also reduced the amount of metal ion release. None of the different surface finishes consistently showed better results for every element. Again, it is important to note that this testing was for only 1 million cycles and two theories will be discussed later about the possibilities of what could be occurring. Even stronger conclusions could be made from further studies of 10 to 20 million cycles of the designs of interest.

Particle Count Results

The contaminated Ringer's solutions from the fatigue test was used to determine the metal ion content, but also some of the solutions were filtered and the particles examined. This was a second way of measuring the contamination that the body would experience in vivo. The filters were analyzed with the SEM and the results were surprising. The parameters analyzed included Proximal, Distal, Sleeve, H preload and Control. These were selected as the parameters of greatest interest. There were no significant particles for the Proximal, Distal, H preload, and Control designs to be seen at 3,000 X magnification as shown. They all had less than 17,827 particles in the 3 ml filtered. It was expected that some particles would have been in the solution and captured on the filter. For the filters investigated with the energy dispersive analysis method very few and very small particles were found. Surprisingly the particles that were found on the filter were usually Co and Cr and not titanium. More titanium was expected because the taper was the rougher surface and it had a lower modulus. Figure 37 shows the energy dispersion analysis and an SEM picture of a Co and Cr particle. The magnification was at 1,500 times and the particle was very small with a length of 7.75 μm. There were higher amounts of particles for the Sleeve design with values of 52 and 32 million titanium, 200000 and 7 million cobalt, and 6 and 23 million chromium particles for the two solutions filtered from the 3 ml of solution. This is still much less than the clinical number of polyethylene particles per year, which is

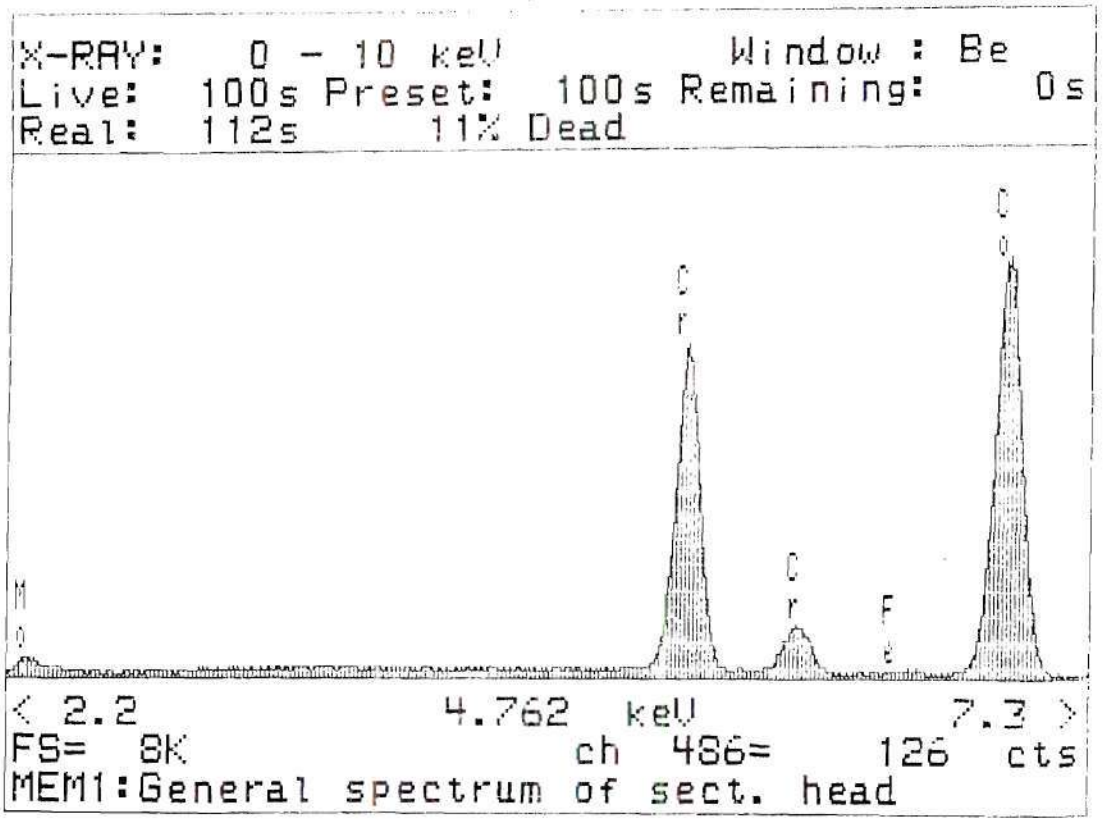

Figure 37. Cobalt chromium particle and energy dispersive analysis

approximately 50 billion per year. Figure 38 shows a SEM picture at 3000 X magnification of the titanium particles filtered from the Sleeved design. This could be expected but not at this extreme. It should be noted that at the present only two Sleeve design solutions were analyzed and one for all other designs that were discussed. It was felt that the metal ion release count was a more accurate measure of the contamination escaping to the body.

Distal and Proximal Contact Theories

As mentioned earlier, there are two ideas of the fluid infiltration of the Distal and Proximal contact designs. The exact electrochemical process that is occurring in the Proximal and Distal designs is not totally understood nor agreed upon by all researchers. Based on the results of this study the results appeared to show that the Distal design simply creates a better mechanical lock and resulted in less metal contamination. From this study the proximal contact appeared to allow fluid to infiltrate the contact surfaces more readily and to carry the particles away to the body. This is obviously undesirable. This type design may however replenish the oxygen in the crevice and allow more free flowing of the fluid, which would help reduce corrosion. This is because relatively stagnant fluid can have oxygen depletion and result in increasing corrosion.

On the other hand, the distal contact design probably reduces the amount of body fluid that can contaminate the contact surfaces. From its design, it appears to essentially create a natural seal between the rim of the head and the taper. This could both help prevent fluid from entering the contact region and trap any fluid that does enter. However, if fluid does get inside the region between the head and the taper it is probably more difficult for it to escape. This could be beneficial because it prevents metal particle and metal ions from reaching the body but this would increase the potential for crevice corrosion. The trapped debris probably acts as third body wear which could accelerate metal wear for longer cycles (i.e. 20 million cycles). The results of this study did not show that the Distal design should

Figure 38. Filtered titanium particles

expect to have any unforeseen problems, but instead that it created a better lock.

It should be noted again that the amount of wear contamination to the body from the head taper lock was much less than the wear from the head and acetabular cup articulation. It is, however, always beneficial to reduce the metal ions and wear particles. Also is should be noted that true in vivo conditions are very difficult to simulate in vitro and this study does not claim to be an exact simulation of in vivo conditions. Clinical trials should be conducted for stronger conclusions.

Impact Head Assembly and Pull-off Loads

From the results of the static and fatigue testing it was shown that having a high preload was beneficial. Along with this it would also be beneficial to have a controlled preload and to not leave it up to the discretion of the surgeon. Figure 39 and Table 11 show the results of the impact testing. Both striking and pushing the impactor had very similar and high values of 814.5 and 880.5 lbs respectively. This showed that the impactor could safely be struck instead of pushed and still get a controlled and consistent load. It should be noted that an additional spring was added in order to increase the load as high as possible with this device, which was higher than the load used for assembling the distal extension. The direct striking using a surgical mallet had a much wider spread from 520 to 750 lbs.

Figure 40 shows the pull-off results after the heads were assembled by impacting them on by both striking the controlled impactor and by directly striking the heads. The controlled impactor test resulted in a pull-off load of 538.8 lbs. When this was compared to the previously discussed static testing the static preload would have been comparable to approximately 980 lb preload. The pull-off loads for the two different operators Tester #1 and Tester #2, were 550.2 and 645.6 lbs respectively. This was a broad range but the difference in the Standard Deviations between using the controlled impactor and a direct

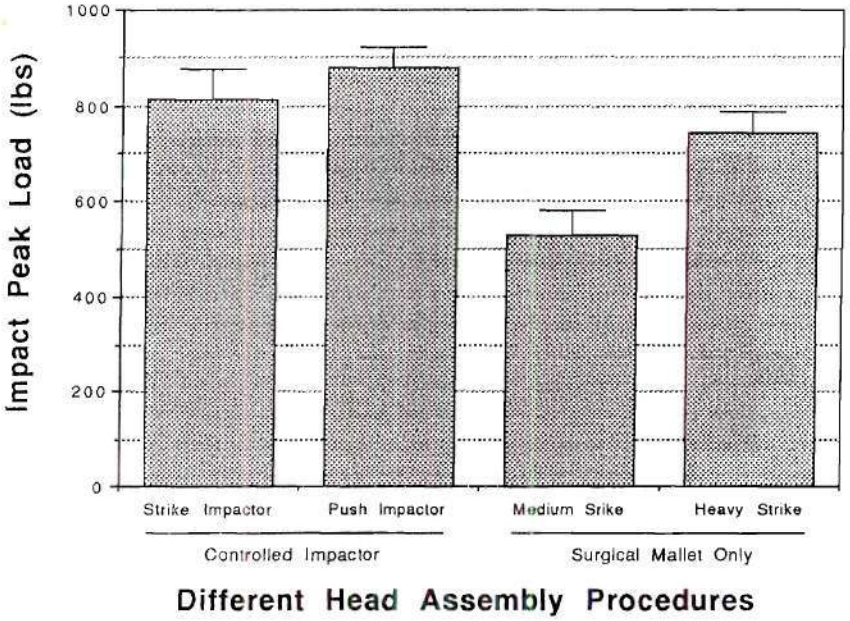

Figure 39. Impact Load Testing

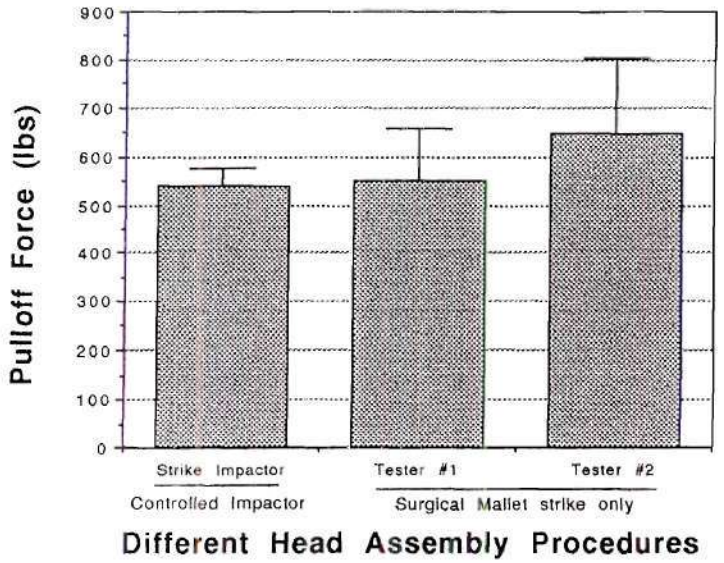

Figure 40. Pull-off testing after impacting heads onto the tapers.

Table 11. Impact Loading and Pull-off Results

Head Assembly Procedure				
	Controlled Impactor		Sugical Mallet only	
	Srike (lbs)	Push	medium	Heavy
	947	903	563	573
	801	902	537	725
	794	897	538	708
	925	884	486	723
	811	734	511	738
	826	894	488	758
	819	886	499	729
	784	902	554	739
	774	895	593	731
	782	883	506	760
	762	899	581	769
	789	885	438	772
	769	895	495	755
	791	900	581	752
	762	897	478	774
	920	890	575	788
	784	891	547	785
	904	881	412	781
	778	813	610	741
	767	878		
Ave	814.45	880.45	525.89	742.16
StDev	59.21	39.47	53.36	46.95

Pull off Load			
Head on Stem	Strike impactor 2 strikes	Surgical mallet only	
		Tester #1	Tester #2
46 on 46	592.2	631.4	639.6
47 on 47	546.4	691.4	930.2
101 on 50	492	546.2	529.2
102 on 51	544.6	453.4	705.8
103 on 57	493.6	406.4	518
104 on 60	558.4	572.4	550.8
Average	537.87	550.20	645.60
StDev	38.87	106.85	157.15

mallet strike were 38.8 and 157.1 respectively. This was even more significant. The controlled impactor value was sufficiently high but it could be changed simply by changing the springs located inside the device. A future design of this device could allow for spring adjustment, which would change the impact load. This would give the surgeon some flexibility, but would still prevent the load from ever being too low.

CHAPTER V

Conclusions and Recommendations

This study considered the interface connection between cobalt chrome femoral heads and titanium taper stems. The surface roughness and taper angle were the primary variables studied. The assembly load, the assembly procedure, and the number of part connections were the secondary variables studied.

* The finite element analysis of the conical taper was used to determine the relative displacements and the stress distributions in the head and taper under loading conditions. They showed that for different taper angles the maximum hoop, effective, and principal stresses were always at the head / taper contact region. The Distal contact design had the highest stresses with approximately a 20 % effective stress increase over the proximal contact design, but they were still well below the ultimate strength of the material. The FE displacement and stress results were similar to the static testing and strain gage experimental results., which showed the validity of the model.

* The static testing showed that the head pull-off loads had a linear relationship with the preload. For the different roughnesses and taper angles the pull-off load was usually 53% of the preload. From the profilometer and SEM analysis the contact region showed plastic deformation, but there was not a consistent trend in the roughness (Ra) values between the low and high static loads.

* From the fatigue testing the distal contact design had a higher head pull-off load and much lower metal ion concentration in the solution. High pull-off loads would demonstrate a stronger mechanical lock and the lower metal ion content shows less contamination escaping

into the body. From the literature, a very important issue in this type testing is the quality of the taper and head manufacturing. Poor quality with either proximal or distal contact would not be beneficial.

* The H preload , or high preload, design had a much larger pull-off load and reduced metal ion content. This would be expected because for higher preloads the locking strength is better. From this it can be concluded that the preload should be as high as the the femur can withstand physiologically.

* The Sleeved design showed a much higher metal particle amount after filtering, which could be attributed to the additional connection.

* There was no correlation found between the small variations in angle mismatch between the head and taper in pull-off loads or metal ion content. Angle mismatches of greater than 11 minutes would be required to show significant differences.

*A study of the different surface roughnesses did not reveal any consistent advantage of one design over the other. They were relatively similar in mechanical integrity and contamination to the body. * It should be noted that from the literature it was found that the wear debris caused by the head / cup articulation is much greater than the wear from the head / taper lock. However, it is always beneficial to reduce metal ions and particles from contaminating the body.

* With the mechanical integrity and contamination to the body as key design issues, the best overall design was the distal contact design. The Distal design was superior in static and post-fatigue pull-off tests and it had a lower metal ion release rate. It should be noted that in this study, the fatigue testing was conducted for only one million cycles and from the literature it is shown that stronger conclusions could be developed if further tests of ten to twenty million cycles were conducted.

* The High Preload design also demonstrated significant benefits. In order to apply a consistently high preload a controlled impactor should be used. The current procedure involves

a surgeon striking the head manually with a surgical mallet resulting in a large variation in the impact loads applied. The controlled impactor device applied a more consistent impact load to the head / taper connection than a direct strike. A device like this would ensure a strong mechanical lock with less metal ion contamination to the body and would be recommended.

APPENDIX

Statistics - t Distribution

Case: Compare two average values with different standard deviations.
This statistic is distributed approximately as t because the variances are not equal.

Significantly different if

$$|t_0| > t_{\alpha/2,\, v}$$

were

$$t_0 = \frac{\overline{X}_1 - \overline{X}_2}{\sqrt{\frac{S_1^{\,2}}{n_1} + \frac{S_2^{\,2}}{n_2}}}$$

$$v = \frac{\left(\frac{S_1^{\,2}}{n_1} + \frac{S_2^{\,2}}{n_2}\right)^2}{\frac{\left(S_1^{\,2}/n_1\right)^2}{n_1 + 1} + \frac{\left(S_2^{\,2}/n_2\right)^2}{n_2 + 1}} - 2$$

v = Degrees of Freedom on t_0
$\alpha = 0.05$ = Significance level
$\overline{X}_1$ = Average value
$\overline{X}_2$ = Average value
S_1 = Standard Deviation
S_2 = Standard Deviation
n_1 = Quantity tested
n_2 = Quantity tested

Statistics for Angle Mismatch

		v	to	t	Conclusion
Proximal					
	Polished	13	4.1766	2.162	Different
	Rough	14	0.28401	2.145	Not Stat. Different
	Distal	13	4.5678	2.162	Different
	Sm Prox	16	-93.7111	2.12	Different
	Sleeve	15	4.8238	2.131	Different
Distal					
	Polished	23	-0.6773	2.069	Not Stat. Different
	Rough	19	-3.6756	2.093	Different
	Sm Prox	16	-48.9145	2.12	Different
	Sleeve	17	-6.474	2.11	Different
Polished					
	Rough	22	-3.3016	2.074	Different

Statistics for Fatigue Testing pulloff

		v	to	t	Conclusion
Proximal					
	Polished	12	-1.778	2.179	Not Stat. Different
	Rough	10	-0.8925	2.228	Not Stat. Different
	Distal	10	-9.3466	2.228	Different
	Sm Prox	10	3.1927	2.228	Different
	H Preload	10	-32.182	2.228	Different
	Sleeve	10	0.3921	2.228	Not Stat. Different
	Control	7	5.228	2.365	Different
Distal					
	Polished	10	5.8907	2.228	Different
	Rough	10	8.9612	2.228	Different
	Sm Prox	10	14.9741	2.228	Different
	H Preload	8	-28.0805	2.306	Different
	Sleeve	8	7.87485	2.306	Different
	Control	9	20.1044	2.262	Different
Polished					
	Rough	11	1.0796	2.201	Not Stat. Different
	Sm Prox	10	4.639	2.228	Different

Statistics for Static Testing pulloff

450 lb		v	to	t	Conclusion
Proximal					
	Polished	10	-0.18892	2.228	Not Stat. Different
	Rough	7	1.4304	2.365	Not Stat. Different
	Distal	6	0.2898	2.447	Not Stat. Different
	Sm Prox	8	2.5551	2.306	Different
	Sleeve	11	0.0666	2.201	Not Stat. Different
1500 lb Proximal					
	Polished	11	-0.1428	2.201	Not Stat. Different
	Rough	7	2.2615	2.365	Not Stat. Different
	Distal	7	-0.09634	2.365	Not Stat. Different
	Sm Prox	11	0.4353	2.201	Not Stat. Different
	Sleeve	11	0.3596	2.201	Not Stat. Different
1500 lb Distal					
	Polished	8	-0.09354	2.306	Not Stat. Different
	Rough	11	5.541	2.201	Different
	Sm Prox	6	0.8118	2.447	Not Stat. Different
	Sleeve	8	0.7264	2.306	Not Stat. Different
3000 lb Proximal					
	Polished	12	1.1408	2.179	Not Stat. Different
	Rough	11	4.0017	2.201	Different
	Distal	10	-1.185	2.228	Not Stat. Different
	Sm Prox	9	-4.085	2.262	Different
	Sleeve	12	-1.2488	2.179	Not Stat. Different
3000 lb Distal					
	Polished	9	2.132	2.262	Not Stat. Different
	Rough	7	4.3464	2.365	Different
	Sm Prox	6	-1.6301	2.447	Not Stat. Different
	Sleeve	11	0.1154	2.201	Not Stat. Different
3000 lb Polished					
	Rough	10	-2.9067	2.228	Different

Statistics for Co Metal Ion Release

		v	to	t	Conclusion
Proximal					
	Polished	7	-4.4176	2.365	Different
	Rough	7	-1.8433	2.365	Not Stat. Different
	Distal	4	5.035	2.776	Different
	Sm Prox	9	-1.405	2.2262	Not Stat. Different
	H Preload	5	2.7239	2.571	Different
	Sleeve	4	-0.7401	2.776	Not Stat. Different
	Control	4	5.5379	2.776	Different
Distal					
	Polished	2	-12.1769	4.303	Different
	Rough	4	-11.4271	2.776	Different
	Sm Prox	5	-8.4837	2.571	Different
	H Preload	6	-4.8041	2.447	Different
	Sleeve	6	-16.5797	2.447	Different
	Control	3	1.2505	3.182	Not Stat. Different
Polished					
	Rough	5	3.5458	2.571	Different
Hpreload					
	Polished	3	-9.2012	3.182	Different
	Rough	6	-7.1713	2.447	Different
	Sm Prox	6	-5.3872	2.447	Different
	Sleeve	6	-7.9523	2.447	Different
	Control	3	6.62	3.182	Different

Statistics for Cr Metal Ion Release

		v	to	t	Conclusion
Proximal					
	Polished	7	2.0492	2.365	Not Stat. Different
	Rough	5	-1.0425	2.571	Not Stat. Different
	Distal	7	2.4165	2.365	Different
	Sm Prox	9	-2.5031	2.2262	Different
	H Preload	7	1.2492	2.365	Not Stat. Different
	Sleeve	5	-0.6425	2.571	Not Stat. Different
	Control	4	4.2683	2.776	Different
Distal					
	Polished	6	-0.4659	2.447	Not Stat. Different
	Rough	3	-2.3684	3.182	Not Stat. Different
	Sm Prox	8	-5.776	2.306	Different
	H Preload	7	-1.7286	2.365	Not Stat. Different
	Sleeve	5	-5.0844	2.571	Different
	Control	3	2.3665	3.182	Not Stat. Different
Polished					
	Rough	3	2.1809	3.182	Not Stat. Different
Hpreload					
	Polished	6	1.2051	2.447	Not Stat. Different
	Rough	3	-1.7535	3.182	Not Stat. Different
	Sm Prox	7	-4.6137	2.365	Different
	Sleeve	5	-3.4374	2.571	Different
	Control	3	5.2587	3.182	Different

Statistics for Ti Metal Ion Release

		v	to	t	Conclusion
Proximal					
	Polished	5	2.5987	2.571	Different
	Rough	4	-1.0153	2.776	Not Stat. Different
	Distal	7	2.6248	2.365	Different
	Sm Prox	9	-4.6496	2.2262	Different
	H Preload	8	0.73098	2.306	Not Stat. Different
	Sleeve	2	-8.9122	4.303	Different
	Control	4	3.2836	2.776	Different
Distal					
	Polished	6	-0.3512	2.447	Not Stat. Different
	Rough	3	-2.1341	3.182	Not Stat. Different
	Sm Prox	6	-8.0667	2.447	Different
	H Preload	6	-1.9566	2.447	Not Stat. Different
	Sleeve	2	-10.2088	4.303	Different
	Control	3	0.4662	3.182	Not Stat. Different
Polished					
	Rough	3	2.0723	3.182	Not Stat. Different
Hpreload					
	Polished	4	1.8889	2.776	Not Stat. Different
	Rough	4	-1.3664	2.776	Not Stat. Different
	Sm Prox	8	-5.6125	2.306	Different
	Sleeve	2	-9.3242	4.303	Different
	Control	3	2.632	3.182	Not Stat. Different

Statistics for Impact Loading

		v	to	t	Conclusion
Controlled Impactor Strike					
	Push	30	-4.148	2.042	Different
Surgical Mallet					
	Medium	30	16.1904	2.042	Different
	Heavy	30	4.278	2.042	Different
Controlled Impactor Push					
Surgical Mallet					
	Medium	30	23.8904	2.042	Different
	Heavy	30	10.083	2.042	Different
Surgical Mallet Medium					
	Heavy	30	13.6081	2.042	Different

Statistics for Pulloff Load after Impacting

		v	to	t	Conclusion
Controlled Impactor Strike					
Surgical Mallet					
	Tester #1	6	-0.2656	2.447	Not Stat. Different
	Tester #2	5	-1.6301	2.571	Not Stat. Different
Surgical Mallet Tester #1					
	Tester #2	10	-1.2297	2.228	Not Stat. Different

ANSYS PROGRAM

```
/PREP7
/show,x11
/TITLE,Conforming
KAN,   0
/COM
/COM NODE DEFINITIONS
iter,-10
wsort,y
waves
CSYS,0
N,1,.31152,-.294956,-1.51E-11
N,2,.28998,-.295,0.
N,3,.267174,-.295,0.
N,4,.242088,-.295,0.
N,5,.214678,-.295,0.
N,6,.184912,-.295,0.
N,7,.152766,-.295,0.
N,8,.118217,-.295,0.
N,9,.08125,-.295,0.
N,10,.041849,-.295,0.
N,11,1.84E-08,-.295,0.
N,12,.310277,-.270374,2.41E-11
N,13,.288854,-.270417,0.
N,14,.266135,-.270417,0.
N,15,.241147,-.270417,0.
N,16,.213843,-.270417,0.
N,17,.184193,-.270417,0.
N,18,.15217,-.270417,0.
N,19,.117757,-.270417,0.
N,20,.080934,-.270417,0.
N,21,.041686,-.270418,0.
N,22,1.84E-08,-.270418,0.
N,23,.30903,-.245793,3.48E-11
N,24,.287726,-.245834,0.
N,25,.265096,-.245834,0.
N,26,.240205,-.245834,0.
N,27,.213008,-.245834,0.
N,28,.183474,-.245834,0.
N,29,.151577,-.245834,0.
N,30,.117297,-.245835,0.
N,31,.080618,-.245835,0.
N,32,.041523,-.245835,0.
N,33,1.84E-08,-.245835,0.
N,34,.307784,-.22121,2.25E-12
N,35,.2866,-.22125,0.
N,36,.264056,-.22125,0.
N,37,.239263,-.22125,0.
N,38,.212173,-.22125,0.
N,39,.182754,-.22125,0.
N,40,.150983,-.22125,0.
N,41,.116838,-.22125,0.
N,42,.080302,-.221252,0.
N,43,.0413605,-.221253,0.
N,44,1.84E-08,-.221253,0.
```

```
N,927,.062603,.422944,0.
N,928,.063444,.44203,0.
N,929,.0643039,.46156,0.
N,930,.0651847,.48156,0.
N,931,.0660867,.502047,0.
N,932,.06701,.523026,0.
N,933,.067957,.54451,0.
N,934,.03127,.386,0.
N,935,.031703,.405388,0.
N,936,.0321405,.42497,0.
N,937,.032583,.44478,0.
N,938,.0330306,.46482,0.
N,939,.0334838,.485107,0.
N,940,.0339426,.50564,0.
N,941,.034407,.52644,0.
N,942,.0348776,.5475,0.
N,943,0.,.386,0.
N,944,0.,.40631,0.
N,945,0.,.42662,0.
N,946,0.,.44693,0.
N,947,0.,.46724,0.
N,948,0.,.48755,0.
N,949,0.,.50786,0.
N,950,0.,.52817,0.
N,951,0.,.54848,0.
/COM
/COM MATERIAL PROPERTIES
EX,        2,  3.1E+07
NUXY,      2,  3.0E-01
DENS,      2,  0
ALPX,      2,  0
KXX,       2,  0
EX,        3,  1.65E+07
NUXY,      3,  3.5E-01
DENS,      3,  0
ALPX,      3,  0
KXX,       3,  0
/COM
/COM REAL CONSTANT TABLE, ELEMENT TABLES, AND
/COM ELEMENT COORDINATE SYSTEM DEFINITION
/COM
/COM PHYSICAL PROP TABLE IN BIN:      1, LABEL:
/COM
R,1,,,,,,
ET,   1,  42,   0,   0,   1,   0,   0,   0
ET,   2,  42,   0,   0,   1,   0,   0,   0
/COM
/COM REAL CONSTANT TABLE, ELEMENT TABLES, AND
/COM ELEMENT COORDINATE SYSTEM DEFINITION
/COM
/COM PHYSICAL PROP TABLE IN BIN:      1, LABEL:
/COM
R,2,,,,,,
mu,4,0.15
/COM
```

```
/COM REAL CONSTANT TABLE, ELEMENT TABLES, AND
/COM ELEMENT COORDINATE SYSTEM DEFINITION
/COM
/COM PHYSICAL PROP TABLE IN BIN:      1, LABEL:
/COM
R,3,2.85-90,.17e9,0.,0.,0.,
ET,   3,  12,   0,   0,   0,   1,   0,   0
TYPE,  1 $ REAL,     2 $ MAT,     3
ESYS,  0
EN,1,1,2,13,12
EN,2,2,3,14,13
EN,3,3,4,15,14
EN,4,4,5,16,15
EN,5,5,6,17,16
EN,6,6,7,18,17
EN,7,7,8,19,18
EN,8,8,9,20,19
EN,9,9,10,21,20
EN,10,10,11,22,21
EN,11,12,13,24,23
EN,12,13,14,25,24
EN,13,14,15,26,25
EN,14,15,16,27,26
EN,15,16,17,28,27
EN,16,17,18,29,28
EN,17,18,19,30,29
EN,18,19,20,31,30
EN,19,20,21,32,31
EN,20,21,22,33,32
EN,21,23,24,35,34
EN,22,24,25,36,35
EN,23,25,26,37,36
EN,24,26,27,38,37
EN,25,27,28,39,38
EN,26,28,29,40,39
EN,27,29,30,41,40
EN,28,30,31,42,41
EN,29,31,32,43,42
EN,30,32,33,44,43
EN,31,34,35,46,45
EN,32,35,36,47,46
EN,33,36,37,48,47
EN,34,37,38,49,48
EN,35,38,39,50,49
EN,36,39,40,51,50
EN,37,40,41,52,51
EN,38,41,42,53,52
EN,39,42,43,54,53
EN,40,43,44,55,54
EN,41,45,46,57,56
EN,42,46,47,58,57
EN,43,47,48,59,58
EN,44,48,49,60,59
EN,45,49,50,61,60
EN,46,50,51,62,61
EN,47,51,52,63,62
```

```
EN,791,111,601
EN,792,100,592
EN,793,89,583
EN,794,78,574
EN,795,67,565
EN,796,56,556
EN,797,45,547
EN,798,34,538
EN,799,23,529
EN,800,12,520
EN,801,1,502
/COM
CSYS,0
/COM Case set number      1
/COM
/COM Restraint set       1
DDELE, 1, ALL,     951
/COM
/COM NODAL DISPLACEMENT RESTRAINTS
D,144,UX,0.,,,
D,144,UY,0.,,,
D,145,UX,0.,,,
D,145,UY,0.,,,
D,146,UX,0.,,,
D,146,UY,0.,,,
D,147,UX,0.,,,
D,147,UY,0.,,,
D,148,UX,0.,,,
D,148,UY,0.,,,
D,149,UX,0.,,,
D,149,UY,0.,,,
D,150,UX,0.,,,
D,150,UY,0.,,,
D,151,UX,0.,,,
D,151,UY,0.,,,
D,152,UX,0.,,,
D,152,UY,0.,,,
D,153,UX,0.,,,
D,153,UY,0.,,,
D,154,UX,0.,,,
D,154,UY,0.,,,
/COM
/COM Load set       1
KRF,1
KSE,1
FDELE, 1, ALL,     951
TDELE, 1,     951
EPDELE, ALL, , ,ALL
/COM
/COM ELEMENT EDGE PRESSURE LOADS
EP,     776,       2,    4401*1/10
EP,     768,       2,    4366.18*1/10
EP,     760,       2,    4277.80*1/10
EP,     752,       2,    4144.66*1/10
EP,     744,       2,    3975.02*1/10
```

```
EP,     736,        2,    3776.62*1/10
EP,     728,        2,    3556.63*1/10
EP,     720,        2,    3321.73*1/10
EP,     712,        2,    3078.83*1/10
EP,     704,        2,    2834.11*1/10
EP,     696,        2,    2592.66*1/10
EP,     688,        2,    2276.69*1/10
EP,     680  1858.47*1/10
EP,     672,        2,    469.67*1/10
lwrite
EP,     776,        2,    4401*2/10
EP,     768,        2,    4366.18*2/10
EP,     760,        2,    4277.80*2/10
EP,     752,        2,    4144.66*2/10
EP,     744,        2,    3975.02*2/10
EP,     736,        2,    3776.62*2/10
EP,     728,        2,    3556.63*2/10
EP,     720,        2,    3321.73*2/10
EP,     712,        2,    3078.83*2/10
EP,     704,        2,    2834.11*2/10
EP,     696,        2,    2592.66*2/10
EP,     688,        2,    2276.69*2/10
EP,     680  1858.47*2/10
EP,     672,        2,    469.67*2/10
lwrite
EP,     776,        2,    4401*3/10
EP,     768,        2,    4366.18*3/10
EP,     760,        2,    4277.80*3/10
EP,     752,        2,    4144.66*3/10
EP,     744,        2,    3975.02*3/10
EP,     736,        2,    3776.62*3/10
EP,     728,        2,    3556.63*3/10
EP,     720,        2,    3321.73*3/10
EP,     712,        2,    3078.83*3/10
EP,     704,        2,    2834.11*3/10
EP,     696,        2,    2592.66*3/10
EP,     688,        2,    2276.69*3/10
EP,     680  1858.47*3/10
EP,     672,        2,    469.67*3/10
lwrite
EP,     776,        2,    4401*4/10
EP,     768,        2,    4366.18*4/10
EP,     760,        2,    4277.80*4/10
EP,     752,        2,    4144.66*4/10
EP,     744,        2,    3975.02*4/10
EP,     736,        2,    3776.62*4/10
```

REFERENCES

1. **Moore, R., Hamburger, S., Jeng, L., Hamilton, P.,** Orthopedic Implant Devices: Prevalence and Sociodemographic Findings from the 1988 National Health Interview Survey, J. of Applied Biomaterials, 1991, vol.2, pp. 127-131.

2. **American Machinist,** What the morse taper really is and how it was measured, 1896, vol. 19, no. 20.

3. **Marks, L., McKay, G.,** Mechanical Engineer's Handbook: fourth ed., McGraw-Hill Book Co., 1941.

4. **Huiskes, R., Weinans, H., Van Rietbergen, B.,** The relationship between stress shielding and bone reabsorption around total hip stems and the effects of flexible materials, J. Clinical Orth. & Related Res., 1992, No. 274, pp. 125.

5. **Skinner, H., Curlin, F.,** Decreased pain with lower flexural rigidity of uncemented femoral prostheses, Orthopedics, 1990, Vol. 13, No. 11, pp. 1223.

6. **Bobyn, D., Mortimer, E., Glassman, A., Engh, C. Miller, J., Brooks, E.,** Producing and avoiding stress shielding, J. Clinical Orth. & Related Res., 1991, pp. 79.

7. **Clarke, I., Mckellop, H., McGuire, P., Okuda, R., Sarmiento, A.,** Wear of Ti-6Al-4V implant alloy and ultra-high molecular weight polyethylene combinations, Amer. Soc. for Testing Mat., 1983, pp. 136-147.

8. **McKellop, H., Clarke, I.,** Degredation and Wear of UHMWPE , in corrosion and Degradation of Implant Materials, ASTM Fraker and Griffin, eds., Am. Soc. for Testing and Mat, Philadelphia, PA, STP 859, 1985, pp. 35-368.

9. **Dobbs, H., Minimumski, M.,** Metal ion release after total hip replacement, J. of Biomaterials, 1980, volume 1, pp. 1933-1938.

10. **Zimmer, Inc.,** Current topics in orthopaedic technology, 1991, vol. 5, no. 3.

11. **Angle, T.**, Analyzing taper fits, WEMCO co., Machine Design, 1983, pp.75-78.

12. **Smith and Nephew Richards**, File number MO 219, material properties, Memphis Tennessee, 1991.

13 **Kalpakjian, S.**, Manufacturing Processes for Engineering Materials, Addison-Wesley Publishing Co., 1985.

14. **Star, M., Colwell, C., Donaldson, W., Walker, R.**, Dissociation of modular hip arthroplasty components after dislocation, Clinical Orthopaedics and Related Research, 1992, vol. 278, pp. 111-115.

15. **Pellicci, P., Haas, S.**, Disassembly of a modular femoral component during closed reduction of the dislocated femoral component, J. of Bone and Joint Surgery, 1990, vol. 72-A, no. 4, pp. 619-620.

16. **Woolson, S., Pottorff, G.**, Disassembly of a modular femoral prosthesis after dislocation of the femoral component, J. of Bone and Joint Surgery, 1990, vol. 72-A, no. 4, pp. 624-625.

17 **Maquet, P.**, Biomechanics of the Hip, Springer-Verlag, New York, 1984, pp. 1-15

18. **Williams, J.**, Biomechanics of total hip replacement, The Hip and Its Disorders: W.B. Saunders Co., Harcourt Brace Jovanovic, Inc., 1991, pp. 876-904.

19. **Dingman, C.**, Determinimumation of an in-vitro load condition to represent the mid-stance phase of gait: a finite element analysis, Richards Medical Co., 1989.

20. **International Organization for Standardization**, Implants for surgery-partial and total hip joint prosteses-determination of endurance properties of stemmed femoral components without application of torsion, ISO 7206-3, 1988.

21. **Rohlmann, A., Mossner, U., Bergmann, G., Kolbel, R.**, Finite-element analysis and experimental investigation in a femur with hip prosthesis., J. of Biomechanics, vol. 16, 1983, pp. 727-742.

22. **Collier, J., Surprenant, V., Jensen, R., Mayor, M.**, Corrosion at the interface of cobalt-alloy heads on titanium-alloy stems, J. of Clinical Orthopaedics and Related Research, 1991, vol. 271, pp. 305-312.

23. **Sauer, W., Kovacs, P., Varnavas, J., Beals, N.**, Potential corrosion-related phenomena at head/taper interfaces: a 3-5 year follow-up of modular head/Ti-6Al-4V femoral stem hip prosthesis, S &N Richards Advanced Technology AT-91-15, 1991.

24. **Howmedica Research**, Modular heads and taper tolerances, Howmedica, Rutherford, N.J., 1992.

25. **Fontana, M.**, Corrosion Engineering 3rd Ed., McGraw Hill, 1986, pp. 40-60.

26. **Davidson, J., Kovacs, P.**, Basic description of issues associated with crevice conditions in modular femoral heads, S & N Richards Orthopaedic Research Department, 1991

27. **Bauer, T., Brown, S., Jiang, M., Panigutti, M., Fleming, C.**, Corrosion in modular hip stems, ORS 38th annual meeting #354, Washington D.C., 1992.

28. **Mathiesen, E., Lindgren, J., Blomgren, G., Reinbolt, F.**, Corrosion of modular hip prostheses, J. of Bone and Joint Surgery, 1991, vol. 73-b, no.4, pp. 569-575.

29. **Rostoker, W., Pretzel, C., Galanta, J.**, Couple corrosion among alloys for skeletal prostheses, J. Biomedical Materials, 1974, vol. 8, pp. 407-419.

30. **Amstutz, H., Campbell, P., Kossovsky, N., Clarke, I.**, Mechanism and clinical significance of wear debris-induced osteolysis, J. of Clinical Orthopaedics and Related Research, 1992, vol. 276, pp. 7-18.

31. **McLean, T.**, Filtration procedures for wear analysis, S & N Richards Inc., Orthopaedic Research Department OR-92-#, 1992.

32. **Goldman, S., Lynch, G.**, Biofit taper evaluation, S & N Richards, Research and Development Division ML-84-72, 1984.

33. **Goldman, S.**, Davidson, J., Ceramic head pull-off testing, S & N Richards, Research and Development Division ML-84-36, 1984.

34. **Goldman, S., Lynch, G.**, Cyclic loading of trunnion-mounted ceramic heads, S & N Richards, Research and Development Division ML-85-16, 1985.

35. **Lynch, G.**, Cyclic loading of extra-smooth biofit trunnion, S & N Richards, Research and Development Division ML-85-55, 1985.

36. **Asgian, C.**, Mechanical testing of oxidized Ar-2.5Nb modular heads, S & N Richards, Orthopaedic Research Department OR-91-70, 1991.

37. **Mishra, A.**, Pull-off testing of Ti-13Nb-13Zr trunnions following static and fatigue loading, S & N Richards, Orthopaedic Research Report, OR-91-08, 1991.

38. **Fricker, D.C.**, Shivanath, R., Fretting corrosion studies of universal femoral head prostheses and cone taper sigots, J. of Biomaterials, 1990, vol. 11, pp. 495-500.

39. **Doino, J.**,, PCB Engineer, personal conversation, 11-19-92

40. **Kovacs, P., Davidson, J., Daigle, K.**, Correlation between the metal ion concentration and the fretting wear volume of orthopaedic implant metals, Standard Technical Publication 1144, ASTM, 1992.

41 **DeSalvo, G., Gorman, R.**, ANSYS users manual version 4.4, Swanson Analysis System Inc., 1989.

42. **Fessler, H., Fricker, D.C.**, A study of stresses in aluminum universal heads of femoral prostheses, J. of Engr. in Medicine, Proc. Institution of Mech. Engrs., IMechE 1989, vol. 203, pp. 15-34.

43. **Harbaugh, M.**, A finite element model of the modular head taper joint", S & N Richards Orthopaedic Research Report OR-92-70, 1992.